Exterior Rotor Permanent Magnet generator In Variable Speed Applications

Rauf Sattar

PEMC Research group

Nottingham University

A thesis submitted in partial fulfillment of the requirements of the Department of engineering at Nottingham University for the Degree of Master of Philosophy (MPhil).

2015

Acknowledgements

Firstly, I would particularly like to thank my supervisors, Professor Christopher Gerada and Dr Mohand Hamiti, for their unfailingly generous support and guidance throughout this work.

I also acknowledge the encouragement of my engineering manager Dr Jawad Al-Tayie for his fruitful discussions about this project, his guidance and encouragement without whom I would never have embarked on this journey.

I would also like to acknowledge Nigel Atkins (Cobham) for the finite element software (Opera).

Finally, special thanks go to my family, without whom I might never have finished.

Contents

1. Nomenclature

A	Area (m)
B_g	Air gap flux density (T)
N	Number of turns
N_m	Number of magnet poles
N_{ph}	Number of turns in series per phase
N_s	Number of slots
N_{sm}	Number of slots per magnet pole
B_r	Magnetic remanence (T)
T	Torque (Nm)
H	Magnetic field intensity (A/
Am	The cross-sectional areas of the permanent magnet
Aag	The cross-sectional areas of the air gap
A_{slot}	The slot area
A_{cu}	The conductor cross-sectional area in mm^2
B_r	Magnet remanent flux density
B_m	Magnet working flux density
e_t	The induced back EMF in one conductor e
Eph	The phase back EMF
h_{slot}	The slot height
H_m	Magnetic field intensities of the permanent magnet
Hag	Magnetic field intensities of the air gap
ia	Phase currents in ampere, A
i_{sc}	The short circuit current
kw	Winding distribution

L_a	Self inductances of each phase in henry, [H]
L_{ab}	Mutual inductances of between phases in henry, [H]
L_{cu}	Total length of the stator winding [m]
L_{mot}	The axial length of the stator core [m]
N_{turn}	The number of conductor turns
P_h	The number of phases
P_{cu}	The copper loss
P_{iron}	The iron loss
P_h	The hysteresis loss
P_e	Eddy current loss
σ	Winding conductor conductivity
μ_{rec}	Magnet recoil permeability
ϕ	Effective flux
Ψ_{am}	Flux linkages of each phase in weber, Wb
K_{fill}	Filling Factor
K_{safe}	Safety factor
K_{sh}	Ratio of interior diameter of rotor and rotor length [m]
l_m	Radial length of magnet [m]
l_r	Rotor length [m]
l_s	Stator length [m]
h_o	Slot opening depth [m]
H	Magnetic field strength [A/m]
h_s	Slot height [m]

h_{sy}	Height of stator yoke [m]
h_t	Tooth height [m]
I_i	Fundamental stator current [A]
J_s	Current density of source [A/m^2]
$\dot{B}$	Amplitude of flux density [T]
$\dot{B}_{g1}$	Amplitude of the fundamental flux density in air gap due to the magnets [T]
$\dot{B}_{r1}$	Amplitude of the fundamental flux density of a tooth [T]
$\dot{B}_{g,0}$	Mean air gap flux density due to the magnet at positions opposite the magnet [T]
$\dot{B}_{g,max}$	Max air gap flux density due to the magnet at positions opposite the magnet [T]
$\dot{B}_{ry}$	Mean flux density of rotor yoke [T]
$\dot{B}_{sy}$	Mean flux density of Stator yoke [T]
B_t	The tangential component of the flux density [T]
A_{cu}	Cross section of Copper wiring [m^2]
A_{slot}	Cross section of slot [m^2]

2. Abstract

This thesis explores approaches for converting rotational mechanical power from diesel engines into electrical power of fixed frequency and voltage. Advances in high energy permanent magnets and power electronics are enabling technologies that provide opportunities for electrical machines with increased efficiency and compact size for variable speed power generation.

The overall objective was to design a permanent magnet machine with concentrated winding that could be used in variable speed application. Specifically, the aim is to extract the maximum power density and torque by utilizing high pole numbers and minimizing magnetic material content.

The concept of variable speed is discussed and suitable electrical machines are reviewed. A radial flux Permanent magnet machine is researched and possible integration methodologies explored within the flywheel housing of the diesel engine. A machine design model is developed based upon a combination of analytical and finite element analysis tools and explore an insight into the design of such machines and optimisation of the overall performances, leading to smaller size, less maintenance, smaller carbon foot print and higher speed.

To take into account the thermal aspects of the design, a basic thermal model was developed to understand the influence of the temperature on the overall performance of the design along with the temperature of the windings and magnets. A number of scientific contributions were generated from the analysis of the above objectives, they are as follows;

- The concept of the variable speed application and its benefits over fixed speed generation
- Design and analysis of a suitable configuration of the PM machine for a variable speed application
- Integration methodology of PM machine into the flywheel of a diesel engine
- Identified power conditioning system topologies which could be applied in variable speed application
- Briefly, explored the selection methodology for engines for fuel reduction which in turn reduces the overall size of the generating set

3. Background

This study constitutes an overall approach to literature review of electrical machines and then a design based selection on permanent magnet synchronous generator topology for automotive and variable speed generators application, Naturally, such an approach involves the making of a series of choices and decisions, some mandated at the outset by the requirements and constraints of the surrounding system, and some gradually introduced in due course by the accompanying technical analyses. The former are mainly about the basic structure of the machine and the latter will be on the specifics of the design parameters and other auxiliary issues such as the power electronic drive.

In recent years power electronics has flourished and new and innovative techniques are available, this in turn opens new perspectives in innovative machine design, furthermore with availability on new materials, such as soft magnetic composites and high performance permanent magnets, renders the possibility of even further improvements in design performance characteristics and the demand such as torque quality aspects is becoming increasingly important. As the demand for power is increasing around the world it has become imperative that the industry designs and develops reliable, high-performance electrical machines at the lowest cost possible. Constraints restricting the business are the efficiency, cooling and mechanical properties of the machines. If industry is offered an opportunity to choose between two alternative electrical machines, which have the same performance, e.g. efficiency, but of which can be built at a lower manufacturing cost, it is obvious that the latter, cheaper design will be preferred. An important tool needed for decision-making is then a performance comparison between the considered electrical machines.

A theoretical comparison between similar machines types can be done reasonably but comparison between the different machine topologies is a cumbersome task since there exist many variables and it is difficult to decide which variables should be kept as constants and which may vary. In order to establish a reliable comparison, a sufficient amount of different machine designs have to be considered. In this review the focus is on PMSM synchronous machine designs. Initially several machine concepts will be explored to understand the fundamentals and to identify possible potential designs and designs techniques.

4. Research Objectives and Benefits

This thesis originates from a research project into the design of a generator in variable speed application.

The aim is to select best possible topology and design optimisation methods. The mechanical aspects of the generator, the diesel engine and design of the converter are briefly highlighted but are beyond the scope of this research. Each application has individual characteristics so that the choice of the generator structure needs to be studied with care. Different application will lead to different choices of structure. With the increasingly stringent emissions legislation as well as the hiking fuel prices, electrification is currently a prime path to meet the environmental and efficiency targets, thus placing the need for high-performance electrical machines.

This study looks at analyzing/designing electrical machines for variable speed options significantly reducing fuel consumption as the system can respond quickly and efficiently to load demands especially during start up. The environmental advantages of the Variable Speed Generators are also apparent with more efficient fuel consumption reducing refueling, thus reducing the total carbon footprint. The selection criteria is based on the following:

- A reduced system weight
- Less demanding maintenance
- Improved efficiency
- Cost Effective
- Fuel efficiency
- Cleaner and safer environment.

4.1. **Permanent Magnet synchronous generators in Variable Speed Application**

Over the past hundreds of years synchronous generators have made up nearly all the worlds electrical power needs. The most common solution for providing electrical power is to use fixed speed engines, this includes shaft generators for marine applications. Due to emissions regulations and fuel prices a compelling shift is required to operate the generating set at variable speed. With recent advances in power electronics it is now possible to condition the variable frequency and output voltage.

4.2. **Fixed Speed Power Generation**

Generators operate at a driven speed to provide an electrical output at the ideal international voltage and frequency appropriate for the connected electrical equipment. Generators are designed to be operated with a speed governing system that will operate at 5% above the nominal synchronous speed at No Load, with the speed drooping to the nominal synchronous speed at full rated output.

Slow running speeds affect the performance of the cooling fan and so promote generator components to conditions of overheating. They also cause the generator to operate at higher magnetic flux levels in attempt to maintain the set output voltage; this situation overheats/overloads all the excitation components and also the stator lamination steel. In synchronous generators the frequency of generation is linked directly with mechanical rotational speed.

$$F = \frac{\mathrm{n} * \mathrm{p}}{60} \qquad \text{Eq.1}$$

F is operating frequency
n is mechanical speed
p is number of pole pairs

When load is applied to diesel generating set, a transient voltage dip occurs this is shown below, whilst the generator excitation system establishes the correct level of excitation.

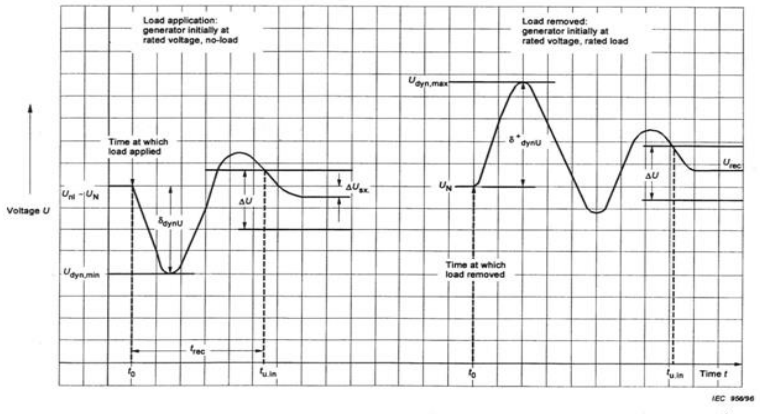

Figure 1. Generator transient voltage versus time for sudden load application and removal, rms voltage versus time [43]

We current innovation diesel engine technology only a percentage of full loads can be applied a given time, when the load is then removed, a transient voltage rise occurs due to the engine speed.

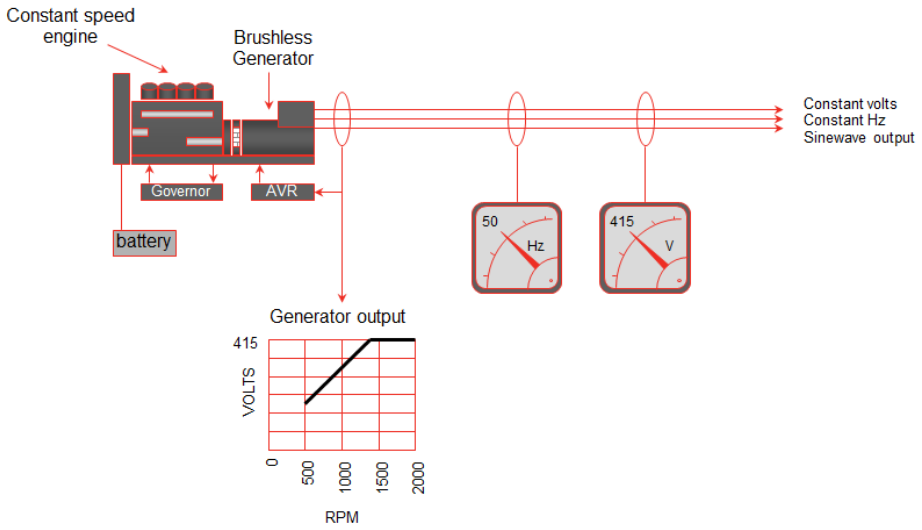

Figure 2. Outline of a convectional generating set [40]

Figure 3. Examples of a diesel driven synchronous generating set [45]

Rotational power is provided by the diesel engine and converted into electrical power by a permanent magnet generator. With variable speed the amplitude and frequency of the voltage provided by the generator will also vary.

To overcome this, the output is rectified and boosted to a reference DC level, so that constant DC link voltage is maintained. This voltage is then converted to the desired output and voltage using Pulse Width Modulation (PWM) techniques.

Variable Speed Decoupled Generation as an **additional degree of freedom** for the prime-mover and for the generator.

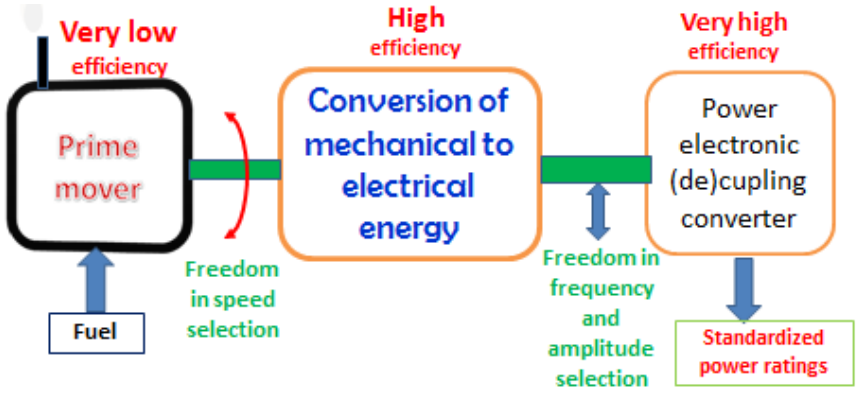

Figure 4. Shows Mechanical to Electrical conversion process through variable speed power generation [40]

The release of the generating set from the fixed speed opens the way for new design related to energy losses reduction, high dynamics and weight of the generating set reduction.

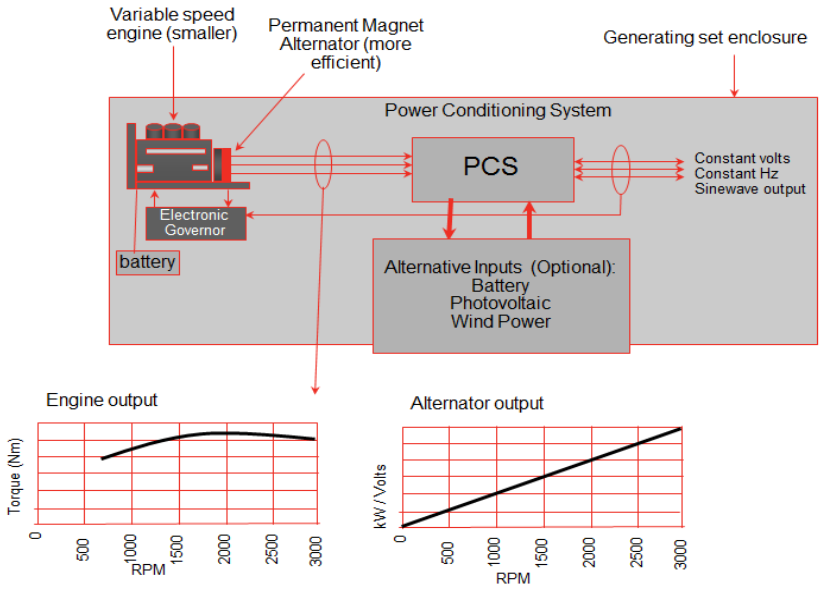

Figure 5. Outline of a Variable Speed generating set [40]

With additional battery charging capability or alternative storage system, allows power to be supplied to the load with the generating set switched off.

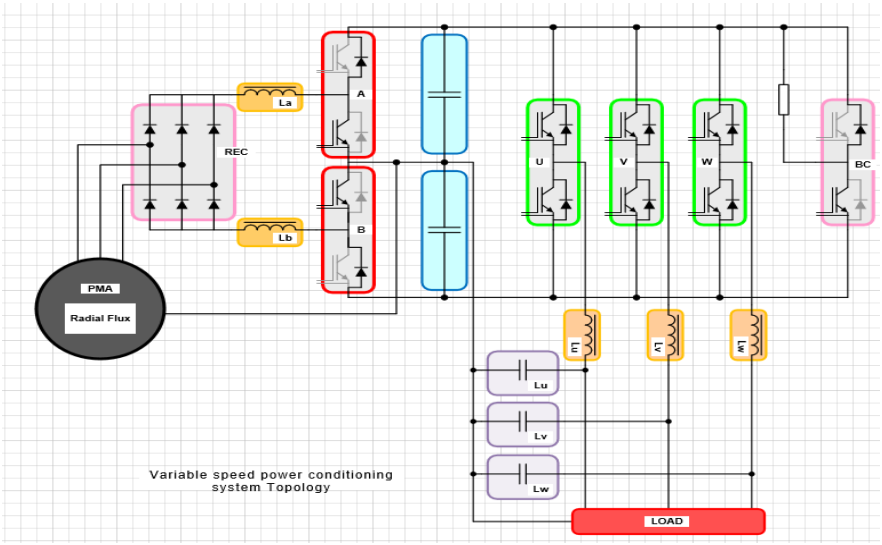

Figure 6. One of the many possible topologies for Power Conditioning System in variable speed application [40]

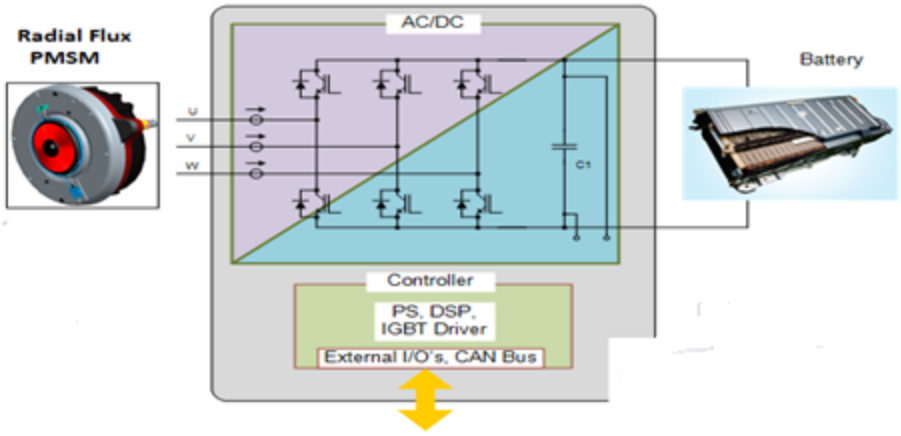

Figure 7. One another possible concept showing PMSM as part of a hybrid system [40]

Comparing engines when sizing a genset, may be necessary to determine optimal performance, torque and horsepower are necessary measures but not helpul when comparing different sizes and designs. Instead engines can be compared by referring to the brake mean effective pressure (BMEP).

The mean effective pressure is an average of the pressure that would need to be present for the power and torque to be produced, BMEP refers to the brake MEP or the useful work done at the engine flywheel.

BMEP is an indicator of much engine torque is available and allows to select an engine based on optimal performance parameter. With variable speed application with no load to run at constant speed the engine can be run at speeds that return minimum fuel consumption for a given power output. System efficiency can be improved further, particularly for light loads as the engine could be switched off and the loads supported by the battery or other energy storage medium. This will lead to lower running costs over `the life cycle of the test. With variable speed the engine can be run at an optimum Break Mean Effective Pressure, which in turn reduces emissions, and increases engine life.

With engine speed control, vibration levels can be reduced and mechanical systems resonance conditions avoided, reducing maintenance and increasing engine life further.

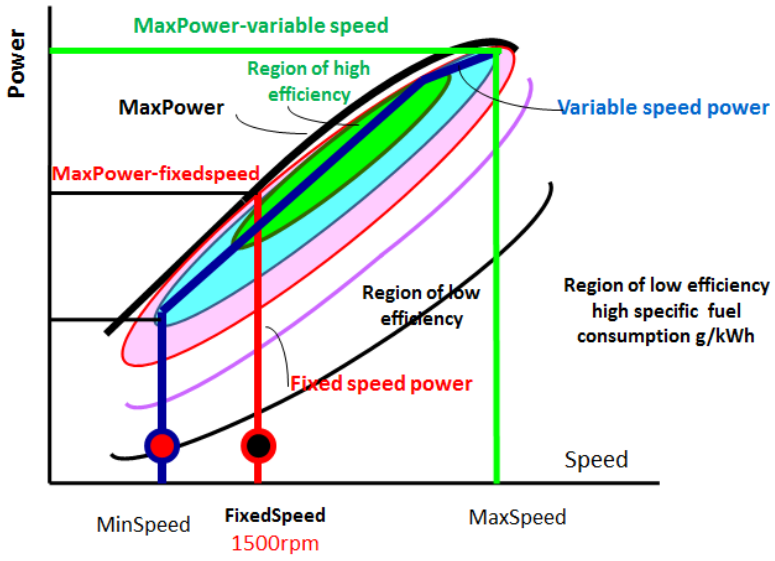

Figure 8. Power and specific fuel consumption of fixed and adjustable speed engine driving generator [40]

Figure 9. Possible coupling arrangement onto the engine flywheel for a permanent magnet variable speed generator [40]

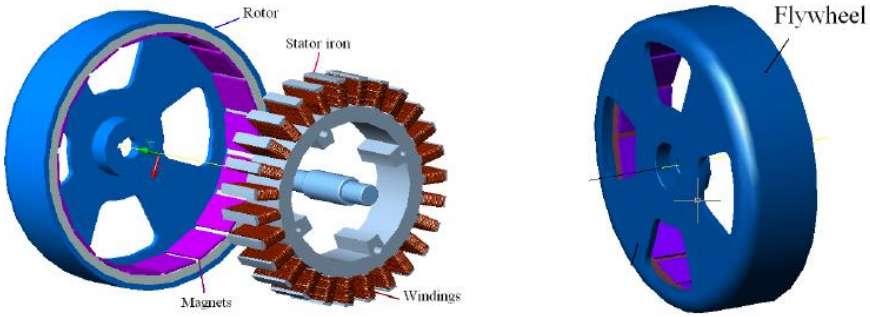

Figure 10. Exterior rotor permanent magnet machine for marine application [20]

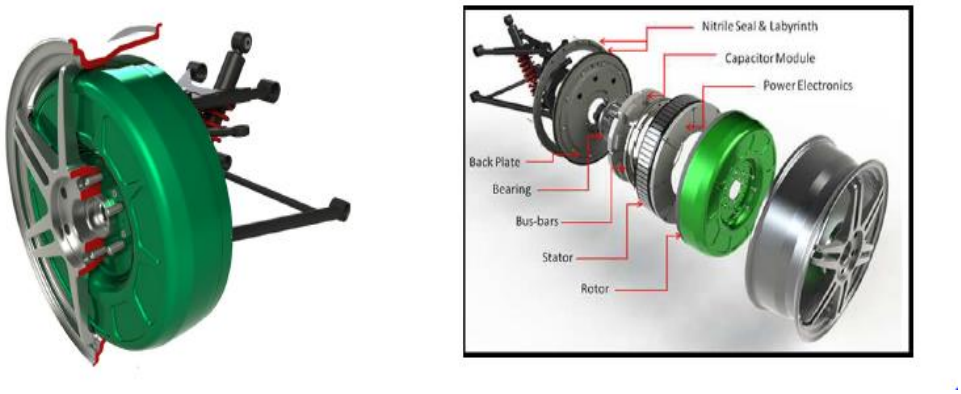

Figure 11. Exterior rotor permanent magnet in wheel hub of electric protean truck, protean electric [44]

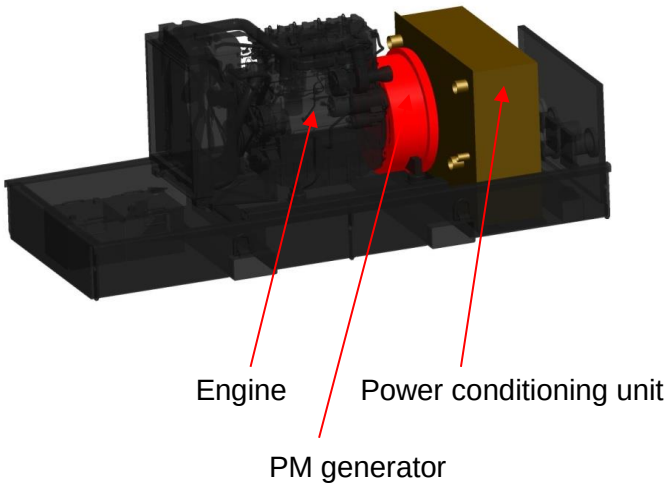

Figure 12. One of the possible ways to integrate a complete generating set for variable speed applications [40]

5. Review of electrical machines

Permanent magnet synchronous machines (PMSM) provide significant advantages in terms of electrical efficiency compared with the traditional electrically excited synchronous machines.

This is because the joule losses of the field winding are eliminated by using permanent magnet (PM) instead of rotor winding. Because permanent magnets are part of the magnetic circuit of the machine, they significantly affect the total reluctance of the machine.

The relative permeability μ_r of the modern PM materials such as NdFeB lead to the fact that the equivalent air gap length in rotor surface magnet in the d-axis direction is considerable thus resulting in magnetizing inductance values, which is beneficial from the viewpoint of high pull-out torque production. There are many different configurations of the permanent magnet (PM) machines. In addition, each application has individual characteristics. Different applications can lead to different choices.

Therefore, the choice of the PM machine configurations can lead to different configurations choices; these can be radial, axial and transverse. The aim is to compare the advantages and disadvantages of permanent machines in order to select the most suitable. There are many ways to asses an electrical machine such as torque per mass, torque per volume, power density and efficiency.

5.1. Transversal Flux Permanent Magnet (TFPM)

The investigation on transverse flux machines (TFM) and their application in direct drive systems has become a topic of intense research since Weh and May proposed a new machine by combining high energy density permanent magnets (PM) and transverse flux configuration in 1986 [16]. TFMs can achieve high specific torque in low-to-medium speed and hence are suitable for direct drive application with reduced weight, cost, losses and maintenance. In normal machines the armature excitation conductors are perpendicular to the direction of motion and the magnetic flux mainly flows within the longitudinal plane. A fundamental constraint on the design of this type of machines is that the armature conductors and the magnetic flux compete for the same space around the circumference of the stator. The force density in an electrical machine can be calculated by the product of electric loading and no-load induction, or the product of the equivalent current loading of the rotor magnet and armature induction.

The armature induction is not restricted to follow in the axial direction. As opposed to the RFPM and AFPM the magnetic flux and current does not compete for the space in this type of machine. The result is that the current loading and thereby the power density can be much higher.

The high current loading has a drawback; high reactance, which again result in a high voltage drop at nominal load, and a need for high induced voltage.

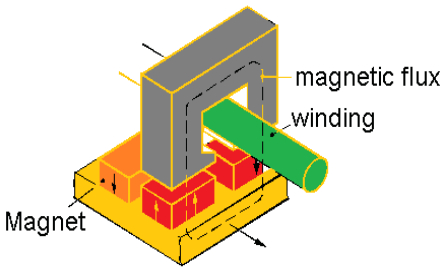

Figure 13. Geometry of TFPM machine with surface mounted magnets [19]

This makes the converter somewhat more expensive since it has to be rated for the high no load voltage. Reducing the inductance also reduces the power density and the TFPM's performance becomes more like the RFPM's and AFPM's. Another challenge with the TFPM is the large amount of small parts that the machine will consist of. This is both costly and challenging concerning assembly. Transversal machines will not be discussed further due to the large number of parts and the cost incurred.

5.2. **Axial flux**

Axial flux machines are defined as rotating electrical motors/generators in which magnetic flux crossing the gap between the rotor(s) and stator(s) does so predominantly in the axial direction. As a result, such machines tend to be disc-shaped, having a relatively large diameter and a short axial length by comparison with the more conventional radial flux machines, which tend to be cylindrical.

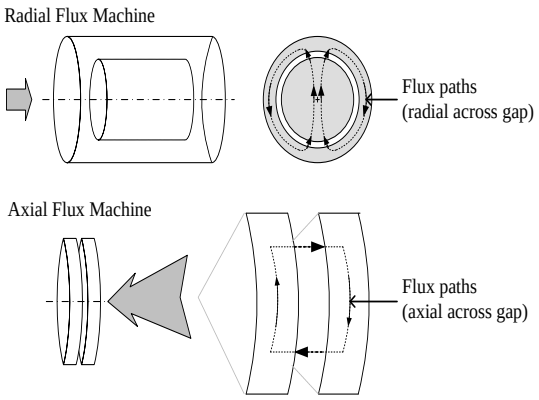

Figure 14. Basic distinction between axial and radial flux [46]

Alternatively, a radial flux machine may be transformed into an axial flux machine as follows. Consider a simplified radial flux machine, having a permanent magnet rotor and a stator with a distributed winding.

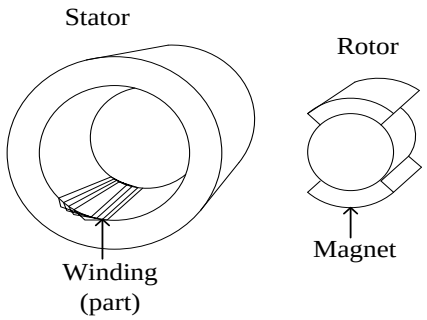

Figure 15. Simplified radial flux machine [46]

In fact, it is the requirement for axial mounting of the rotating part that creates disc-type components. Compare this with the radial flux machine where both the diameter and the axial length of the air-gap determine the active area. This decoupling of the active area from the axial length is a significant feature of axial flux machines and is fundamental to the application of this concept.

Another significant feature is the arc-shape of each magnet, commonly implemented as a trapezium. Also, the axial flux configuration is naturally suited to high pole numbers since increasing the number of poles in an electrical machine reduces the flux per pole and hence the back iron requirement in the stator and rotor components.

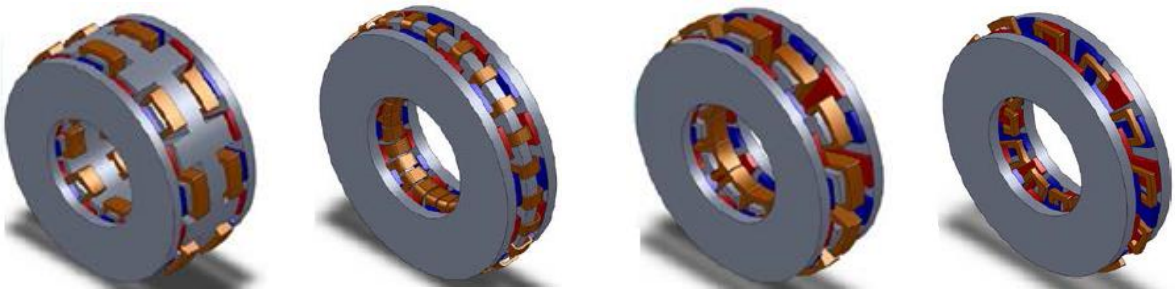

Figure 16. Interior slotted stator N-N lap winding (A) Interior slotless stator N-N toroidal winding (B) Interior ferromagnetic core stator N-S machine (C) Interior coreless N-S machine [43]

Design variations, stator inner and diameters are the most important design parameters. Hence, for cases where the stator outer diameter is limited or imposed by the rest of the system, the ratio of inner to outer diameter are the key parameters to consider and it has a crucial impact on the determination of the machine characteristics, such as torque, torque to weight ratio, iron losses, copper losses, and efficiency. Other important design parameters are the pole number, magnet thickness, conductor size, number of turns and material types. On the other hand, every design has it particular constraints and they differ with the type of application.

5.3. **Radial flux Permanent magnet machines**

Radial flux machine is the classical type of electric machine. Close to all commercial induction and wound synchronous machines are radial flux machines. A cylinder rotates inside another, usually supported by bearings in the Centre. The magnets can be placed in many ways on the rotor and the radial field [6] shown below figure, the high power density synchronous machines have surface PM's with radial orientation whereas the interior magnet versions is intended for high speed application.

Regardless of the manner how the magnet is fitted, the principle of operation remains same, however due to the position of the magnets the main difference is between the direct and quadrature axis inductance values.

Considering the permeability of high flux density PM's is almost similar of that air. This results in the magnet thickness becoming an extension of the air-gap by that amount. The stator inductance when direct axis or magnet is aligned with the stator winding is known as direct inductance.

By rotating the magnets from the aligned position by 90^{o}, the stator sees the interpolar area of the rotor containing on the iron path and the inductance measured in this position is referred to as Quadrature Axis inductance, inductance is derived from the device dimensions, air gap and number of turns.

$$L = \frac{\lambda}{\mathrm{I}} = \frac{\mathrm{Tph}\phi}{\mathrm{I}} = \frac{\mathrm{TphF}}{\mathrm{I}\Re} = \frac{\mathrm{Tph\ Tph\ I}}{\mathrm{I}\Re} = \frac{\mathrm{T^2ph}}{\Re} \qquad \text{Eq.2}$$

Tph is number of turns
ϕ is the flux
F is MMF
I is the current
$\Re$ is reluctance

$$\mathrm{L} = \frac{\mathrm{l}}{\mu_o\, \mu_r\, \mathrm{A}} \qquad \text{Eq.3}$$

l is the length of the flux line
A is the area of the cross section
μ_r is the relative permeability of the steel laminations

The magnetic force has a radial and tangential component, were the sum of radial forces around the air gap ideally is zero and the sum of tangential forces yields the output torque. In contrast to axial-flux machines, which are manufactured almost exclusively with surface mounted magnets, radial flux permanent magnet machines can presented in various forms of magnet placement on the rotor which leads to certain unique operating characteristics. The principle of operation of synchronous machines with PM rotors is explored and the fundamental relationships such as the magnetomotive force (mmf), induced emf (also known as back emf), and torque are derived for PMSMs with sinusoidal-induced emf but they can be extended along the same lines to brushless dc machines with trapezoidal-induced emf.

To understand these relationships, the understanding of stator windings and how the number of turns and their placement in the stator laminations affect them. Factors that affect the windings are pitch, distribution and skew.

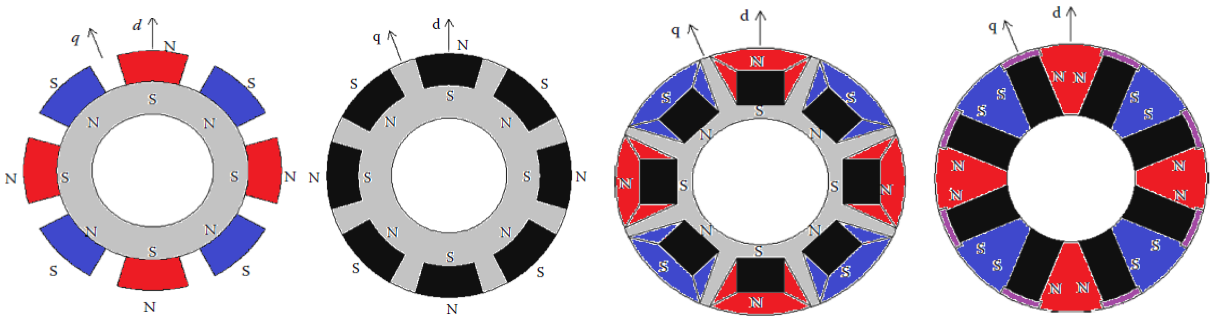

Figure 17. Rotor structures and the definitions for the direct (d) and quadrature (q) axes. Surface PM synchronous machine (A) Surface inset PM synchronous machine (B) Interior PM synchronous Machine (c) Interior PM synchronous with circumferential orientation(D) [24]

The synchronous machines are always magnetically unsymmetrical and are thus observed usually with respect to the d- and q-axes. The geometrical structure of the rotor influences strongly the *L*d and *L*q inductances.

5.4. **Surface mounted PMSM**

The magnets mounted on the surface of the outer periphery of rotor laminations. This arrangement provides the highest air gap flux density as it directly faces the air gap without the interruption of any other medium such as part of rotor laminations.

Drawbacks of such an arrangement are lower structural integrity and mechanical robustness as they are not snugly fitted into the rotor laminations to their entire thickness, the magnets are bound to the rotor, thus reinforcing the mechanical strength of the rotor and magnet combination. They are not preferred for high-speed applications, generally greater than 3000 rpm but machines with very small rotor diameter can be found to have speeds in the range of 50,000 rpm also. The reluctance variation between the direct and quadrature axes is fairly small in this machine as seen from its construction. Accordingly, there is very little (less than 10%) variation between the quadrature and direct axes inductances in this machine.

5.5. **Surface-Inset PMSM**

The magnets placed in the grooves of the outer periphery of the rotor laminations, providing a uniform cylindrical surface of the rotor.

In addition, this arrangement is much more mechanically robust compared to surface mount machines as the magnets do not protrude out of the rotor laminations as in the case of the synchronous permanent magnet (SPM) and therefore they are fully and mechanically embedded in the rotor giving it mechanical strength from flying out.

Bracing magnets on to the rotor with tapes in the case of SPM with lateral air gaps between magnets does not give the greatest mechanical strength. Whereas in the surface inset PMSM, it is mostly unwarranted and even if it is used, it can be bound uniformly as the rotor lamination and magnet surfaces make a uniform surface unlike that of the SPM. The ratio between the quadrature and direct axes inductances can be as high as 2–2.5 in this machine.

5.6. **Interior PMSM**

The interior PM rotor construction is mechanically robust and therefore suited for high-speed applications. The manufacturing of this arrangement is more complex than the surface mount or inset magnet rotors.

Note that the ratio between the quadrature and direct axes inductances can be higher than that of the inset magnet rotor and generally is the range of three even though there has been claims of much higher ratio for various other interior type PM rotor configurations. The interior PM rotor shown in Figure 17 has steel removed to create large air gaps between the magnets in the rotor. They are intended to discourage the flow of flux between adjacent PMs within the upper rotor surface. Without these air barriers known as flux barriers, the flux will flow from one magnet to the adjacent one within the rotor and thereby bypass the stator structure. It will result in reduced mutual flux linkages, and, therefore, the flux barriers are essential to this arrangement of PMs. The barriers also reduce the weight of the rotor itself thus giving the lowest rotor inertia.

Consequently, it facilitates higher acceleration rates usually required in servo drives. Surprisingly, in spite of this advantage, these machines are seldom used in those applications today. The circumferential inset PM rotor shown in Figure 17 seems to require a large volume of the PMs and, therefore, as such this configuration is not suitable for high energy density PMs since they are expensive. Accordingly, this configuration can only be confined to low energy density and low-cost magnets such as ferrites. Uniquely this configuration bestows a rotor arrangement that can yield a higher air gap flux density than that of the magnets themselves. It is achieved by the fact that the area of cross section of the magnets is much larger than the rotor surface area that conducts the flux from a magnet to the stator.

Because of its higher air gap flux density compared to, say, the surface mount ferrite PMSMs, this configuration is very desirable from the point of view of higher efficiency and smaller stator excitation for the same power output. But higher air gap flux density is achieved at the expense of higher rotor volume compared to that of the rotor with high energy density PMs has to be noted. The inset magnet construction has the advantages of high mechanical robustness and a high ratio between the quadrature and direct axis inductances, respectively. Many more arrangements of the magnets on the rotor are possible and they are very rarely used in general industrial practice and hence they are not considered any further in this review.

5.7. **Radial flux versus Axial Flux PM Machines**

Compared to axial flux PM machines (AFPM), radial flux PM machines (RFPM) are more suitable to integrate in the flywheel of a diesel engine and more robust

Axial and Radial flux machines tend to have the same performance in terms of torque density, torque per mass and efficiency [6].

However, axial flux machines do normally have two rotors or two stators in order to obtain the balance required. The air gap therefore is higher (two air gaps), more magnets mass and also more windage loss [19]. Therefore the cost of AFPM is much higher than that of RFPM also the costs of a RFPM are lower due to its maturity in terms of technology.

COMPARISION BASED ON NUMBER OF COMPONENTS								
	Axial Flux PM 48/16			Radial Flux PM 24/20			Radial Flux PM 24/22	
S.No		QTY	S.No		QTY	S.No		QTY
1	DE ROTOR PLATE	1	1	ROTOR	1	1	ROTOR	1
2	NDE ROTOR PLATE	1	2	STATOR	1	2	STATOR	1
3	11mm MAGNETS	32	3	6mm MAGNETS	20	3	6mm MAGNETS	22
4	Universal Widget	32	4	ADAPTOR PLATE	x	4	ADAPTOR PLATE	x
5	5.1 Spider	2	5	COPPER COILS	xKg	5	COPPER COILS	xKg
	Stator Sub Assembly		6	BALANCE WEIGHT	x	6	BALANCE WEIGHT	x
6	STATOR HALF	2	7	GLUE	x	7	GLUE	x
7	DE STATOR RETAINIG RING	1	8	MAGNET RETAINER	1	8	MAGNET RETAINER	1
8	NDE STATOR RETAINIG RING	1	9	RETAINING	1	9	RETAINING	1
9	COPPER WINDINGS	x Kg	10			10		
10	INSULATION /SLOT LINER	x	11			11		
11	GLUE	x	12			12		
12	Balance weight	x						
13	Bolts	x						
14	Rivets	32						
15								
16								
17	TOTAL COMPONENTS	104		TOTAL COMPONENTS	24		TOTAL COMPONENTS	26

Table 1. Illustrates components based comparison for currently axial PM manufactured by Cummins and the new design based on radial flux technology [40]

5.8. **Exterior versus interior PM machines**

Exterior rotor permanent magnet machine is normally the surface-mount or the inset shown above. The surface mount PM machine has simple structure, so it is widely used in many applications. To reduce the ripple of the air gap flux density, voltage and torque, the varying air gap length is made curving the surface of the magnets to improve [49], [50]. The inset PM machine can be used to improve the reluctance torque in some cases.

The exterior PM machine with buried magnets is rare, because its rotor yoke would be made from iron laminations, it would be weaker in mechanical structure and higher in cost that the solid rotor yoke.

The interior rotor PM machine is used in many application, static part is put externally as a safety measure.

However, for application which require integrating the electric machine in a flywheel, the outer rotor PM machine has the following main advantage in comparison with interior rotor PM machines.

5.9. **Conclusions**

The application requirements decide the type of PM material used due to the cost, size and weight. It very important to consider operating temperature range, external demagnetizing field, weight constraints and space limitation at the design stage itself.

According to the rotor configuration there are two possibilities: inner and outer rotor. The outer rotor solution is well adapted to be integrated since the rotor can be directly fixed to the flywheel. It is also easier to wind the stator since the stator teeth point outwards. Moreover, outer rotor designs are around 15% lighter than an inner rotor machine with the same torque because of their longer air gap diameter. Since the torque of the machine depends on this value squared, the axial length can be reduced with the subsequent weight reduction. However, outer rotor machines may be more difficult to cool in some applications since the windings, which can generate the high losses, are placed in the inner part of the machine.

The inset magnet construction has the advantages of high mechanical robustness and a high ratio between the quadrature and direct axis inductances, for this type of machine, the rotor is mounted outside and the magnets are placed in the internal surface of the rotor. This configuration presents a large rotor diameter allowing a greater number of poles.

Furthermore the above external rotor design is advantageous in terms of cooling arrangement. The way, the axial or centrifugal impellers can be mounted on the rotating rotor, hence compact dimensions, especially in an axial direction, this makes cooling arrangement much simpler and as the circulating air from the fan is also cooling the motor housing.

Conditioned by the cooling arrangement, the external rotor motor can achieve a higher torque (magnet volume, air gap surface, and radius) than the internal rotor motor of the same package length, the same magnet system and the same magnet thickness (reduced magnet volume, reduced air gap surface, smaller radius).

According to [42] the torque of the exterior rotor grows extensively for a large air gap radius r (with a value close to the outer machine radius *R*).

The exterior rotor machine however requires the stator area to be as large as possible, just leaving enough space for the rotor to produce the required magnetic field. In this configuration, the exterior rotor machine could theoretically produce a much higher torque than achievable with the optimal interior rotor setup. For real conditions however, the torque is reduced due to the lowered air gap field in case of magnetic saturation. Thus, the main design task consists in finding the optimum between a high number of ampere-turns and a high air gap field. Many aspects, such as pole pair number, number of stator teeth, shape of stator, current density and, as shown in this paper, the factors cw (winding space factor) and xr (ratio of air gap radius to motor radius) influence the resulting torque.

The interior rotor PM machine is used in many application, static part is put externally as a safety measure. However, for application which require integrating the electric machine in a flywheel, the outer rotor PM machine has the following main advantage in comparison with interior rotor PM machines.

- It’s a compact method to integrate the generator with a flywheel.
- The air gap is larger than that of interior rotor PM machines with the same rated power and volume, so it might allow for a higher torque density.
- Moment of inertia is higher than that of interior rotor PM generator, because of the higher rotor diameter. This is requirements for application in which the PM generators is mounted on the flywheel of the diesel engine.

6. Operating principles of PMSM Machines

Nowadays there are several different topologies of rotating electrical machines. Most rotating machines are normally distinguished according to their direction of the flux field such as radial, axial, and transversal. The majority of machines are still designed basing on the inner-rotor-radial-flux layout, as it is the most established in design, analysis, and production.

The radial permanent magnet motor is maintaining approximately the same torque density and the same outer dimensions as its counterpart machines. For an example, a PM synchronous machine (PMSM) requires a rotor flux field from permanent magnet and a stator carries stator windings flux when supplied with alternating currents.

Its counterpart machines however, the rotor flux field is generated by a field winding. This rotor flux passes the airgap, encircles the stator windings and passes the airgap again back to the rotor backiron where thereby providing the magnetic flux linkage. The flux flows about radially in the machine airgap while the current flow about in the axial direction in the main region of the machine. The radial permanent magnet motor is being increasingly used in industries such as aerospace application, consumer, medical, automotive industries, industrial automation etc [11]. This motor does not use any brushes for commutation; instead, it is electronically commutated and thus it is well known as a brushless permanent magnet motor. This motor exists in single phase and multiphase but the 3-phase motors are most popular and widely used.

Typically the stator of a brushless machine consists of a three phase winding similar to that of induction machine hosted inside the slots of a cylindrical ferromagnetic core. The rotor of the motor includes permanent magnets and a ferromagnetic core that may feature different shapes. The motor characteristics depend on the stator winding and the way magnets are located on the rotor. The PMSM are traditionally classified into two variants basing on the waveform of the back EMFs which reflects the design peculiarities of the machine.

6.1. Mathematical Model of BLAC Machine

BLAC is essentially a three-phase AC motor with sinusoidal back EMF driven by a DC source, which is converted to three-phase alternating currents supplying to the three stator windings of a BLAC by a controller unit such as a vector controlled drive.

In order to drive a BLAC smoothly, a controller shall be designed such that the stator current space vector, which is the sum of the three phase currents, shall be always in the quadrature direction with respect to the rotor and has constant magnitude, irrespective of rotation speed and back EMF frequency.

This results in maximum torque and minimum torque ripple and such model is valid for any instantaneous variation of voltage and current and adequately describes the performance of the machine under both steady-state and transient operation. The operation of vector-controlled drive of any AC supplied motor such as PM synchronous motor is to imitate one of DC motor where the torque and flux are independently controlled by armature and field currents.

The idea of the space vector permits to work with two variables instead of three and the motor can be considered a 2-phase machine.

This technique is based on projections which transform a three phase time and speed dependent system into a two d-q axis coordinates (direct and quadrature) time invariant system known as field oriented frame which reduces the number of equations and simplifies the control design [37]. This field orientated frame controlled machines need two constants as input references: the torque component (q coordinate) and the flux component (d coordinate). The transformation of the three-phase stationary coordinate system to the field oriented frame is made in two steps:

1) A transformation from the three-phase stationary coordinate system to the two-phase stationary coordinate system.

2) A transformation from the two-phase stationary coordinate system to the d-q rotating coordinate system.

These direct and quadrature components are obtained from the three phases variables; a, b and c, through the Park transformation as below [13].

$$\begin{bmatrix} id \\ iq \\ io \end{bmatrix} = \frac{2}{3} \begin{bmatrix} \cos(\theta) & \cos(\theta - \frac{2\pi}{3}) & \cos(\theta + \frac{2\pi}{3}) \\ \sin(\theta) & \sin(\theta - \frac{2\pi}{3}) & \sin(\theta + \frac{2\pi}{3}) \\ 1/2 & 1/2 & 1/2 \end{bmatrix} \begin{bmatrix} ia \\ ib \\ ic \end{bmatrix} \quad \text{Eq.4}$$

Vice versa; a, b and c components are obtained from the direct and quadrature variables through the inverse of the Park transformation as defined below:

$$\begin{bmatrix} ia \\ ib \\ ic \end{bmatrix} = \begin{bmatrix} \cos(\theta) & \sin(\theta) & 1 \\ \cos(\theta - 2\pi/3) & \sin(\theta - 2\pi/3) & 1 \\ \cos(\theta + 2\pi/3) & \sin(\theta + 2\pi/3) & 1 \end{bmatrix} \begin{bmatrix} id \\ iq \\ io \end{bmatrix} \quad \text{Eq.5}$$

The principal operation of PMSM is similar to the traditional synchronous motor operation. The different is that the electrically excited field winding is replaced by the permanent magnets. The representation of the machine in d and q axis is developed by analyzing the armature winding on the stator and the permanent magnet rotor.

Each winding coil and the magnet are considered to produce flux density distribution in the air gap, which are perfectly sinusoidal functions at the space angle θ. The direct axis component of the armature flux, Φ_{ad} is produced by id and has the same direction as the magnet flux Φ_m whereas the quadrature component of the armature flux Φ_{aq} is produced by i_q.

The voltage equation for the quadrature and direct axis can be written as;

$$Vq = Riq + \frac{d\lambda q}{dt} + \omega e \lambda \mathrm{m} + \omega e \lambda \mathrm{d} \quad \text{Eq.6}$$

$$Vd = Rid + \frac{d\lambda d}{dt} - \omega e \lambda \mathrm{q} \quad \text{Eq.7}$$

Where,

Vd and Vq: the d and q axis voltages

λd λq: d and q axis armature flux linkages

λm: flux linkage due to the permanent magnet rotor linking the stator

id and iq: d and q axis armature current

R: the stator resistance

ωe: Electrical angular frequency

The term $\frac{\mathrm{d}\lambda \mathrm{d}}{\mathrm{dt}}$ simply represents the induced voltage associated with quadrature inductance Lq, which has equivalent equation relationship as $\frac{\mathrm{d}\lambda \mathrm{q}}{\mathrm{dt}} - \frac{\mathrm{dLq}}{\mathrm{dt}}$ x iq. The term ωm λm is the motional EMF induced by the magnet flux normally referred to as E and the term ωm λd is the speed EMF by the armature in the d axis flux.

Thus,

$$\mathrm{Vq} = \mathrm{Riq} + \frac{\mathrm{d}\lambda\mathrm{q}}{\mathrm{dt}} + \mathrm{E} + \omega\mathrm{m}\lambda\mathrm{d} \qquad \text{Eq.8}$$

By substituting $\omega\mathrm{m}\lambda\mathrm{m}$ for E

The term $\frac{\mathrm{d}\lambda\mathrm{d}}{\mathrm{dt}}$ simply represents the induced voltage associated with the direct axis inductance Ld, which has equivalent equation relationship $\frac{d\lambda q}{dt} - \frac{dLq}{dt}$ x iq. However all the components $\frac{\mathrm{d}\lambda}{\mathrm{dt}}$ represent transient terms only and during the steady state condition, $\frac{\mathrm{d}\lambda}{\mathrm{dt}} = 0$ and the above equations can be simplified as below:

$$Vq = Riq + E + \omega e\lambda\mathrm{d} \qquad \text{Eq.9}$$

$$Vd = Rid - \omega e\lambda\mathrm{q} \qquad \text{Eq.10}$$

Where V is the resultant voltage $V = \sqrt{Vd^2 + Vq^2}$) Eq.11

And i is the resultant current $\mathrm{i} = \sqrt{\mathrm{id}^2 + \mathrm{iq}^2}$ Eq.12

The electromagnetic torque can be found directly from the total input power to the machine, Pin, in the a, b and c components;

$$\mathrm{Pin} = \mathrm{Va\ ia} + \mathrm{Vb\ ib} + \mathrm{Vc\ ic} \qquad \text{Eq.13}$$

While in direct and quadrature axis components, the total input power will be:

$$\mathrm{Pin} = 3\ (\mathrm{Vd\ id} + \mathrm{Vq\ iq})/2 \qquad \text{Eq.14}$$

By substituting for Vd and Vq equations into equations (above) respectively;

$$Pin = 3\ [(Rid - \omega e\ \lambda\mathrm{q})\ \mathrm{id} + (Riq + E + \omega e\ \lambda\mathrm{d})\mathrm{iq}\ ]/2 \qquad \text{Eq.15}$$

By assuming that the voltage across resistance is small compare to the E and voltage produced from the flux linkage value, the equation shall be simplified as below:

$$Pin = 3\,[Eiq - \omega e\,\lambda q\,\mathrm{id} + \omega e\,\lambda d\,\mathrm{iq}\,]/2 \qquad \text{Eq.16}$$

Finally, the total electromagnetic torque is defined as the total input power to the machine divided by the motor's mechanical speed which is, $= \frac{P_{in}}{\omega_m}$. Thus, the total electromagnetic torque equation is as below where rotor mechanical speed and electrical angular frequency ωm is related as ωe = P ωm with number of pole pairs P.

$$Te = 3\left(\frac{E_{iq}}{\omega_m} - P\,\lambda q\,\mathrm{id} + P\,\lambda d\,\mathrm{iq}\right)/2 \qquad \text{Eq.17}$$

By substituting the $\lambda d = \mathrm{Ld\,id}$ and $\lambda q = \mathrm{Lq\,iq}$ into the total electromagnetic torque equation below:

$$Te = 3\left(\frac{E_{iq}}{\omega_m} - PL_q\,i_q\,i_d + PL_d\,i_d\,i_q\right)/2 \qquad \text{Eq.18}$$

As i_d is set to be zero, then

$$\mathrm{T_{E=}}\ 3\left(\frac{\mathrm{Ei_q}}{\omega_\mathrm{m}}\right)/2 \qquad \text{Eq.19}$$

$$or \quad \mathrm{T_{E=}}\ 3\ \mathrm{P}\left(\frac{\mathrm{Ei_q}}{\omega_\mathrm{e}}\right)/2 \qquad \text{Eq.20}$$

Since $\frac{E}{\omega_\mathrm{m}}$ is equivalent to the magnetic flux linkage which is a constant waveform with respect to the rotor position, thus, the torque is directly dependent to the quadrature axis current. Then, the above shall be represented as per equation below:

$$\mathrm{T_e} = \mathrm{K_t i_q} \qquad \text{Eq.21}$$

Where

$$K_t = 3\,P\,\frac{\left(\frac{E}{\omega_e}\right)}{2}/2 \qquad \text{Eq.22}$$

The electromagnetic torque value also appears in the mechanical equation of the machine, therefor the mechanical torque dynamics equation is described below:

$$T_e = J\,\frac{d\omega_m}{dt} + B\omega_M + T_L \qquad \text{Eq.23}$$

Where, TL is the external load torque, J is the motor shaft inertia and B is the damping coefficient of viscous friction.

11] [**BLAC** (brushless AC or PM synchronous): sinusoidally excited and sinusoidal back-EMF as shown below:

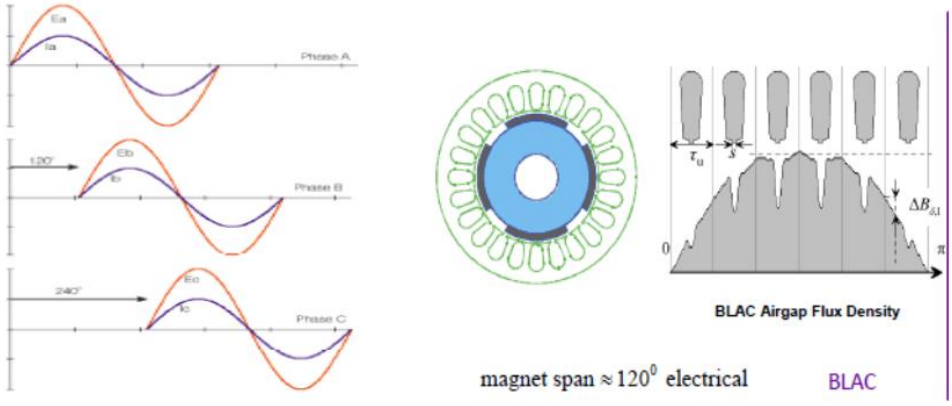

Figure 18. Brushless AC sinusoidally exited and sinusoidal back-EM [9]

6.2. **BLDC Operation**

A BLDC motor rotates as a result of the interaction of its permanent magnet field at the rotor with a magnetic field generated when a DC voltage is connected across a set of its stator coils. To maintain rotation, the orientation of the stator magnetic field in the stator has to be rotated sequentially. Moreover, in order to deliver a higher power and torque which is ideally free from ripple, the desired rectangular AC wave back EMF and current would be preferred.

Each phase current should be switched corresponding to machine back EMF as a function of the rotor position. At each rotor position, a constant current multiplies the constant part of the back EMF which the sum of the product produces the output power of the machine. Thus, in order to maintain synchronization with the rotating stator magnetic field and identify the commutation sequence for the above purpose, the rotor position must be known at fixed angular intervals.

The rotor position could be identified by the use of position sensors such as encoder, resolver or Hall sensors which could detect the position of the rotor field, and hence the position of the rotor shaft. The current commutation from one phase to the other phase corresponding to that particular state of the back EMF is synchronized by these position sensors. For Hall position sensors, three sensors are used to determine each back EMF and hence the position of the rotor field. These particular Hall position sensors generate a logic high signal that goes low when the corresponding back EMF starts falling and remains low till that back EMF starts rising.

6.3. **Mathematical Model of BLDC Motor**

A simple three-phase two-pole star connected BLDC motors and a 1-phase equivalent circuit schematic is shown in figure below.

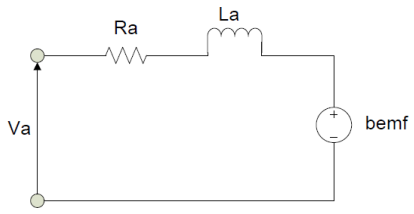

Figure 19. Illustrates one phase equivalent circuit [48]

The circuit equations of the three windings in phases are [37];

$$V_{a=\,R_a}\, i_a + \frac{d\Psi_a}{dt} \qquad \text{Eq.24}$$

$$V_{b=\,R_b}\, i_b + \frac{d\Psi_b}{dt} \qquad \text{Eq.25}$$

$$V_{c=\,R_c}\, i_c + \frac{d\Psi_c}{dt} \qquad \text{Eq.26}$$

Where

R_a, R_b, R_c: Winding Resistances of each phase in ohm, Ω

V_a, V_b, V_c: Phase voltages on motor winding in volt, V

i_a, i_b, i_c: Phase currents in ampere, A

ψ_a, ψ_b , ψ_c :Flux linkages of each phase in weber, Wb

The flux linkages for each phase are defined as follows:

$$\Psi_a = L_a i_a + L_{ab} i_b + L_{ac} i_c + \Psi_{am} \quad \text{Eq.27}$$

$$\Psi_b = L_b i_b + L_{ba} i_b + L_{bc} i_c + \Psi_{bm} \quad \text{Eq.28}$$

$$\Psi_c = L_c i_c + L_{ca} i_a + L_{cb} i_b + \Psi_{cm} \quad \text{Eq.29}$$

Where

L_a, L_b Lc: Self-inductance of each phase in Henry, H

L_{ab}, L_{ac}, L_{ba}, L_{bc}, L_{ca} L_{cb}: Mutual inductances of between phases in Henry, H

Ψ_{am}, Ψ_{bm}, Ψ_{cm}: Flux linked with each phase due to the permanent magnet at each phase in weber, W_b.

From the above two series of equation, the matrix form can be written as follows:

$$\begin{bmatrix} Va \\ Vb \\ Vc \end{bmatrix} = \begin{bmatrix} Ra & 0 & 0 \\ 0 & Rb & 0 \\ 0 & 0 & Rc \end{bmatrix} \begin{bmatrix} ia \\ ib \\ ic \end{bmatrix} + \frac{d}{dt} \begin{bmatrix} La & Lab & Lac \\ Lba & Lb & Lbc \\ Lca & Lcb & Lc \end{bmatrix} + \frac{d}{dt} \begin{bmatrix} \Psi am \\ \Psi bm \\ \Psi cm \end{bmatrix} \quad \text{Eq.30}$$

The rate of change of the flux linkages established by the permanent magnet at each phase is equal to the induced back EMF in the winding. By assuming that there is no change in the rotor

reluctances, then the self and mutual inductances of every phase will be similar respectively. It is also assumed that the winding resistances are equal.

Hence the above equation can be written as:

$$\begin{bmatrix} Va \\ Vb \\ Vc \end{bmatrix} = \begin{bmatrix} R & 0 & 0 \\ 0 & R & 0 \\ 0 & 0 & R \end{bmatrix} \begin{bmatrix} ia \\ ib \\ ic \end{bmatrix} + \frac{d}{dt} \begin{bmatrix} L & M & M \\ M & L & M \\ M & M & L \end{bmatrix} \begin{bmatrix} ia \\ ib \\ ic \end{bmatrix} \begin{bmatrix} ea \\ eb \\ ec \end{bmatrix} \qquad \text{Eq.31}$$

The sum of the currents in the three phases, connected in star configuration with no neutral equals to zero.

ia = -ib -ic

Therefore, the equation 31 may be written as below:

$$\begin{aligned} L\ \frac{d_{\mathrm{ia}}}{dt} + M\ \frac{d_{\mathrm{ib}}}{dt} + M\ \frac{d_{\mathrm{ic}}}{dt} &= L\ \frac{d_{\mathrm{ia}}}{dt} + M\ \left\{\frac{d_{\mathrm{ib}}}{dt} + \frac{d_{\mathrm{ic}}}{dt}\right\} \\ &= L\ \frac{d_{\mathrm{ia}}}{dt} + M\ \left\{\frac{d_{\mathrm{ia}}}{dt}\right\} \\ &= L - M\ \frac{d_{\mathrm{ia}}}{dt} \end{aligned}$$

Similarly

$$\begin{bmatrix} Va \\ Vb \\ Vc \end{bmatrix} = \begin{bmatrix} R & 0 & 0 \\ 0 & R & 0 \\ 0 & 0 & R \end{bmatrix} \begin{bmatrix} ia \\ ib \\ ic \end{bmatrix} + \frac{\mathrm{d}}{\mathrm{dt}} \begin{bmatrix} L-M & 0 & 0 \\ 0 & L-M & 0 \\ 0 & 0 & L-M \end{bmatrix} \begin{bmatrix} ia \\ ib \\ ic \end{bmatrix} + \begin{bmatrix} \mathrm{ea} \\ \mathrm{eb} \\ \mathrm{ec} \end{bmatrix} \qquad \text{Eq.32}$$

The above differential equation may be put in canonical form by multiplying by the inverse inductance matrix, L^{-1}.

$$\frac{\mathrm{d}}{\mathrm{d_t}} \begin{bmatrix} ia \\ ib \\ ic \end{bmatrix} = -L^{-1}\ R \begin{bmatrix} 1 & 0 & 0 \\ 0 & 1 & 0 \\ 0 & 0 & 1 \end{bmatrix} + -L^{-1}\ R \begin{bmatrix} Va \\ Vb \\ Vc \end{bmatrix} + -L^{-1}\ R \begin{bmatrix} \mathrm{ea} \\ \mathrm{eb} \\ \mathrm{ec} \end{bmatrix} \qquad \text{Eq.33}$$

The electromagnetic torque is given by following equation:

$$\mathrm{T_e} = \frac{\mathrm{e_a\, i_a}\ \mathrm{e_b\, i_b}\ \mathrm{e_c\, i_c}}{\omega_{\mathrm{m}}} \qquad \text{Eq.34}$$

Or by using the expression of co-energy [31];

$$T_e = \frac{P}{2} \frac{\delta W_c\ (\theta_{re})}{\delta \theta_r} \quad \text{Eq.35}$$

Where P, W_c and θ_{re} are the number of poles, co-energy and electrical rotor position respectively.

$$W_c(\theta_{re}) = \frac{1}{2} \quad [i_a i_b i_c]\, L \begin{bmatrix} i_a \\ i_b \\ i_c \end{bmatrix} + [i_a i_b i_c] \begin{bmatrix} \Psi_m \sin\theta_{re} \\ \Psi_m \sin\theta_{re} - 2\pi/3 \\ \Psi_m \sin\theta_{re} + 2\pi/3 \end{bmatrix} + W_{pm} \quad \text{Eq.36}$$

For surface-mounted PM machines, the direct and quadrature axis inductances are approximately equal, thus the inductance matrix, L and the energy stored in the permanent magnet, Wpm are not functions of θ_r [41].

Therefore;

$$T_e = \frac{P}{2} \frac{\delta W_c\ (\theta_{re})}{\delta \theta_r} = \frac{P}{2} \quad [i_a i_b i_c] \frac{\delta}{\delta \theta_r} \begin{bmatrix} \Psi_m \sin\theta_{re} \\ \Psi_m \sin\theta_{re} - 2\pi/3 \\ \Psi_m \sin\theta_{re} + 2\pi/3 \end{bmatrix} \quad \text{Eq.37}$$

$$T_e = \frac{P}{2} \frac{\delta W_c\ (\theta_{re})}{\delta \theta_r} - \frac{P \Psi_m}{2} \quad \left[i_a cos\theta_{re} + i_b \cos\left(\theta_{re} - \frac{2\pi}{3}\right) + i_c \cos(\theta_{re} + \frac{2\pi}{3}\right] \quad \text{Eq.38}$$

The mechanical equation is as below:

$$T_e = j \frac{d\omega_m}{dt} + B\omega_m + T_L \quad \text{Eq.39}$$

The mechanical differential equations shall be derived by equating the above two equations (38) and (39)

$$T_e = \frac{P}{2} \frac{\delta W_c\ (\theta_{re})}{\delta \theta_r} = j \frac{d\omega_m}{dt} + B\omega_m + T_L \quad \text{Eq.40}$$

$$\frac{d\omega_{\mathrm{m}}}{dt} = \frac{P}{2j}\frac{\delta W_c\ (\theta_{re})}{\delta\theta_r} - \frac{B}{j}\ \omega_{\mathrm{m}} - \frac{1}{j}\ \mathrm{T_L} \qquad \text{Eq.41}$$

$$\frac{d\theta_{\mathrm{rm})}}{dt} = \omega_{\mathrm{m}} \qquad \text{Eq.42}$$

By using the conversion of electrical-mechanical angular speed and displacement relationship as below, the mechanical differential equations are described below;

$$\omega_{\mathrm{rm}} = \frac{2}{P}\ \omega_{\mathrm{re}} \ \text{ and } \ \theta_{\mathrm{rm}} = \frac{2}{P}\ \theta_{\mathrm{re}}$$

$$\frac{2}{P}\ \frac{d\omega_{\mathrm{re}}}{dt} = \frac{P}{2\mathrm{J}}\frac{\delta W_c}{\delta\theta_{re}} - \frac{B}{\mathrm{J}}\frac{2}{P}\omega_{\mathrm{rm}} - \frac{1}{\mathrm{J}}\ \mathrm{T_L}$$

$$\frac{d\omega_{\mathrm{re}}}{dt} = \frac{P^2}{2\mathrm{J}}\frac{\delta W_c}{\delta\theta_{re}} - \frac{B}{\mathrm{J}}\omega_{\mathrm{rm}} - \frac{P}{2\mathrm{J}}\ \mathrm{T_L}$$

$$\frac{d\theta_{\mathrm{re})}}{dt} = \omega_{\mathrm{re}} \qquad \text{Eq.43}$$

[11] **BLDC** (brushless DC): square wave excited and trapezoidal back-EMF also known as Trapezoidal PM motors.

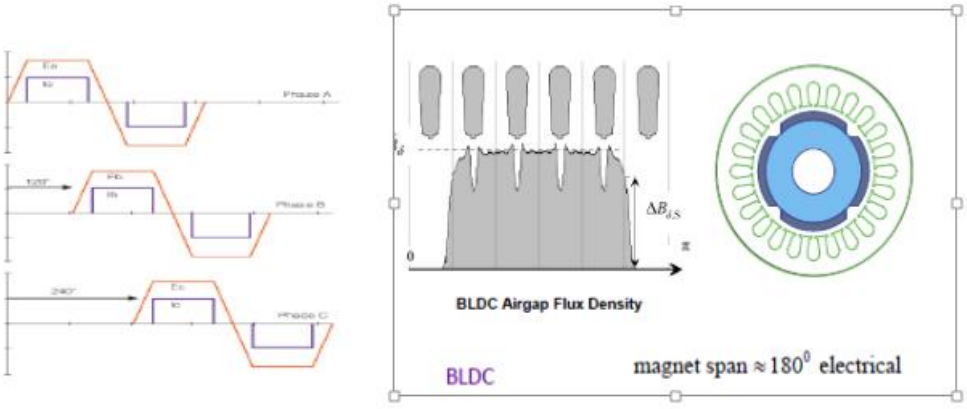

Figure 20. Brushless DC square wave excited and trapezoidal back-EMF [9]

BLDC motors are also fed from a multi-phase supply (generally three phases – and shifted by 120^0 one from another) but these wave shapes rectangular BLAC are rectangular. Only two phase windings out of three conducts current simultaneously. Such a control scheme (electronic commutation) is functionally equivalent to the mechanical commutation in D.C. machines.

7. Design procedure

7.1. Main equations and the starting process of the design

Shaping Coefficient: The ratio of the diameter of the rotor D_{ir} to the length of the rotor l_r

$$k_{SH} = D_{ir} / l_r \quad \text{Eq.44}$$

Air gap sheer stress σ (tangential force) per unit area: $\sigma_{m\,is}$ the value of the sheer stress that a permanent magnet material can suffer, magnet **$\sigma_{m\,is}$** around 20 to 50 Kpa and the safety factor is equal to 2/3.

$$\sigma = \frac{0.5\ T_e}{\frac{\pi}{4}\ D_{ir}{}^2 / l_r} = \frac{\sigma_m}{k_{safe}} \quad \text{Eq.45}$$

Interior rotor diameter D_{ir}:

$$D_{ir} = \sqrt[3]{\frac{2\ T_e\ k_{sh}}{\pi\sigma}} \quad \text{Eq.46}$$

Length of the rotor:

$$l_r = D_{ir} / k_{SH} \quad \text{Eq.47}$$

Magnet length in the radial direction:

$$l_m = \frac{\mu_{rm}\ g_{eff}}{B_r / B_{g.0} - 1} \quad \text{Eq.48}$$

Magnet Width:

$$w_m = k_m \frac{\pi\ D_{ir}}{2_p} \quad \text{Eq.49}$$

Tooth Width:

$$w_t = \frac{\phi_{t1}}{l_s\ B_{t1}} \quad \text{Eq.50}$$

Slot Opening:

$$b_s = 2\ g \qquad \text{Eq.51}$$

Stator Yoke width:

$$\mathrm{h_{sy}} = \mathrm{B_{g.0}\ w_m / \left(2\ B_{sy}\right)} \qquad \text{Eq.52}$$

Number of phases:

$$N_w = \frac{U_1}{\sqrt{2}\ K_{w1}\ w_m\ B_{g1}\ l_s\ r_s} \qquad \text{Eq.53}$$

Diameter of copper wiring:

$$A_{cu} = \frac{I_1}{J}$$

$$d_{cu} = 2\sqrt{\frac{A_{cu}}{\pi}} \qquad \text{Eq.54}$$

Average length of a turn:

$$I_{cu} \simeq\ 2\ (l_s + \frac{\pi}{2}\ \frac{T_s\ +\ W_t}{2}) \qquad \text{Eq.55}$$

Slot top width:

$$w_{s2} = \frac{\pi\ (D_s - 2h_0 - 2h_1\ )}{Q} - w_t \qquad \text{Eq.56}$$

Slot area:

$$A_{slot} = \frac{2\ N_c\ A_{CU}}{K_{fill}} \qquad \text{Eq.57}$$

Slot bottom width:

$$w_{s1} = \sqrt{w_{s2}^2 - 4\pi \frac{A_{slot}}{Q}} \quad \text{Eq.58}$$

Slot Height:

$$h_s = \frac{2\,A_{slot}}{w_{s1} + w_{s2}} \quad \text{Eq.59}$$

Rotor yoke thickness:

$$h_{ry} = \frac{B_{g,0}\ W_m}{2\,B_{ry}} \quad \text{Eq.60}$$

7.2. **Winding arrangement**

The winding arrangement of an electrical machine determines the configuration of the coils in the stator. Coils can be placed in the air gap or in the slots around a tooth in the stator. The placement of the coil can concentrate in one slot or can be distributed over several slots when a slotted designs or around the air gap circumference when it comes to a slotless design. When a slotted construction is considered, the number of slots and the poles can still wary. [23] The traditional distributive wound machine, the minimum number of slots for three-phase 20-pole machine would be 60. This results in a machine with large end winding length, low copper packing factor, and with windings highly coupled both physically and magnetically. Going for a concentrated wound motor, having the number of slots close to the number of poles is inductive to a high fundamental coil pitch factor, as well as a high-frequency low-magnitude cogging torque. The main disadvantage of these types of windings is the high harmonic content of the stator MMF.

The key benefit of concentrated is the elimination of end winding length leading to lower copper loss, decreased changes of phase to phase fault and reduced axial length of the machine [3-6]'.Concentrated windings also leads to a substantial increase in slot fill factor if the stator is wound using methods illustrated below.

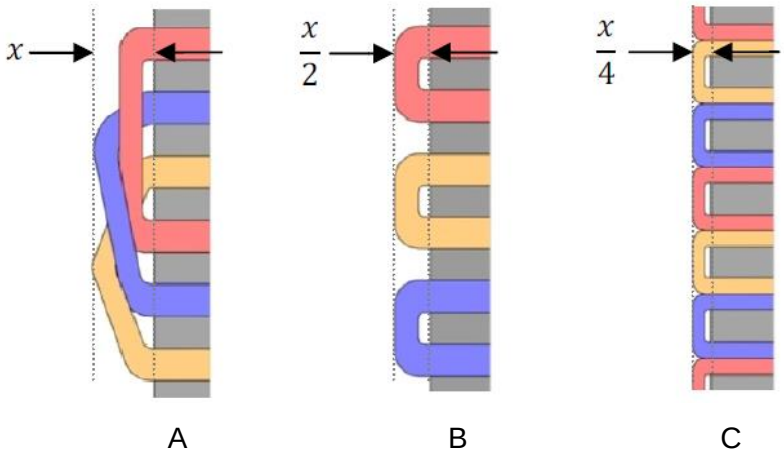

Figure 21. Side sectional showing end windings lengths of (A) Single-layer distributed winding (B) Single-layer concentrated winding (C) Double layer concentrated winding [47].

7.3. **Fractional slots/pole and the pitch factor**

The basic idea of “pitch factor” is to measure the effectiveness of a coil or winding in producing or linking flux, relative to that of a “full-pitch” coil. The fundamental pitch factor of a coil is the ratio

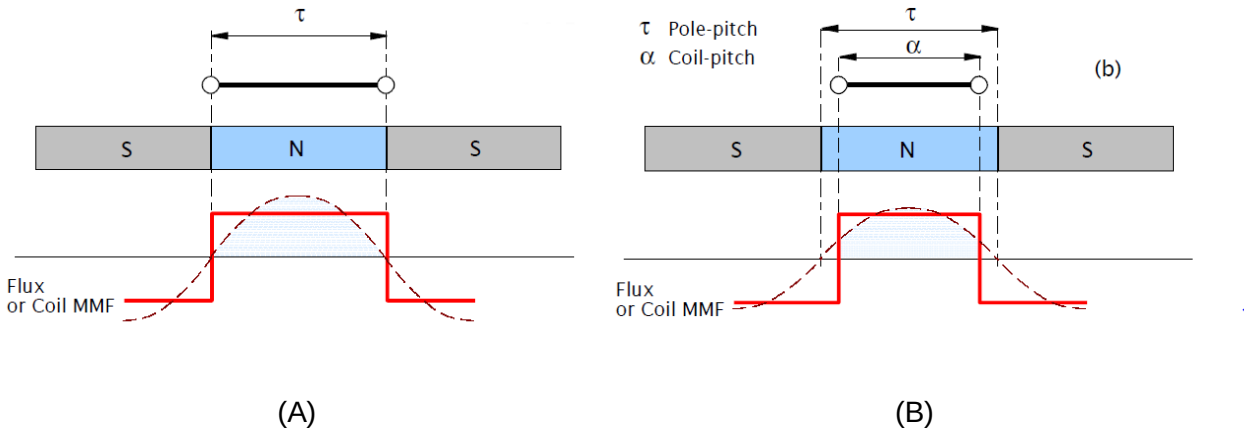

Figure 22. Illustrates Pitch Factor (A) full-pitch coil and an array of full-pitch magnets and (B) short-pitched factor coil having a span $\alpha < \tau$ together with its fundamental component [22]

$$Kp_1 = \frac{\text{Fundamental MMF produced by the coil}}{\text{Fundamental MMF produced by the full pitch coil}} \quad \text{Eq.61}$$

This definition can be shown below to be identical to

$$Kp_1 = \frac{\text{Fundamental flux linked coil}}{\text{Fundamental flux linked by the full-pitch coil}} \qquad \text{Eq.62}$$

Figure 21 above shows a full-pitch coil and an array of full-pitch magnets which are included to define the pole pitch each magnet spans exactly 180 electrical degrees. The coil has a span t = 180º and produces the MMF distribution shown by the solid line. The fundamental of this MMF wave is shown by the dashed line by the well-known Fourier analysis of a square wave, its amplitude is 4/π times the amplitude of the rectangular wave and figure 22 (B) above shows a short-pitched coil having a span together with its fundamental component.

The fundamental pitch factor is given by:

$$K_{P1} = \frac{\int_{-\alpha/2}^{\alpha/2} 1\, Cos_\theta \, d_\theta}{\int_{-t/2}^{t/2} 1\, Cos_\theta \, d_\theta} \; sin = \frac{\alpha}{2} \qquad \text{Eq.63}$$

For example, a coil with a span of 150° has a fundamental pitch factor K_{P1} = sin 75° =0.966.

The pitch factor can be extended to include harmonics. For the *n*'th harmonic we have

$$K_{Pn} = \frac{\int_{-\alpha/2}^{\alpha/2} 1 \; Cos\, n_\theta \; d_\theta}{\int_{-t/2}^{t/2} 1\, Cos\, n_\theta d_\theta} \; sin = \frac{n\,\alpha}{2} \qquad \text{Eq.64}$$

Note that K_{P1}= 0, If $\frac{n\,\alpha}{2}$ = 180°. For example, if α = 150° and n = 5, K_{P5} = 0. A coil with a span or pitch of 150° produces no 5th harmonic MMF and therefore it produces no 5th harmonic flux. It also links no 5th harmonic flux produced by the magnet. Similarly a coil with a span of 120° produces no 3rd harmonic MMF and links no 3rd harmonic flux.

The denominator of this expression represents the pitch-factor of the winding that would result if all the coils had a span of 180° and were concentrated together with the same MMF axis.

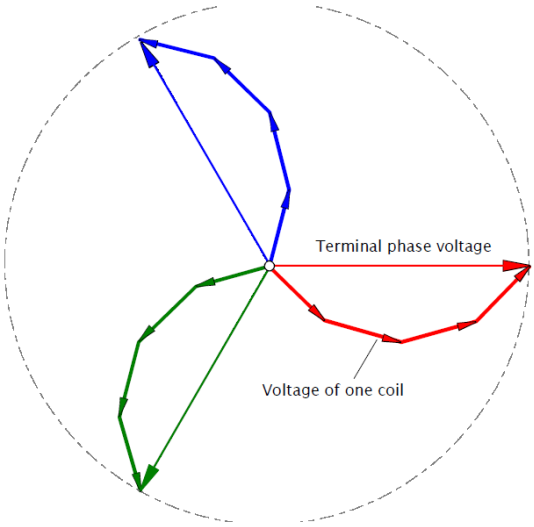

Figure 23. Illustrates addition of EMF's, composition factor for any harmonic [22]

The number of zones will be 2*pm*. The number of slots for each zone is expressed in terms *q*, as a number of slots per pole and phase;

$$q = \frac{Q}{2pm}\,\frac{z}{n} \qquad \text{Eq.66}$$

m: number of phases

z: numerator of q

n: denominator of q, reduce to the lowest term.

	1st-Grade	2nd-Grade	2nd-Grade
Denominator, n	Odd	Even	Even
t	p/n	$2p/n$	$2p/n$
Layer	One or two	One	Two
Q^*	Q_s/t	$2 \cdot Q_s/t$	Q_s/t
p^*	n	n	$n/2$
t^*	1	2	1

Table 2 winding definitions [33]

A variable *t* is needed to calculate other values as e.g. *Q** and *p*. Q** is the number of slots in asymmetrical base winding. *p** is the number of poles in a symmetrical base-winding. *t** is the number of base windings in a stator winding. In integrals slot windings q is an integer. However q can also be a fraction. In this case, the winding is called a fractional slot. The phase zones are distributed symmetrically to different phase winding so that the phase zones U.V and W are positioned on the periphery of the machines at equal distances in electrical degrees.

$$\frac{360\,p}{Q} \qquad \text{Eq.67}$$

The phasors are numbered from 1…to *Q** so that the phasor number 2 is placed to 360·*p*/*Q** electric degrees, now 150° electric degrees (24/20) and 165° electric degrees (24/22), from the phasor 1 and so on.

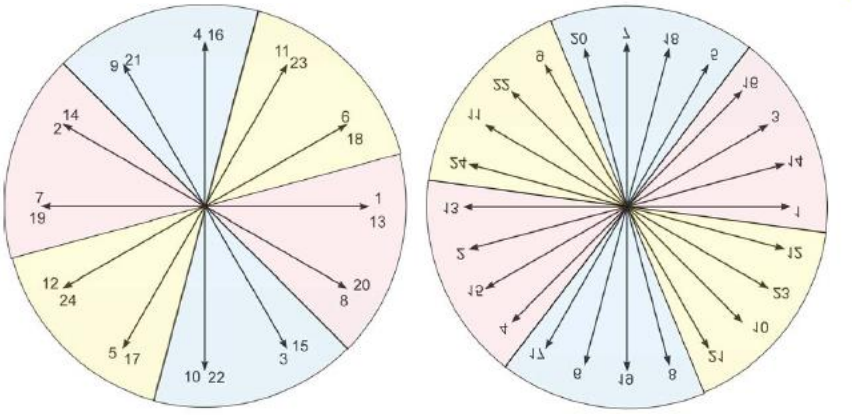

(A) (B)

Figure 24. Illustrates Coil EMF phasor diagram (A) 24 slots 20 pole, (B) 24 slots 22 pole for fractional double slot layer windings [23]

Conductor slot locations 24/20					Conductor slot locations 24/22				
Slot #	PhaseA	PhaseB	PhaseC	Total	Slot #	PhaseA	PhaseB	PhaseC	Total
1	15	0	0	15	1	-30	0	0	30
2	0	-7.5	0	-7.5	2	30	0	0	30
3	0	7.5	0	7.5	3	-30	0	0	30
4	0	0	7.5	7.5	4	15	-15	0	30
5	0	0	-7.5	-7.5	5	0	30	0	30
6	15	0	0	15	6	0	-30	0	30
7	-15	0	0	-15	7	0	30	0	30
8	0	7.5	0	7.5	8	0	-15	15	30
9	0	-7.5	0	-7.5	9	0	0	-30	30
10	0	0	-7.5	-7.5	10	0	0	30	30
11	0	0	7.5	7.5	11	0	0	-30	30
12	-15	0	0	-15	12	-15	0	15	30
13	15	0	0	15	13	30	0	0	30
14	0	-7.5	0	-7.5	14	-30	0	0	30
15	0	7.5	0	7.5	15	30	0	0	30
16	0	0	7.5	7.5	16	-15	15	0	30
17	0	0	-7.5	-7.5	17	0	-30	0	30
18	15	0	0	15	18	0	30	0	30
19	-15	0	0	-15	19	0	-30	0	30
20	0	7.5	0	7.5	20	0	15	-15	30
21	0	-7.5	0	-7.5	21	0	0	30	30
22	0	0	-7.5	-7.5	22	0	0	-30	30
23	0	0	7.5	7.5	23	0	0	30	30
24	-15	0	0	-15	24	15	0	-15	30

Table 3 illustrates conductor slot locations

7.4. **Coil placement**

Placing coils in the air gap leads to slotless design. By doing this, the air gap length between stator and rotor will increase and the reluctance seen by the magnets will increase, which leads to a decrease in flux density. Additional PM material or copper windings are needed to compensate for the decrease in flux density. A slotless design has less steel and therefore less hysteresis and eddy current losses.

7.5. **Coil Winding Distribution**

In slotted stator, the windings can be placed as concentrated coils around the teeth or the winding can be distributed in the slots. According to [FIR 08] concentrated coil constructions have the advantage of the higher winding factor; this increases the amplitude of the induced output voltage. Less copper is needed, due to shorter end windings. These are also easier to manufacture. The disadvantage of concentrated winding is the increase of harmonic component in the air gap flux. This causes an increase of losses in the rotor magnets and back iron due to the eddy current losses.

7.6. **Air gap flux density**

Increasing the air gap flux density increases the force generated. The amount of flux density improvement achievable is limited by the ability of the stator teeth to pass the flux without excessive saturation. Any increase in the flux density requires an increase in the PC of the magnetic circuit or the use of a magnet with a higher remanence. Increasing the PC implies increasing the magnet length or decreasing the effective air gap length. In addition, decreasing the air gap length increases the cogging force.

7.7. **Slot pole combination**

The combination of the number of the stator slots and the number of magnet that can be used in electrical machines design are countless. Therefore the choice of slot pole combinations needs to be based on detailed analysis. The number poles should be inversely proportional to the maximum speed of rotation. The reason for the above is to limit the commutation frequency to avoid excessive switching losses in the transistors and iron losses in the stator [10]. Every time the number of poles is doubled the required thickness of rotor yoke or back iron is reduced by one half, as is the thickness of the stator yoke [10]. As the number of the poles increases, the stator ampere-conductors per pole decrease in inverse proportion, so that the per-unit inductance and synchronous reactance decrease in motors of higher pole number. As the number of poles goes up, the copper packing factor is reduced if the number of slots per pole per unchanged, in order to reduce the number of slots and maximise the slot fill factor, as well as to achieve necessary isolation between phase windings. The number of poles was chosen as a compromise between the restriction of the electrical supply frequency and the minimum rotor internal diameter.

7.8. **Rotor Radius**

For a given torque, magnetic and electric loading, and the machine length the overall machine rotor diameter can be determined as follows [11];

$$T = \frac{\pi}{2} \; B \; \Delta I \; L \qquad \text{Eq.68}$$

B is called magnetic loading (T),

ΔI is called electrical loading A/M

L is motor length and R is rotor radius

Therefore the rotor radius is given:

$$R_r = \sqrt{\frac{T}{2\pi * B * \Delta I * L}} \quad \text{Eq.69}$$

7.9. **Magnet thickness**

Permanent magnet used in PM motors is magnetized and has a remaining remanent flux density and responds to a normal hysteresis characteristic. The useful portion of a magnet in PM operation is in the second quadrant of the hysteresis loop and is usually called the demagnetization curve of the magnet. It represents the relationship between B and H of the magnet once it has been magnetized. Typical demagnetization curve for permanent magnet is shown in figure below.

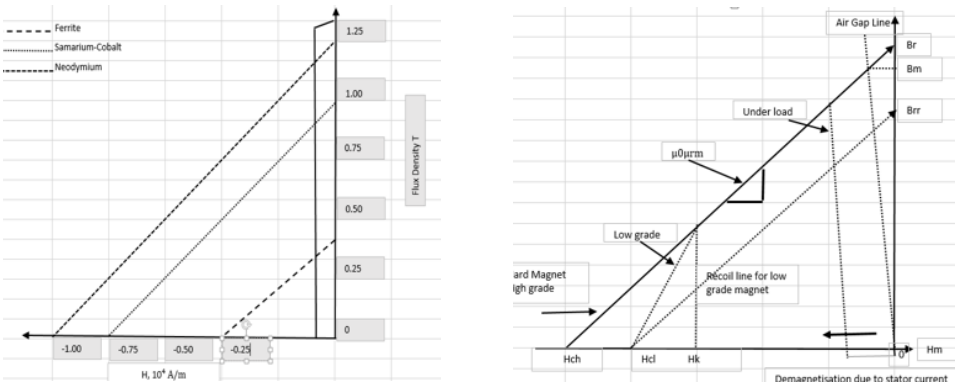

(A) (B)

Figure 25. Illustrates (A) Second quadrant BH characteristics (B) Operating points of magnets [24]

To find the operating point on the demagnetization characteristics of the magnet consider the flux path in the machine. The flux crosses from the north pole of the rotor magnet to stator through an air gap and then closes the flux path from stator to the rotor south pole, via air gap. In the process, the flux crosses two times the magnet length and two times the air gap.

$$H_m \; l_m + \; H_g \;\; l_g = 0 \quad \text{Eq.70}$$

Where

H_m: The magnetic field intensities of the permanent magnet

H_g: The magnetic field intensities of the air gap.

l_m: The lengths of the magnetic paths in the permanent magnet or magnet thickness

l_g: The lengths of the magnetic paths in the air gap

Am: The cross-sectional areas of the permanent magnet

$$H_m\, l_m + \frac{B_m}{\mu_o} * L_g = 0 \qquad \text{Eq.71}$$

$$H_m = -\frac{B_m}{\mu_o} * \frac{L_g}{L_m} \qquad \text{Eq.72}$$

The equation for the linear section at the second quadrant of the B and H characteristic is:

$$\mathrm{B_m} = \mu_o * \mu_{rec} * \mathrm{H_m}\ \mathrm{B_r} \qquad \text{Eq.73}$$

$$\mathrm{B_m} = -\frac{\mu_o\ \mu_{rec}}{\mu_o} * \frac{\mathrm{L_g}}{\mathrm{L_m}} * \mathrm{B_m}\ \mathrm{B_r} \qquad \text{Eq.74}$$

$$\mathrm{B_r} = B_m * \left(1 + \frac{\mu_o * \mu_{rec} * L_g}{\mu_o * L_m}\right) \qquad \text{Eq.75}$$

Rearranging the above equations, it gives that the length of magnet thickness as:

$$\mathrm{L}_M \approx \frac{B_g * \mathrm{L_g} * \mu_{rec}}{\mathrm{B_r} * B_G} \qquad \text{Eq.76}$$

7.10. **Number of phases**

The choice of number of phases depends upon several reasons and factors. Single phase motors are easy to wind and low cost and require only one or two power switches.

However, they have poor conductor utilization, high torque ripple, and are difficult to start [2].Two-phase motors also have poor conductor utilization, but the torque ripple is greatly reduced, and the cost is higher because a minimum of four power switches are required.

In a contrast, a three phase motors have better conductor utilization, no starting problems, and greatly reduced torque ripple.

They can get by with as few as three power switches, but they generally cost more to wind the motors. Increasing the number of phases to four or greater realizes small gains in copper utilization and torque ripple, but the costs of winding and power switches usually outweigh the gains in small medium machines [2].

7.11. **Inductance & Flux Linkage**

Machine models depend on phase inductances [24 - 25] and also on the direct and quadrature axis inductances. Analytical derivations relating the machine dimensions to various inductances are the most important information that designers require to provide them to power conversion and control engineers to do their respective tasks. As the air gap in the PM machines are far more than that of other machines because of manufacturing constraints and the magnet shave permeability's that are close to that of air, resulting in high air gap and magnet path reluctance for this machine.

The high reluctance due to the air gap is more dominant than that of the iron in these machines in comparison to other machines whose reluctance is not simple to compute. Therefore, higher accuracy is made possible in predicting these machine inductances. To make these derivations, basics such as representation of sinusoidal distributed winding, flux in a winding turn, and the mutual flux linkage associated with a winding due to a flux in the airgap or magnets have to be derived.

The flux linkage in a turn is the flux connecting to a winding turn. It is obtained from flux density, stack length, and bore radius as:

$$\lambda_t = \int_{\theta}^{\theta+\Pi/Pp} B(\theta) L_r \, D_\theta \qquad \text{Eq.77}$$

λ_t is the flux linkage in a turn
B (θ) is the flux density at a given electrical spatial position
L is the stack length
r is the bore radius. The flux density can be represented in the air gap as

$$\mathrm{B}\ (\theta) = \mathrm{B}\ \mathrm{Cos}\ (P_p w_t + \alpha - P_p\ \theta\ ) \qquad \text{Eq.78}$$

Where

ω is the electrical rotor speed
α is the angle between the centre of the pole and d-axis of the magnet and stator phase winding.

Then the flux linkage in the turn or the flux in the turn is given by substituting for the flux density in the integral equation over a pole as;

$$\lambda_t = \int_{-(\Pi/2Pp)}^{\Pi/Pp} B(\theta) L_r\ d\theta \qquad \text{Eq.79}$$

$$\lambda_t = \int_{-(\Pi/2Pp)}^{\Pi/Pp} Bpk\ Cos\ (\omega\tau + \alpha - P_p\ \theta) L_r\ d_\theta \qquad \text{Eq.80}$$

$$= 2 + \frac{Bpk\ \ Lr}{Pp}\ \ Sin\ (\omega\tau + \alpha - P_p\ \theta) \qquad \text{Eq.81}$$

$$= \theta_m\ \mathrm{Sin}\ (\omega\tau + \alpha - P_p\ \theta) \qquad \text{Eq.82}$$

The peak flux in the turn or flux linkage associated with a turn is given by:

$$\theta_m = 2\frac{Bpk\ Lr}{Pp} = \frac{Bpk\ DL}{Pp}\ =\ \frac{Bpk\ DL}{P/2}\ =\ 2\ \frac{Bpk\ DL}{P} \qquad \text{Eq.83}$$

D is the bore diameter
P is the number of poles

7.12. **Modern Machine Manufacturing Techniques**

It is well known that electrical power has wide and diverse application in all fields of human activity. The utilization of electrical power is going up day by day and this calls for increased generating capacity.

This necessity will continue increase and a great variety of electrical machines over wide range of range of power outputs. The growing needs of both electric generation and electric utility industries have to be met by continuously expanding electrical machines over a wide range of power outputs. The modern trends in manufacturing of electrical machines are described below:

1. The modern electrical machines are characterised by a very wide range of power outputs.
2. The range rotational speeds of electrical machines are very wide ranging. One machine may have a speed of few revolutions per second while other may have several thousand revolutions.
3. The type of construction adopted depends upon the power output of the machine and also in its rotational speeds.

No universally accepted classification of electrical machines based upon constructional features and power supplies exist as yet. However, a broad classification of electrical machines can be made because machines having power outputs within a particular range have some typical common constructional features. The type of construction to be adopted is considerably influenced by the operating of the machine. Low speed machines have larger diameter and small axial length, while speeds of (3000rpm) has small diameter and long core length.

Another important feature of modern electrical machines manufacture is the trend to build machines which are smaller in size and therefore involve the use of lesser material and at the same time have the same efficiency and overload capability. The increase in power ratings using smaller size coupled with good overall performance has been has been possible only due to the following:

1. There has been considerable development and refinement in the techniques relating to construction and arrangement of conductor and some other parts of the machine and this resulted in drastic reduction in stray load issues and these are basically the losses which are caused by variation in load but their values cannot be determined accurately at any point of time, examples below;

1.1 Skin effect resulting from same source conductors.

1.2 The proximity effect resulting from the field induced from adjacent conductors sharing the same slot.

1.3 The skin effect is caused by electromagnetic induction in the conducting material.

2. With a vast development in the cooling and ventilation systems for machines, the new methods are much effective for dissipation of heat generated inside the machine.

Another important factor in the manufacture of modern machines is the use of magnetic materials which have a high permeability, low iron loss and a high mechanical strength.

The materials permit use of the high values of flux density and therefore result in reduction in the size of the machine and promote the extension of power output.

Modern machine building is marked with use of higher electro-magnetic loadings for active parts and increased mechanical loading for construction materials. In order to accelerate the process of machine manufacture at reduced cost, different improved and refined manufacturing techniques are used for individual machine parts. Modern electrical machines have a field of applications. They are used in varied environment and under different operating conditions. The design of the machine and the manufacture should be such that it (the machine) operates satisfactorily under the desired environmental condition.

8. Results & analysis

The PMA topology in use at the VSIG is based on axial configuration. Radial flux alternator topology offers a number of advantages when compared to axial flux designs. The machine configuration allows the construction of a compact machine with high number of poles. The alternator rotor shaft is bolted directly on the engine flywheel whilst its stator is fixed to the engine bell housing.

The generator is modular in design where variation of magnet width and wire size can accommodate for different power delivery capabilities within a common frame size. The cross section through a bearing-less radial flux PMA is where each armature coil is wound concentrically round the stator core.

The advantage of this winding arrangement is that it is very simple and lends itself to automatic winding. The rotor has single disk (Can) carrying radially polarized neodymium iron boron (NdFeB) magnets.

Torque, speed and power requirements

Generator Power/Speed curve	
speed [rpm]	**power [kW]**
800	7.5
1000	10
1500	16
2000	25
2500	35
3000	44
3300	48

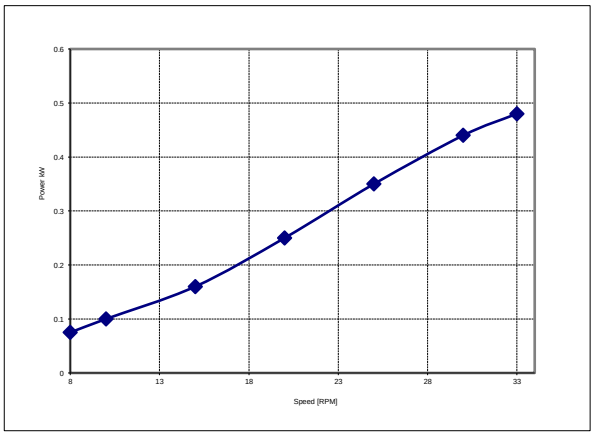

Figure 26. Power Speed Characteristics table and graph [40]

From the above review a pole-slot choice of 24/20 and 22/24 was used for the first machine design. When the allowed outer dimensions of the active machine parts had been fixed, the electrical design was started with exterior topologies were modelled with SPEED software.

Up to this point in time the FE package had not been used to model the machine. To correctly solve for the magnetic vector potential in the model the FE package had to be adapted to use positive boundary conditions. After the implementation of the positive boundary conditions on the modelled machine section an optimization will be performed. Being able to perform optimizations as part of this FE analysis.

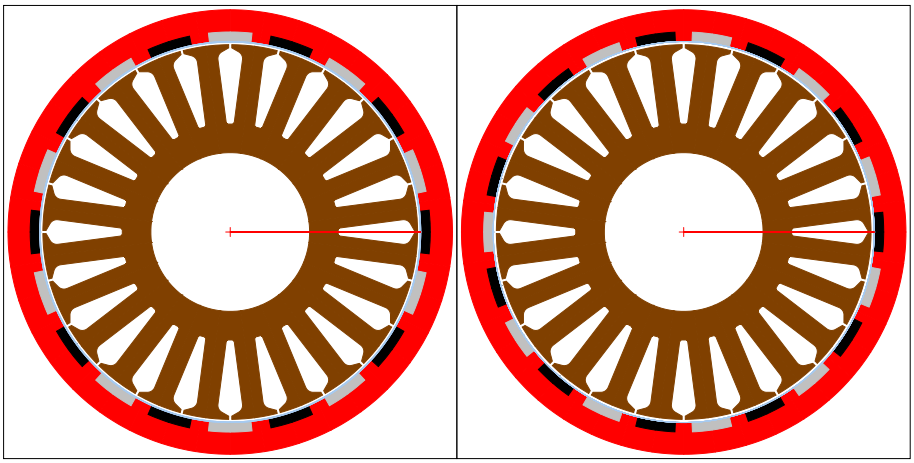

(A) (B)

Figure 27. Illustrates 24/20(A) and 24/22(B) exterior rotor (inset) PM geometry

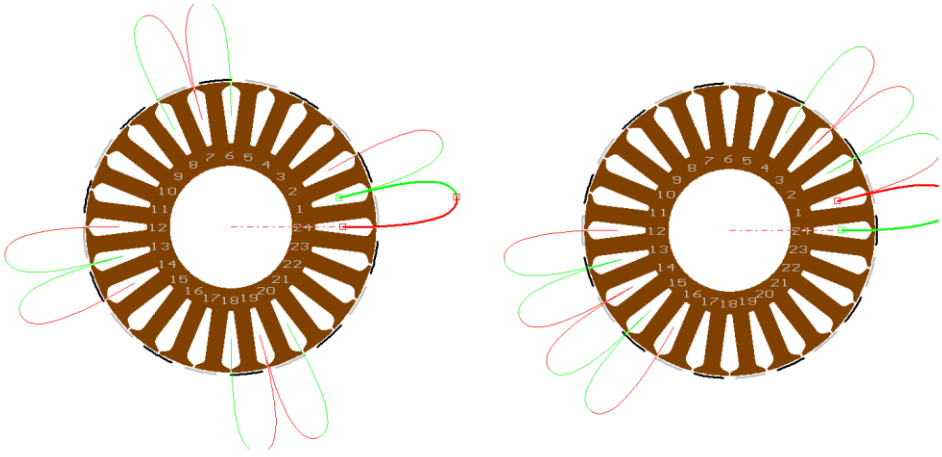

(A) (B)

Figure 28. Illustrates 24/20(A) and 24/22(B) Double layer fractional concentric windings

The Total number of conductors is given by:

Turns in series/phase

$$T_{ph} = \frac{T_c \; C_p \; \text{No.of poles}}{a} \qquad \text{Eq.84}$$

One turn = 2 conductors (“go and return “)

Each turn and each conductor carries the current $\frac{I_{ph}}{\text{a}}$ Eq.85

Total number of conductors

$$Z = T_{ph} \; C_p \; N_{ph} \; a \qquad \text{Eq.86}$$

Turns/coils: Tc

Coils/pole: Cp

Parallel paths: a

Turn in series/phase: Tph

Total numbers of conductors: Z

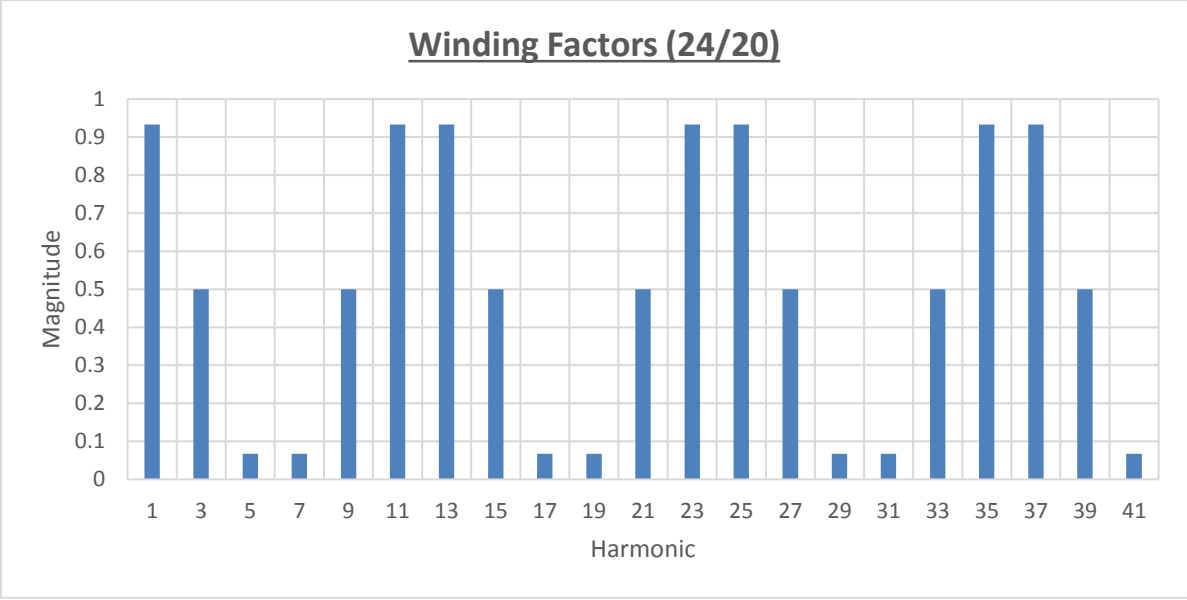

Figure 29. Illustrates Fundamental Winding factors and MMF harmonics normalised to full-pitch winding for 24 slots 20 poles

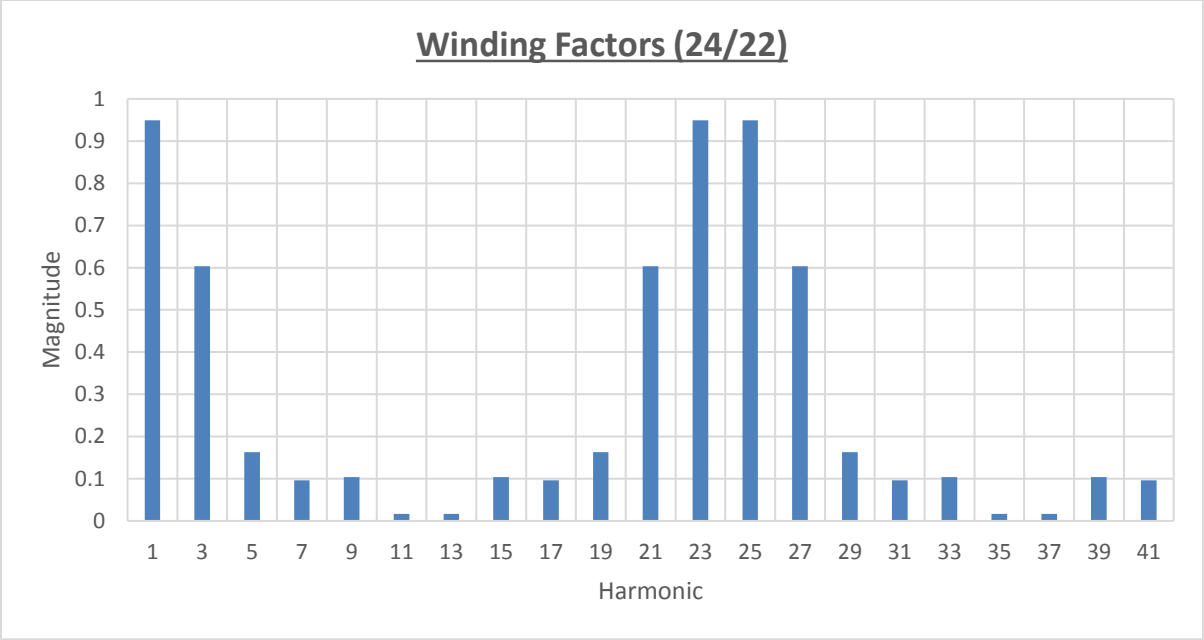

Figure 30. Illustrates Fundamental Winding factors and MMF harmonics normalised to full-pitch winding for 24 slots 22 poles

The winding factors of an electrical machine are proportional to the generated electromagnetic torques. So, the fundamental winding factor of the machine must be high and its sub- and super-harmonic winding factors as low as possible. A machine with a low fundamental winding factor needs to compensate its low torque with a high current or with more winding turns, which both are inversely proportional to the winding factor. The winding factor can be defined through a voltage vector graph or it can be solved from the analytical equations. (When the winding factors of a particular machine are solved by using the equations, it should be remembered that this must be done accurately, because there are different equations to be applied for the different winding types). Analytically, the winding factor can be solved from [33].

$$\xi v = \xi p \ \ \xi d \ \ \xi sk \qquad \text{Eq.87}$$

Where ξp is the pitch factor, ξd is the distribution factor and ξsk is the skewing factor. The pitch factor ξp is defined for concentrated two layer-layer winding as [33].

$$\xi p = \sin\frac{v\pi\tau_s}{2\tau_p} = \sin\frac{v\pi}{Q_s} \qquad \text{Eq.88}$$

The skewing factor can be solved by [33]

$$\xi sk = \frac{\sin v\pi\tau_{sk}/2\tau_p}{v\pi\tau_{sk}/2\tau_p} \qquad \text{Eq.89}$$

Where Tsk is the skewing pitch. Skewing is used to minimize the cogging torque. As to the concentrated fractional slot machine, there are cases, where the amplitudes of the cogging torque are low. This is due to the fact that in a fractional slot machine the different stator slot pitch multiples do not coincide with the rotor pole pitch.

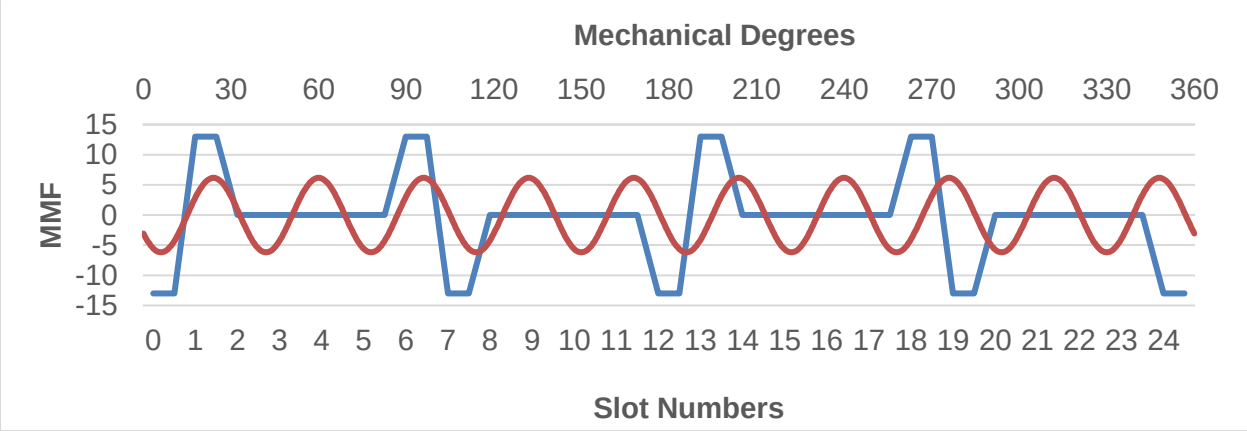

Figure 31. Illustrates, MMF that would result from current flowing in any one phase (24slots, 20 poles)

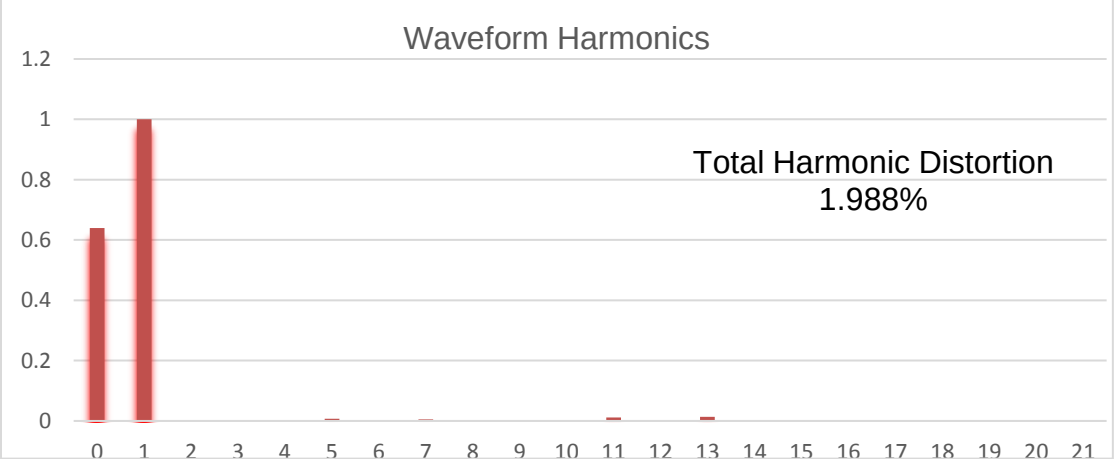

Figure 32. Illustrates Line EMF Waveform Harmonics 24/20 generator

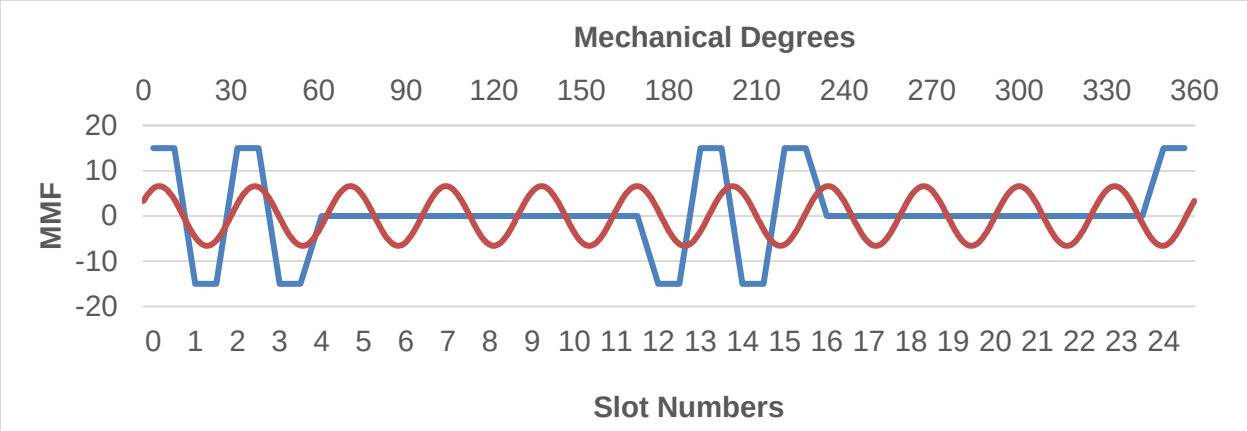

Figure 33. Illustrates, MMF that would result from current flowing in any one phase (24slots, 22 poles)

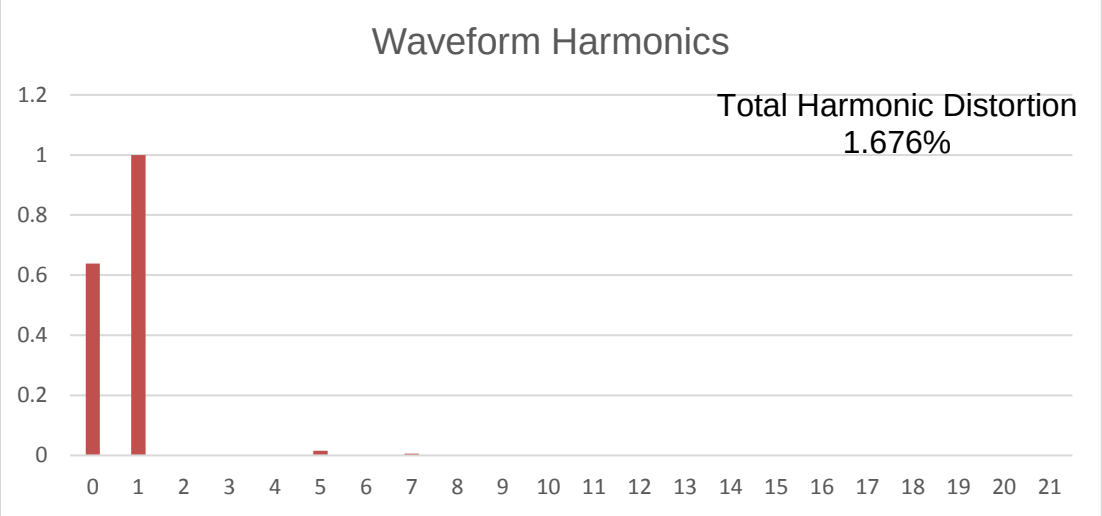

Figure 34. Illustrates Line EMF Waveform Harmonics 24/22 generator

The MMF illustrated above figures that would result from current flowing in any phase, or all phases. In simple terms, this is proportional to the radial magnetic field strength across the airgap that would be produced by the current. The "armature reaction" flux-density in the airgap is proportional to this MMF.

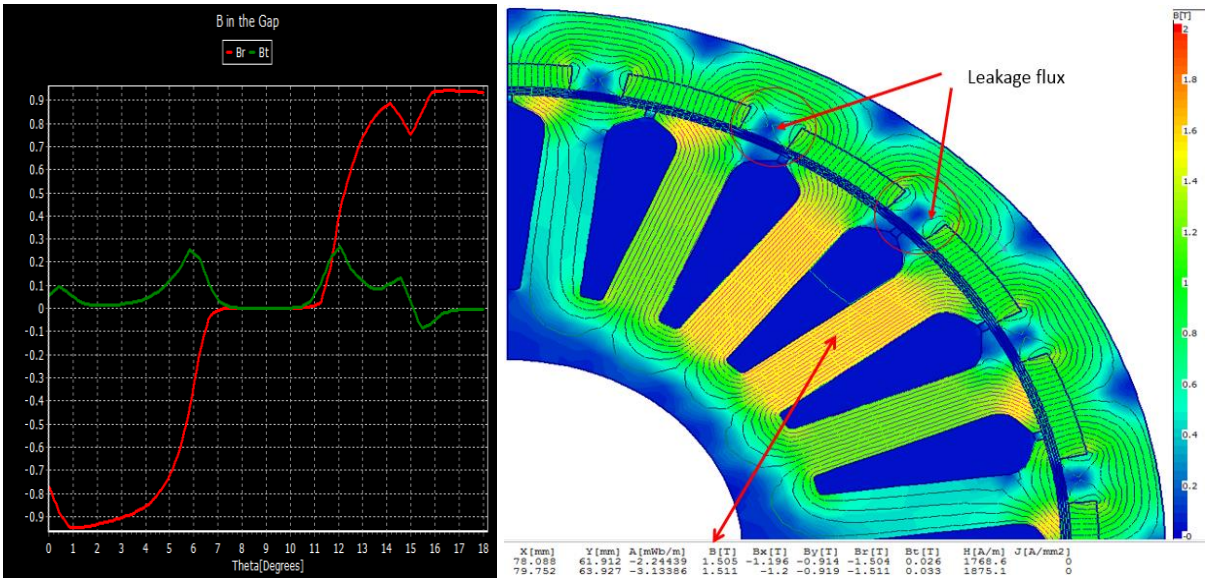

Figure 35. Illustrates Open circuit finite analysis on distribution of air gap flux density with fixed rotor position and graph of radial and tangential flux-densities around the airgap (24/20)

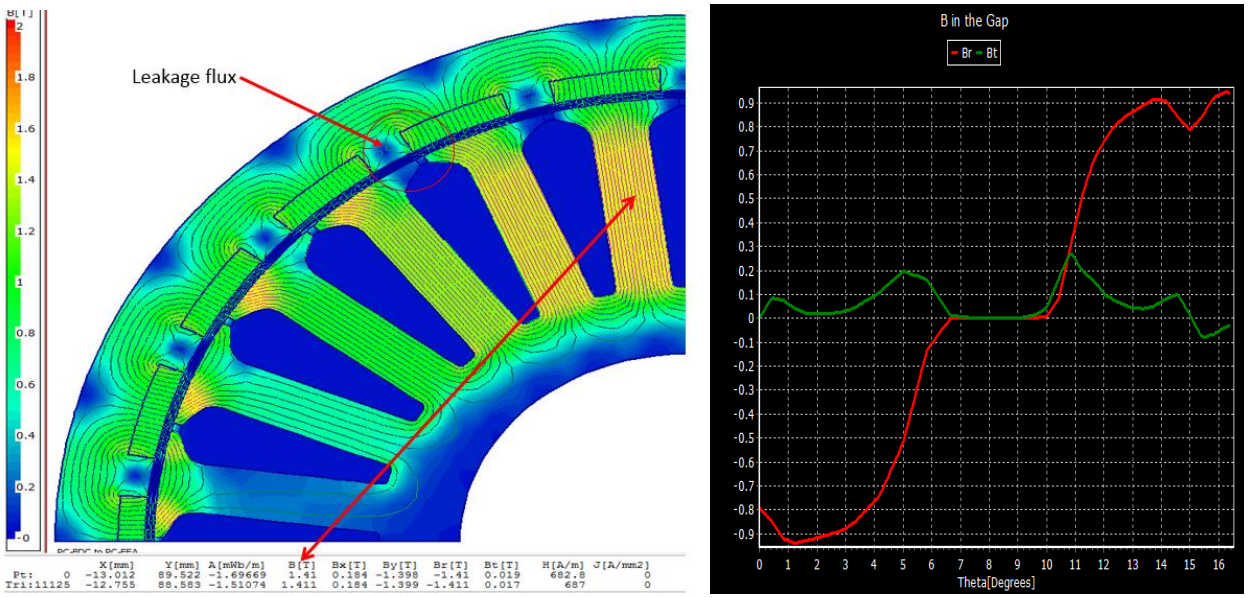

Figure 36. Illustrates Open circuit finite analysis on distribution of air gap flux density with fixed rotor position and graph of radial and tangential flux-densities around the airgap (24/22).

Cogging torque

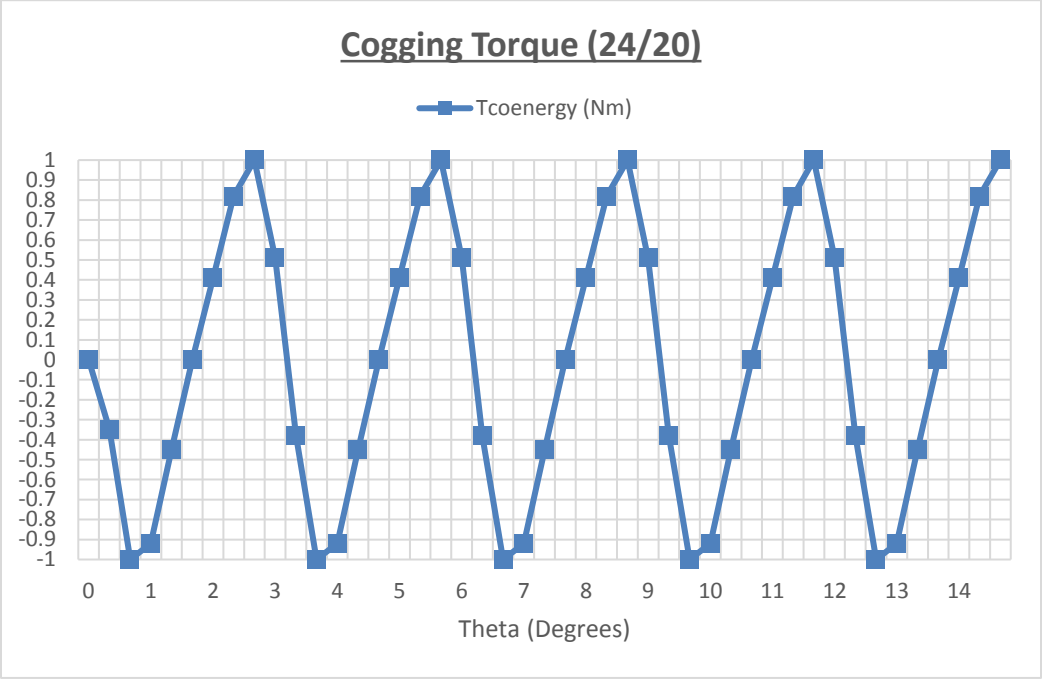

Figure 37. Illustrates The variation of cogging torque caused by the interaction of the magnetised rotor with slotted stator (24/20) Inset

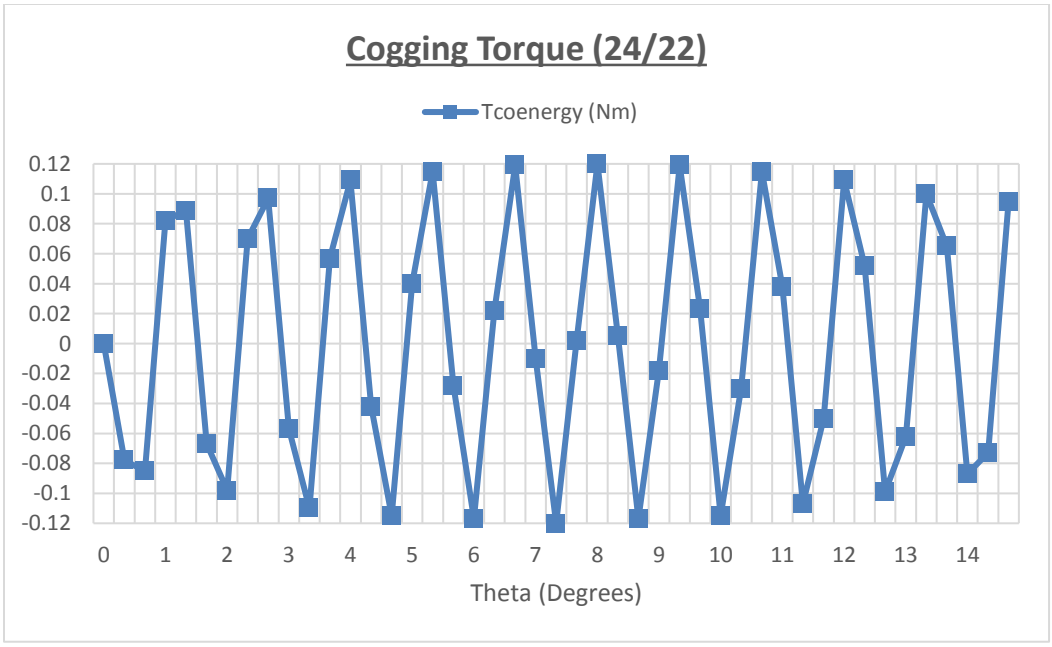

Figure 38. Illustrates The variation of cogging torque caused by the interaction of the magnetised rotor with slotted stator (24/22) Inset

Cogging torque results from the interaction of the rotor permanent magnets with the stator teeth. The use of a fractional number of pole not only reduces the amplitude of the cogging torque, but also increases the order, since the stator slots are located at different relative circumferential positions with respect to the edges of the magnets [30]-[31]. In general, the higher the least common multiple between the number of poles and the number of slots, the lower cogging torque, while the smaller the greatest common divider between the number of poles and the number of slots, the lower the cogging torque.

Neglecting the armature reaction and magnetic saturation, the cogging torque is independent of the stator current. The fundamental frequency of the cogging torque is a function of the number of slots s1, number of pole pairs p and input frequency f. One of the cogging frequencies (usually fundamental) can be estimated as:

$$F_{C=}\ s_1\ n_{s=}\ s_1\ \frac{f}{p} \qquad \text{If} \qquad N_{cog}\ \frac{2p}{GCD\,(S1,2p)} = 1 \qquad \text{Eq.90}$$

$$F_{C\,=\,N_{cog}} \qquad N_{cog} = \frac{L_{cm}\,(S_1\ 2p)}{2p} \qquad If\ =\ N_{cog}\ \geq 1 \qquad \text{Eq.91}$$

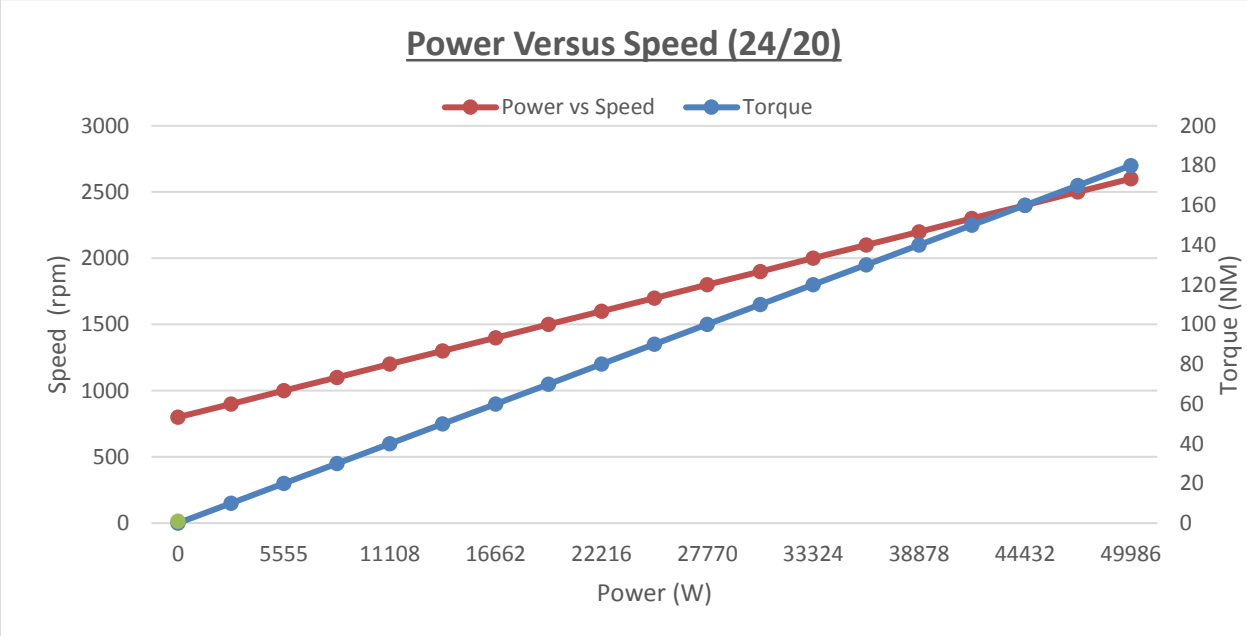

Figure 39. Illustrates Power versus Speed and Torque graph (24_20)

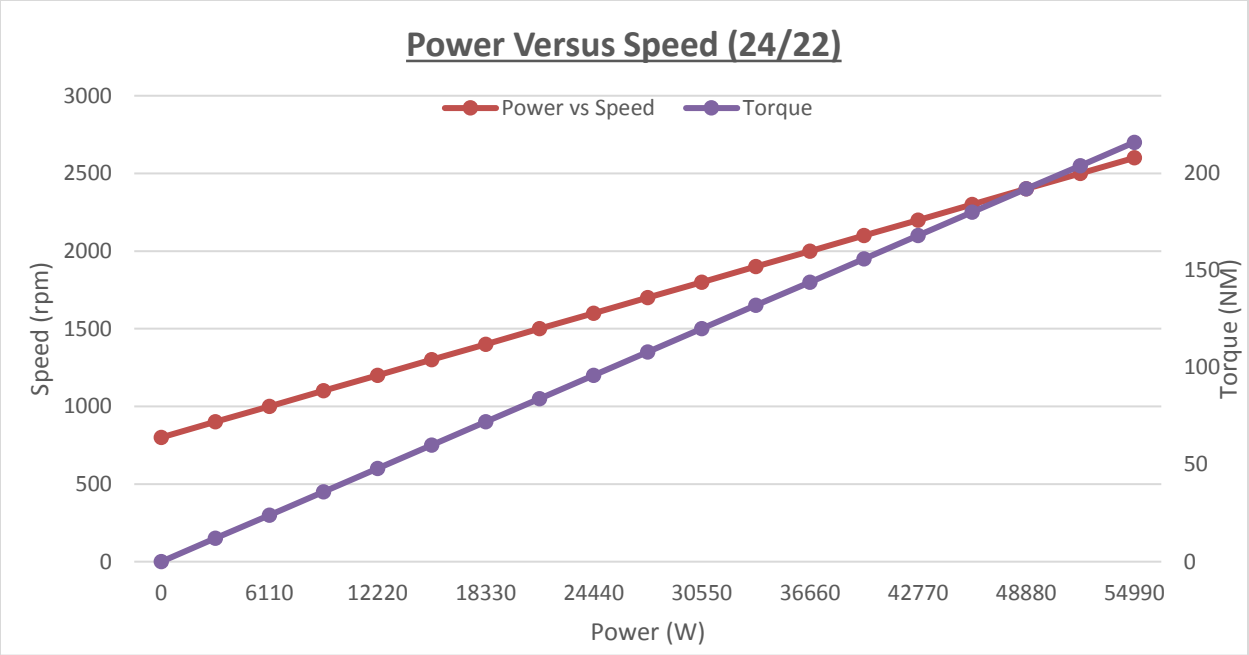

Figure 40. Illustrates Power versus Speed and Torque Graph (24_22)

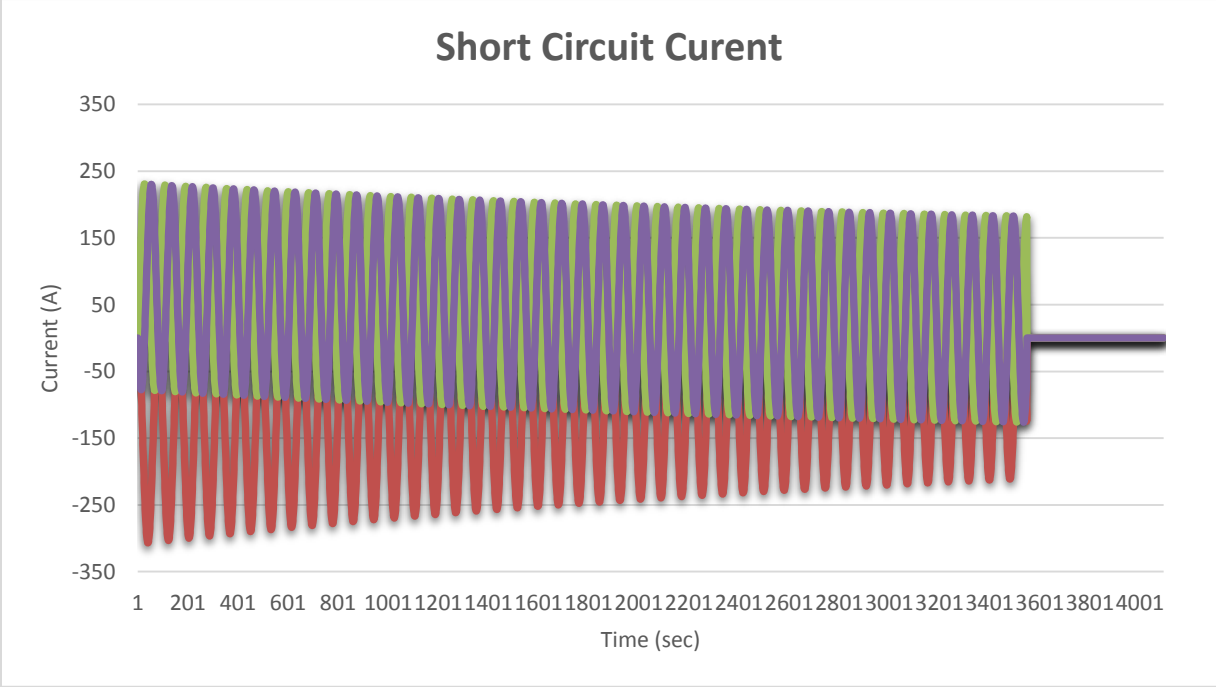

Figure 41. Short circuit currents (24_20) Inset

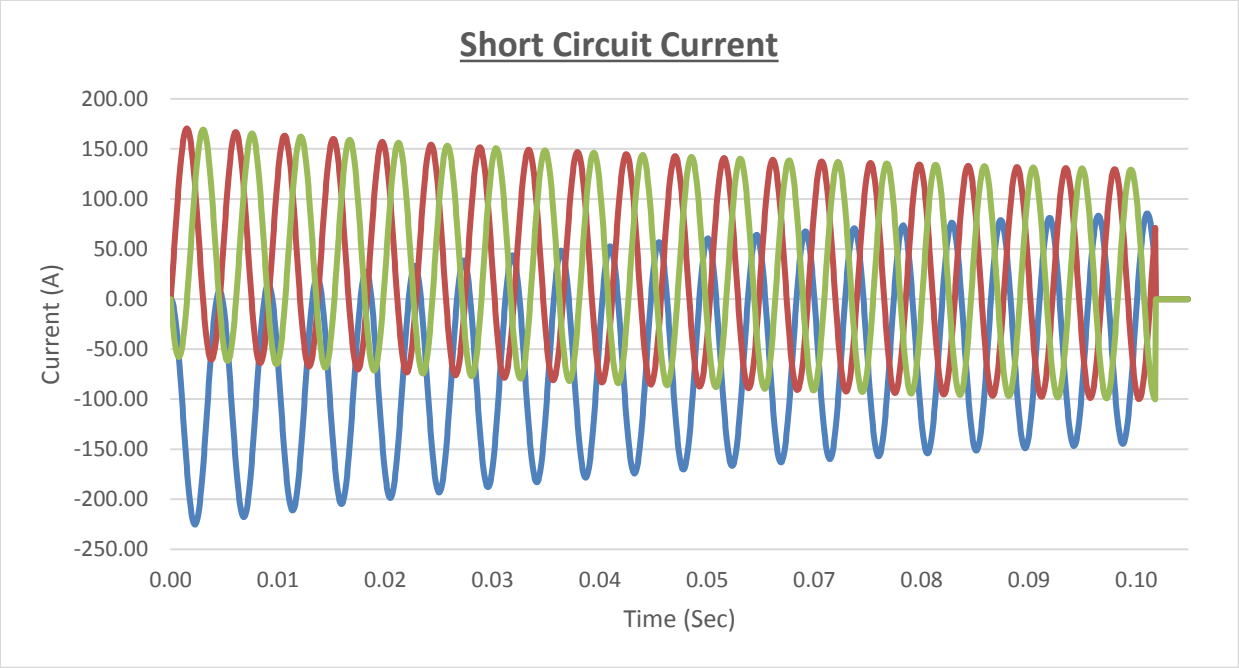

Figure 42. Short circuit currents 24_22 Inset

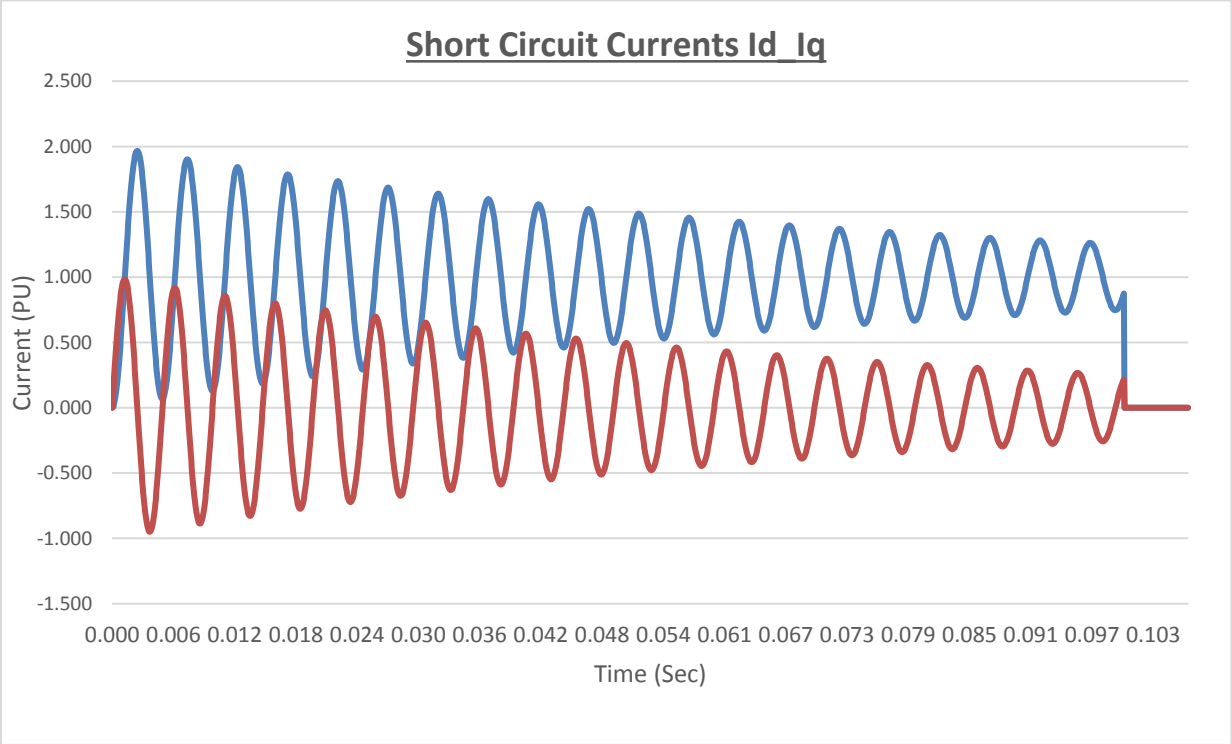

Figure 43. Short circuit currents Id-Iq 24_20 Inset

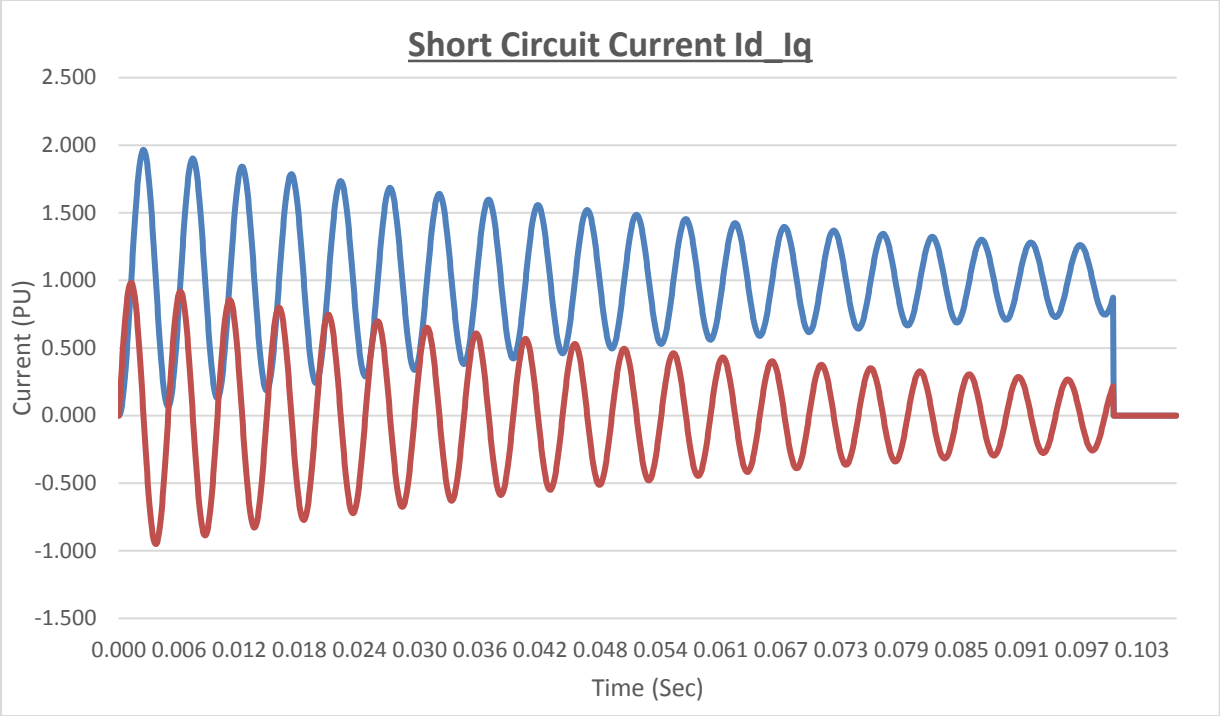

Figure 44. Short circuit currents Id Iq 24_22

The symmetrical short-circuit of an alternator is analysed in many classic texts. [41] Gives the following formula for the phase current.

$$\left(i_{\mathrm{a}} = E\left(\frac{1}{Xd} + \left[\frac{1}{X\prime d} - \frac{1}{Xd}\right] e^{-\frac{t}{T\prime d}} + \left[\frac{1}{X\prime\prime d} - \frac{1}{X\prime d}\right] e^{-\frac{t}{T\prime\prime d}}\right) \cos(\omega t + \lambda) - E e^{-\frac{t}{Ta}}\left[\frac{\cos\lambda}{Xm} + \frac{\cos(2\,\omega t+\lambda)}{Xn}\right]\right) \quad \text{Eq.92}$$

Transient AC Sub-transient DC 2F

Where $E = \sqrt{2\,Eq1}$ is the peak phase EMF, therefore

$$\mathrm{Xm} = \frac{2\,\mathrm{X''d}\;\mathrm{X''q}}{\mathrm{X''d+X''q}}\;; \qquad \mathrm{Xn} = \frac{2\,\mathrm{X''d}\;\mathrm{X''q}}{\mathrm{X''d-X''q}} \quad \text{Eq.93}$$

The equations above contains an AC component cos ($\omega t + \lambda$), a DC offset component cos λ for salient-pole machines and double-frequency component 2F. λ is the angle between the *d*-axis and the axis of phase *a* at time *t = 0*. The worst-case DC offset would occur when λ = 0. It decays with a time-constant *T*a, the armature time-constant.

The AC component has a “steady-state” part controlled by the synchronous reactance *X*d =$W\ L_d$, a “transient” part controlled by (1/*X’*d-1/*X*d); and a “sub-transient” part controlled by (1/*X*’’d -1/*X’*d). The permanent-magnet machine has no field winding, so the transient part does not appear. This can be represented in eqn. (93) by setting *X’*d = *X*d, which has the effect of eliminating the transient term and leaving the correct sub-transient term. After the decay of the sub-transient the current is limited solely by *X*d.

The transient time-constants *T’*d and *T*d’’0 are meaningless in the permanent-magnet machine, but there is no harm in setting them equal to *T*’’d and *T*d’’0, on the grounds that once the sub-transient has decayed the period in which the current is limited by *X*d establishes itself immediately.

The sub-transient part decays with a time-constant *T’’*d, called the sub-transient time-constant, or sometimes the “short-circuit” sub-transient time-constant. Both *X*’’d and *T’’*d depend on the conductive components on the rotor, including the magnets and any retaining can and even the shaft.

In conventional wound-field machines the sub-transient decays rapidly within a small number of cycles, but the transient persists much longer because of the large inductance of the field winding. Considering a non-salient-pole machine with λ = 0. After half a cycle, ωt = π, and assuming that the exponential decay terms are still substantially equal to 1, therefore:

$$\mathrm{i_a} = -\sqrt{2}\ \frac{\mathrm{Eq1}}{\mathrm{X''d}}\ -\sqrt{2}\ \frac{\mathrm{Eq1}}{\mathrm{X''d}} = -2\sqrt{2}\ \frac{\mathrm{Eq1}}{\mathrm{X''d}} \qquad \text{Eq.94}$$

Thus the DC offset is at most equal to the AC sub-transient term, and doubles the peak current at the beginning of the transient.

Torque ripple

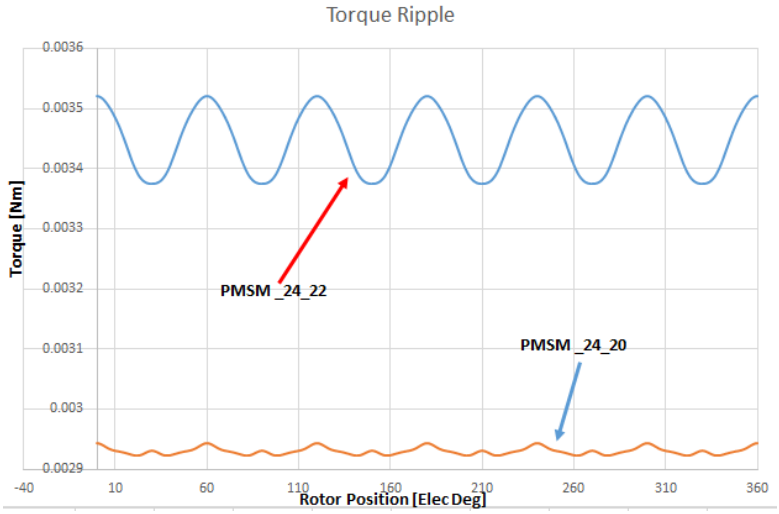

Figure 45. Shows Torque ripple due to the distortion of EMF and current waveform

The instantaneous torque of an electrical motor

$$\mathrm{T}(\alpha) = \mathrm{T0} + \mathrm{Tr}\ (\alpha) \qquad \text{Eq.95}$$

Has two component:

- Constant or average component T0;
- Periodic component Tr (*α*), which is a function of time or angle *α*, superimposed on the constant component.

The periodic component causes the *torque pulsation* called also *torque ripple*, there are many definitions of the torque ripple. Torque ripple can be defined in any of the following ways:

$$t_r = \frac{T_{\max} - T_{min}}{T_{\min} + T_{max}} \qquad \text{Eq.96}$$

$$t_r = \frac{T_{\max} - T_{min}}{T_{av}} \qquad \text{Eq.97}$$

$$t_r = \frac{T_{\max} - T_{min}}{T_{rms}} \qquad \text{Eq.98}$$

$$t_r = \frac{[Torque\ Ripple]\ RMS}{T_{av}} = \frac{Tr_{rms}}{T_{av}} \qquad \text{Eq.99}$$

Where the Average torque in Eq.100

$$T_{av} = \frac{1}{Tp} \int_{\propto}^{\propto = tp} T^2(\propto)\, d\propto = \frac{1}{TP} \int_0^{tp} T(\propto)\, d\propto \qquad \text{Eq.100}$$

And the *rms* or effective torque in Eq.101

$$T_{rms} = \sqrt{\frac{1}{T_p} \int_0^{tp} T^{2\,(\propto)}\, d(\propto)} \qquad \text{Eq.101}$$

The torque ripple T_{rms} in Eq.100 is calculated according to Eq101 in which *T* (*α*) is replaced by *Tr* (*α*).

T_p *i*s the period of the torque waveform. For a sinusoidal waveform the half-cycle average value is (2/*π*) T_m , where T_m is the peak torque and the *rms* value would be equal to $\frac{T_m}{\sqrt{2}}$.

For the waveform containing higher harmonics, the rms value of the torque ripple.

$$T_{rms} = \sqrt{T_{rms1}^2 + T_{rms2}^2 + T_{rms3}^2 \ldots\ldots} \qquad \text{Eq102}$$

Finite Element Analysis (Opera)

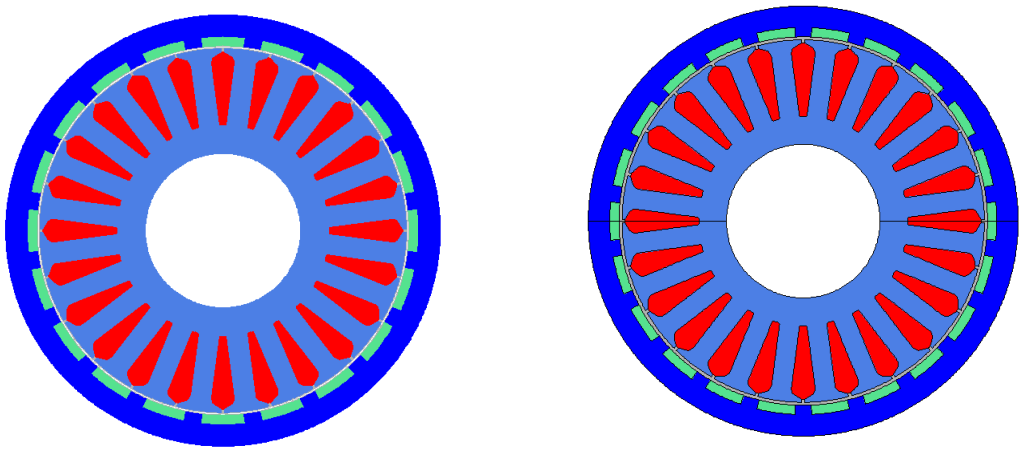

(A) (B)

Figure 46. Illustrates 24 slots/20 poles (A) and 24slots /22 poles (B) exterior rotor PM geometries (Opera)

Vector field Opera is the software used for the finite element method. The results are used to verify the analytical calculations. The machine geometry is drawn and the different machine parts are assigned a specific material. In a magnetic simulation, the non-magnetic materials are represented by vacuum. The magnet material is created in order to describe the required remanence flux density.

The above two motors where examined dynamically using the rotating machines analysis (RM). Opera-2d/RM can also be used to quickly and easily establish some basic characteristics of the motor, namely the motor open-circuit back-emf at speed as well as the cogging torque. The model that was employed to ascertain the start-up characteristic of the motor on no-load can quickly be modified to achieve this goal. When no conducting materials are present, the same model can be used to evaluate both the open-circuit back-emf as well as the cogging torque in the BPM motor. Opera-2d Pre-Processor and read in the Opera-2d RM model previously prepared. A time-stepping solution to the transient electromagnetic equation is obtained allowing the rotor to rotate by the appropriate angle at each time step.

There are two types of simulations namely:

1) Static Analysis, used for calculation of the flux density created by the magnets.

2) Rotating Machine Analysis (RM), used for calculations of the torque and the iron losses at rated speed

Many electromagnetic devices are operated while connected to an electric circuit. However, under time varying conditions, the inductance of the coil and reactance in the external circuit may also be significant. For example, the coil inductance could be time dependent due to magnetic saturation and eddy currents. Consequently, the current in the coil will not be known. To allow models of this nature to be solved Opera-2d supports external RM solver. The circuits illustrated in figures below were used to simulate open circuit condition for the above two motors.

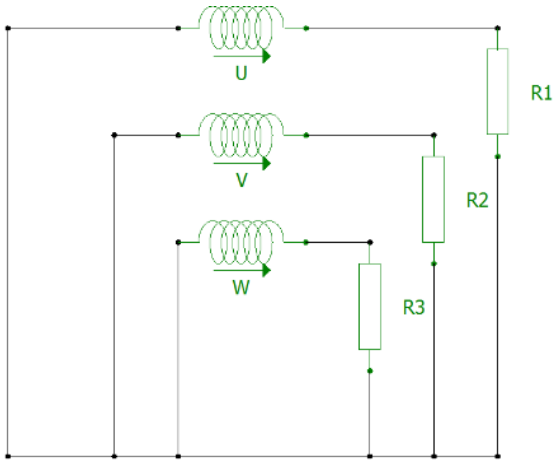

Figure 47: Circuit used for open circuit simulation

Resistors:

Name	Value	Notes
R1	1000000 MO	
R2	1000000 MO	
R3	1000000 MO	

Windings:

Name	Conductor set	Circuit type	Resistance per unit length	Turns per conductor	Length	Model symmetry	Symmetry factor	Notes
U	-1,2,3,-4	Filamentary	0.0100 O/m	13	60 mm	Yes	4	
V	5,-6,-7,8	Filamentary	0.0100 O/m	13	60 mm	Yes	4	
W	-9,10,11,-12	Filamentary	0.0100 O/m	13	60 mm	Yes	4	

Table 4 shows components parameters set for open circuit simulations in this instance for 24/20

For full load magnetic simulation, a circuit shown below was used in order to impose the rated

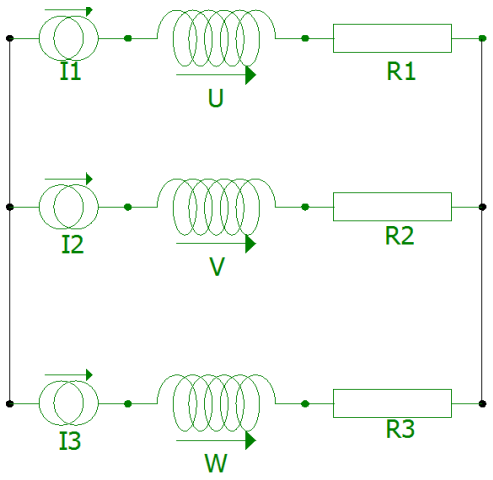

Figure 48: Circuit used for full load (resistive) simulation

Resistors:

Name	Value	Notes
R1	0.5 O	
R2	0.5 O	
R3	0.5 O	

Windings:

Name	Conductor set	Circuit type	Resistance per unit length	Turns per conductor	Length	Model symmetry	Symmetry factor	Notes
U	1,-2,-3,4,5,-6,-7,8	Filamentary	0.0150 O/m	13	60 mm	Yes	2	
V	-9,10,11,-12,-13,14,15,-16	Filamentary	0.0150 O/m	13	60 mm	Yes	2	
W	17,-18,-19,20,21,-22,-23,24	Filamentary	0.0150 O/m	13	60 mm	Yes	2	

Currents:

Name	Type	Peak current	Frequency	Phase	Internal Resistance	Notes
I1	"AC Current"	91.9 A	476.66 Hz	60	1 MO	
I2	"AC Current"	91.9 A	476.66 Hz	300	1 MO	
I3	"AC Current"	91.9 A	476.66 Hz	180	1 MO	

Table 5 shows components parameters set for full load simulations in this instance for 24/20

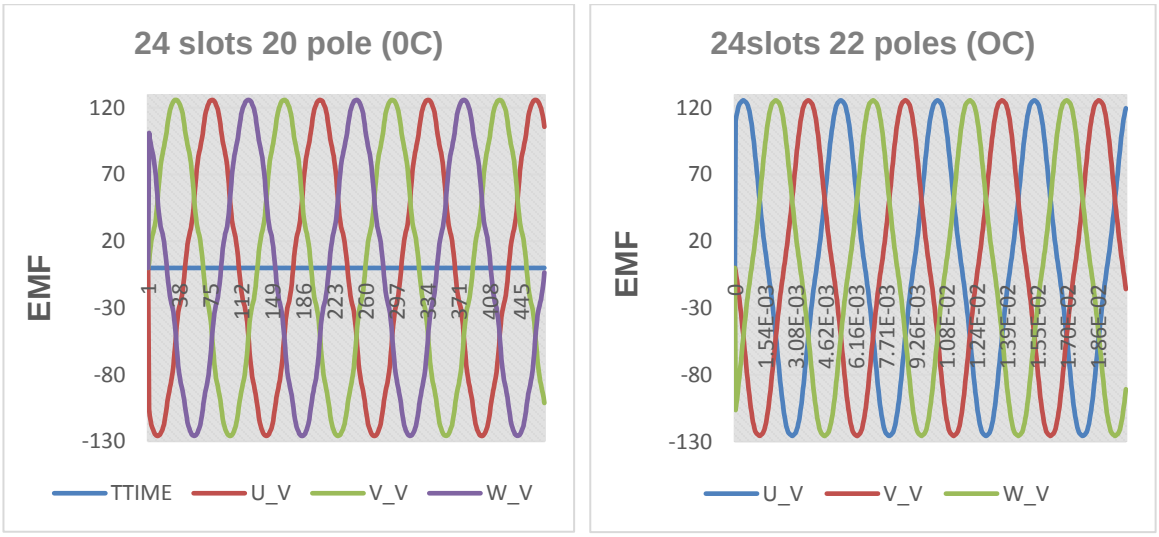

(A) (B)

Figure 49. Illustrates 24/20 (A) and 24/22 (B) open circuit EMF simulated at 1100 rpm (Opera)

The circuit equations of the three phase winds are described below;

$$Va = Ra\ ia + \frac{d\Psi a}{dt} \quad \text{Eq.103}$$

$$Vb = Rb\ ib + \frac{d\Psi b}{dt} \quad \text{Eq.104}$$

$$Vc = Rc\ ic + \frac{d\Psi c}{dt} \quad \text{Eq.105}$$

Ra, Rb, Rc: Winding Resistances of each phase in ohm, Ω

Va, Vb, Vc: Phase voltages on motor winding in volt, V
ia, ib, ic : Phase currents in ampere, A
ψa, ψb, ψc : Flux Linkage of each phase

The flux linkages for each phase are defined as

$$\Psi a = l_{a\,I_a} + l_{ab\,I_b} + l_{ac}\,i_c + \Psi am \qquad \text{Eq.106}$$

$$\Psi b = l_{b\,I_b} + l_{ba\,I_a} + l_{bc}\,i_b + \Psi bm \qquad \text{Eq.107}$$

$$\Psi c = l_{c\,I_c} + l_{ca\,I_a} + l_{bc}\,i_b + \Psi cm \qquad \text{Eq.108}$$

Where

l_a, l_b, l_c : Self inductances of each phase in henry, H

l_{ab}, l_{ac}, l_{ba}, l_{bc}, l_{ca}, l_{cb}: Mutual inductances between phases in henry, H

$\Psi am, \Psi bm, \Psi cm$: Flux linked with each phase due to the permanent magnet in each phase in weber, WB.

The above equations can then be written in matrix form.

$$\begin{bmatrix} Va \\ Vb \\ Vc \end{bmatrix} = \begin{bmatrix} Ra & 0 & 0 \\ 0 & Rb & 0 \\ 0 & 0 & Rc \end{bmatrix} \begin{bmatrix} ia \\ ib \\ ic \end{bmatrix} + \frac{d}{dt} \begin{bmatrix} La & Lab & Lac \\ Lba & Lb & Lbc \\ Lca & Lcb & Lc \end{bmatrix} + \frac{d}{dt} \begin{bmatrix} \Psi am \\ \Psi bm \\ \Psi cm \end{bmatrix} \qquad \text{Eq.109}$$

The rate of change of the flux linkages established by the permanent magnet at each phase is equal to the induced back EMF in the winding. By assuming that there is no change in the rotor reluctances, then the self and mutual inductances of every phase will be similar respectively. It is also assumed that the winding resistances are equal. Hence the above equation can be written as:

The electromagnetic torque is given by:

$$\mathrm{T_e} = \frac{\mathrm{e}a\ ia \quad \mathrm{e}b\ ib \quad ec\ ic}{\omega \mathrm{m}} \qquad \text{Eq.110}$$

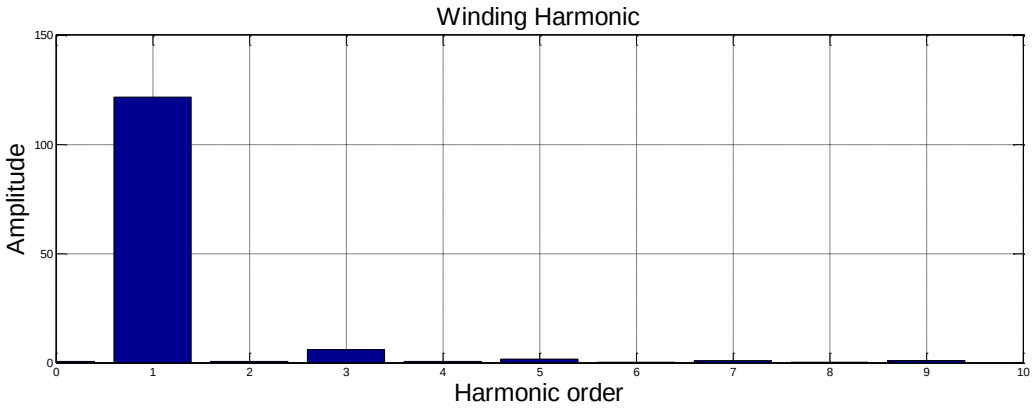

Figure 50. Spatial harmonics due to the winding distribution 24/20

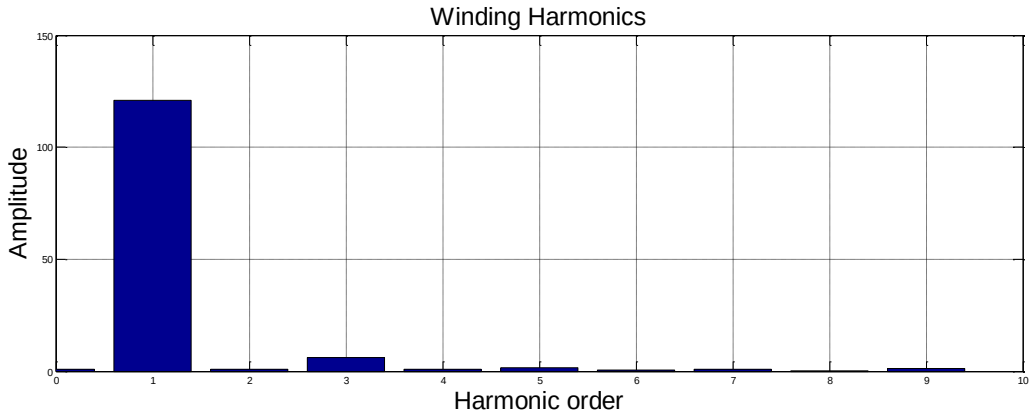

Figure 51. Spatial harmonics due to the winding distribution 24/22

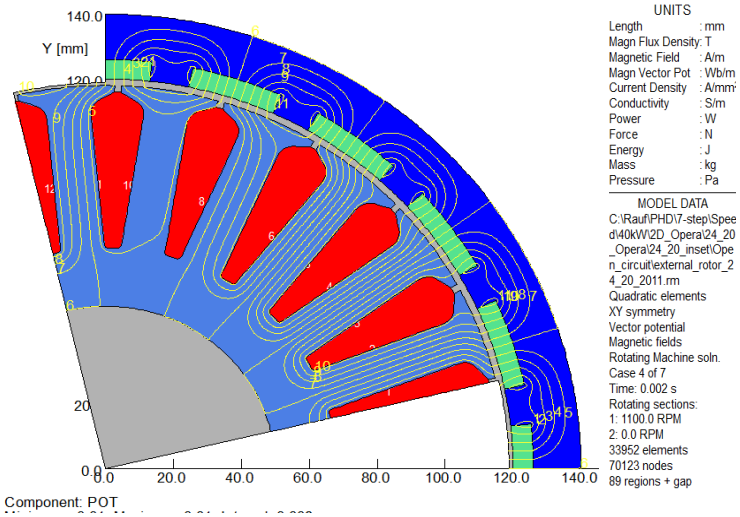

Figure 52. Illustrates, generator on open circuit flux plot at 2 ms (24/20)

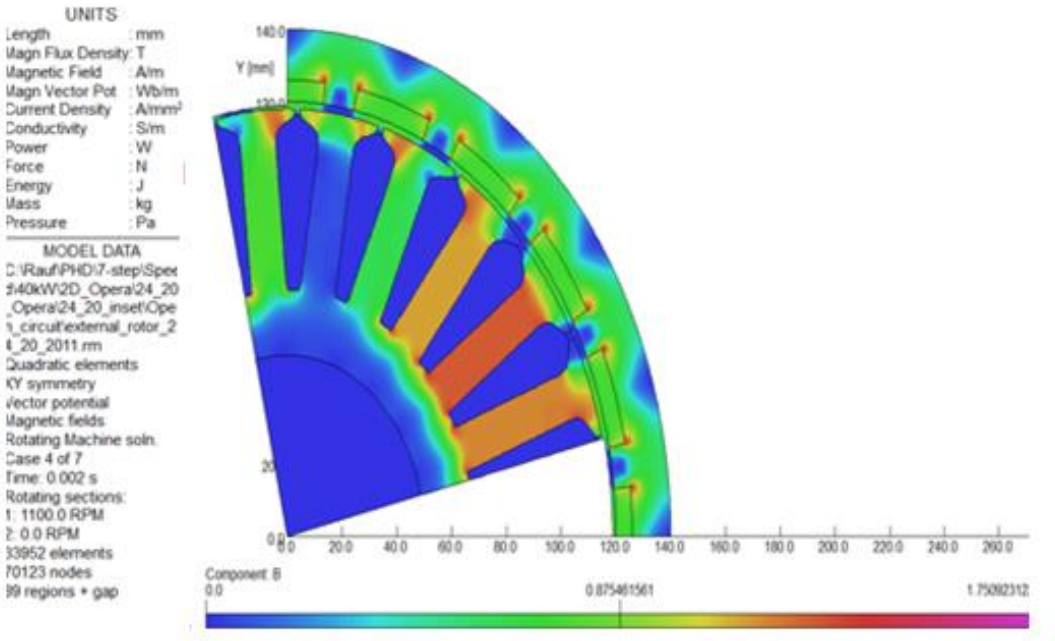

Figure 53. Illustrates, generator on open circuit flux density plot at 2 ms (24/20)

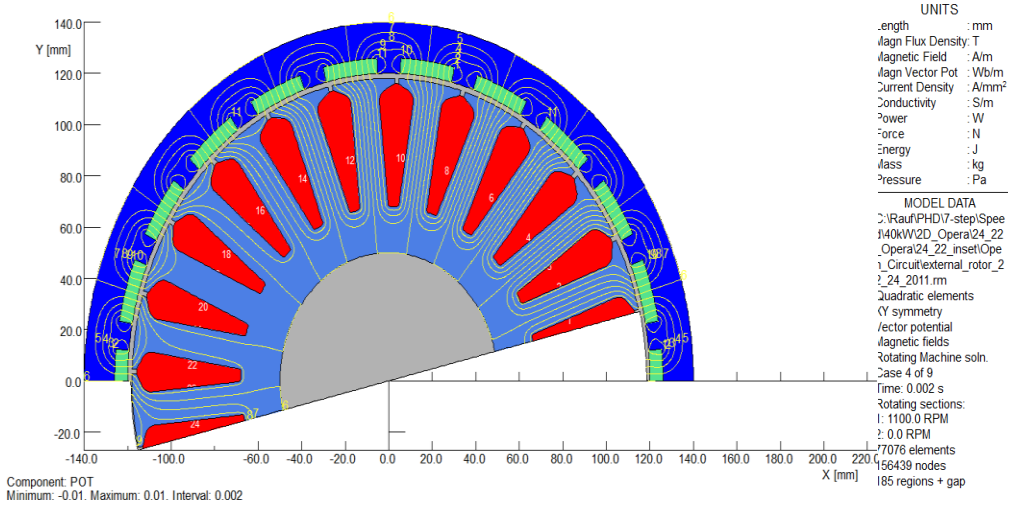

Figure 54. Illustrates, generator on open circuit flux plot at 2 ms (24/22)

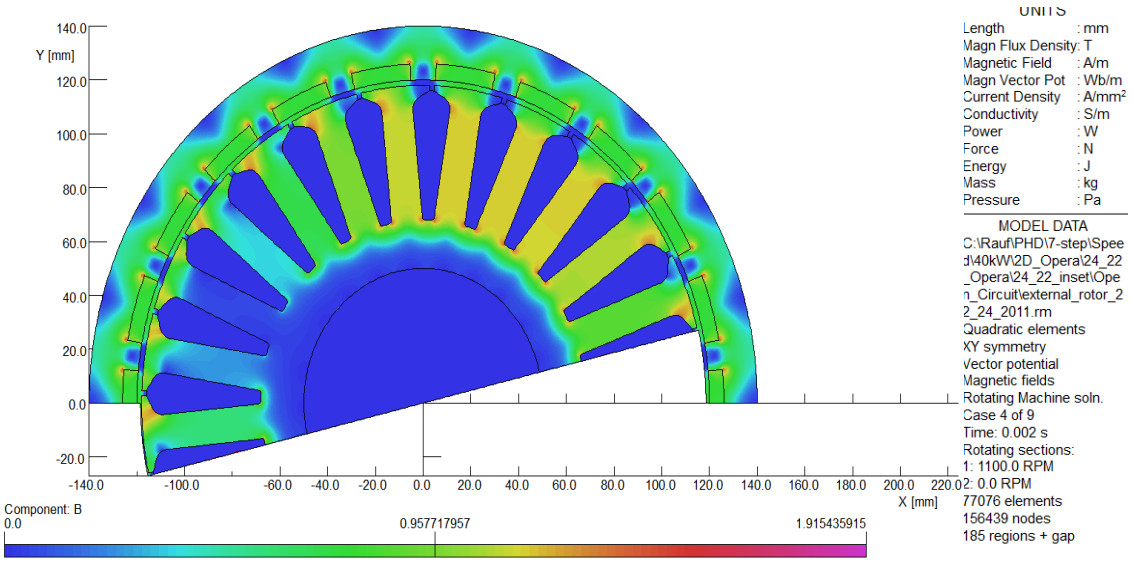

Figure 55. Illustrates, generator on open circuit flux density plot at 2 ms (24/22**)**

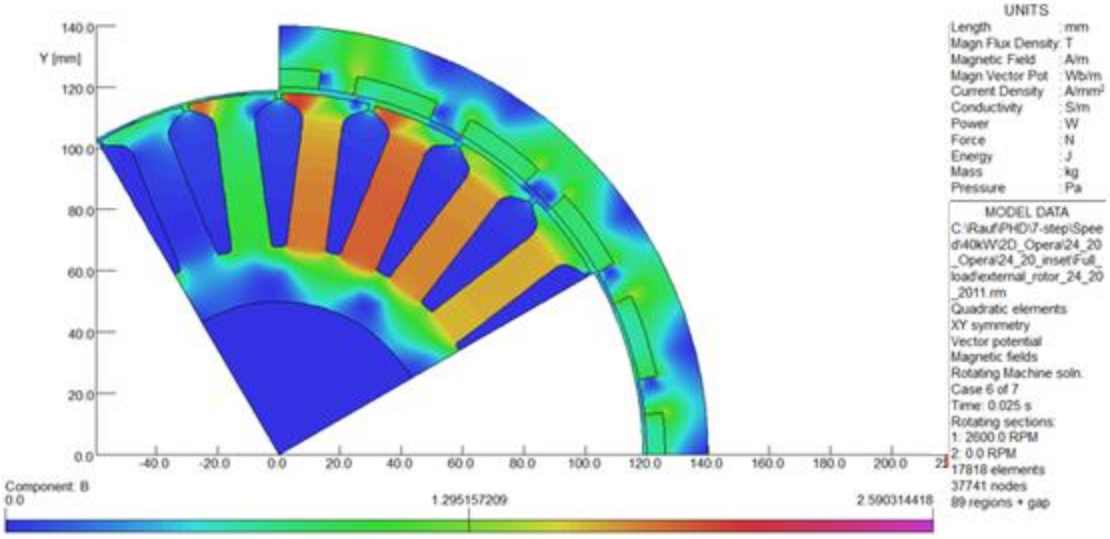

Figure 56. Illustrates, generator on full load flux density plot at 2.5 ms (24/20)

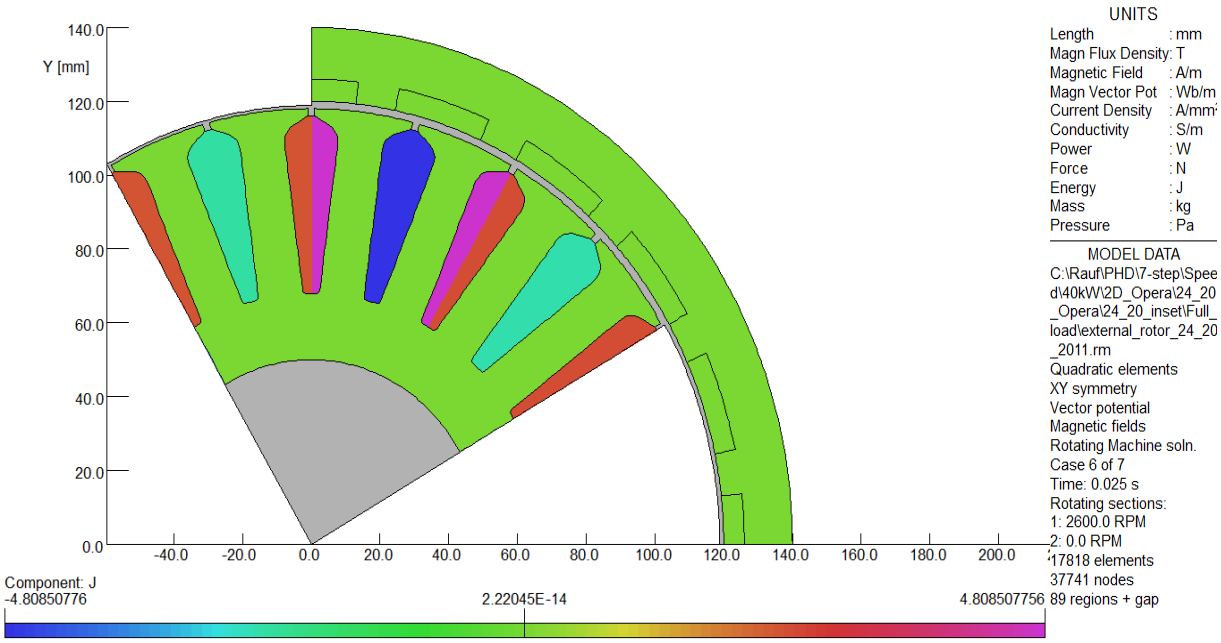

Figure 57. Illustrates, generator on full load current density plot at 2.5 ms (24/20)

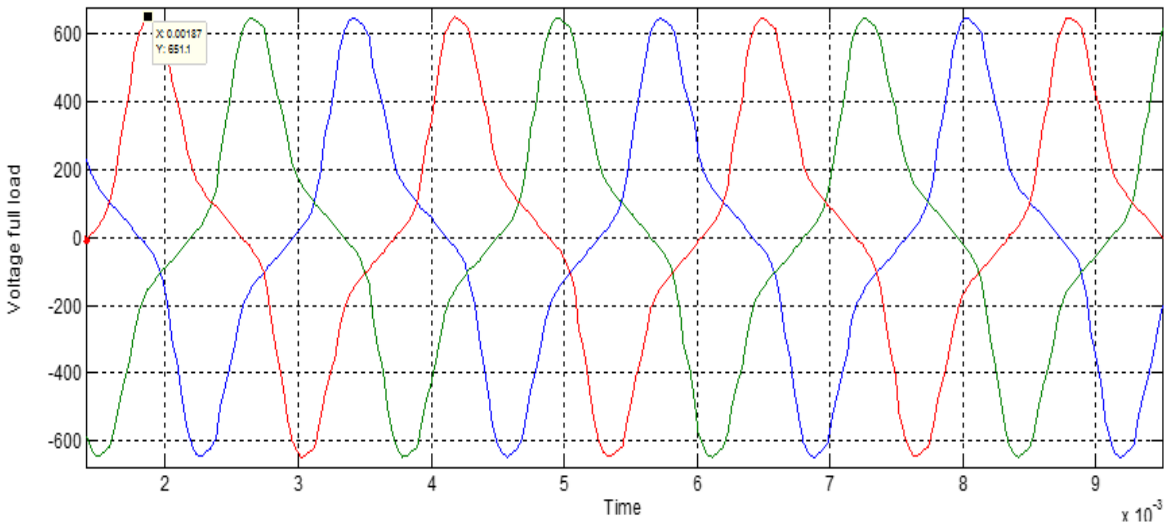

Figure 58. Illustrates 24/20, full load voltage vs time at 2600 rpm (Opera)

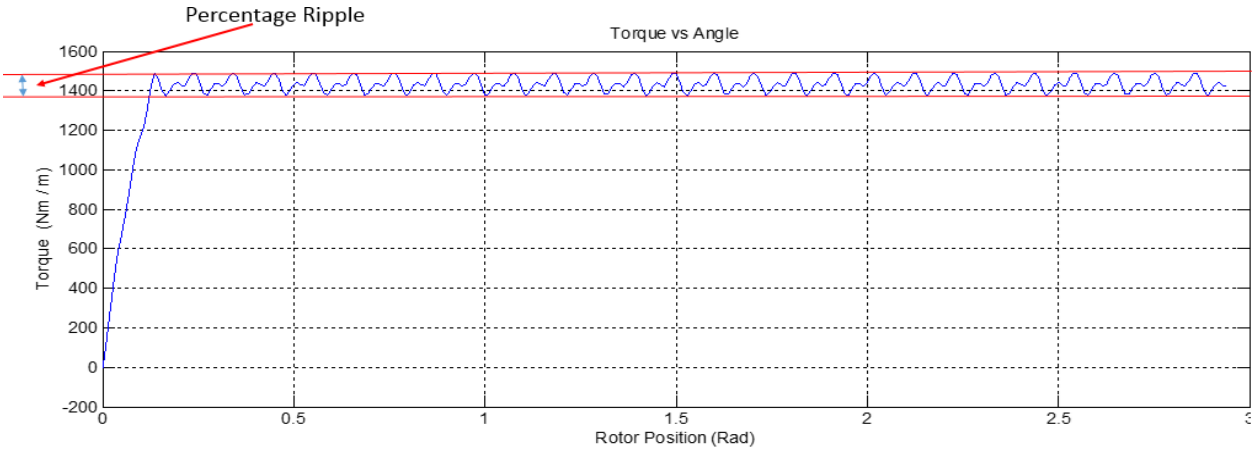

Figure 59. Illustrates 24/20, full load Torque vs Rotor Position at 2600 rpm (Opera)

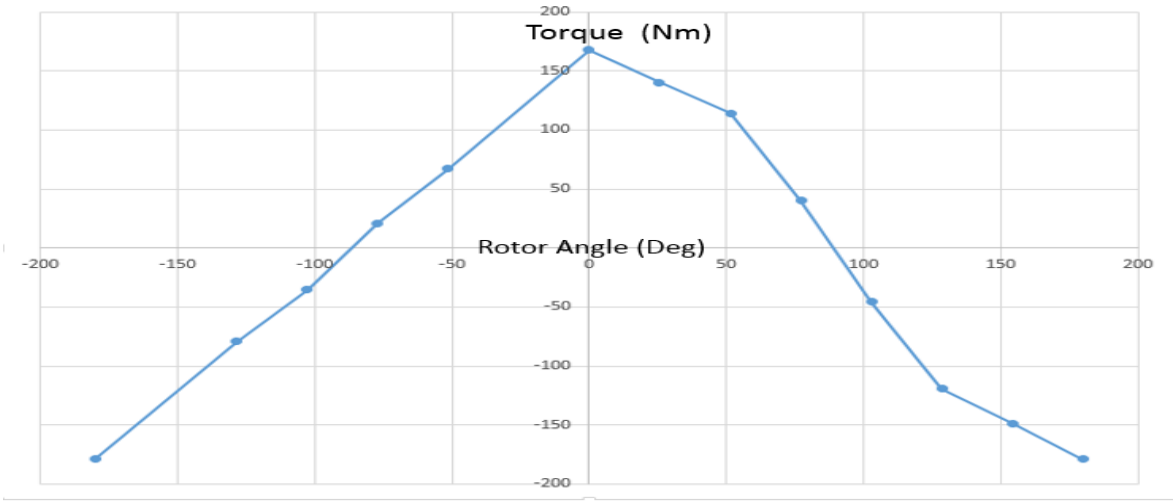

Figure 60. Illustrates 24/20, the effects in torque values with varying angle values between -180 to 180 degrees (24/20)

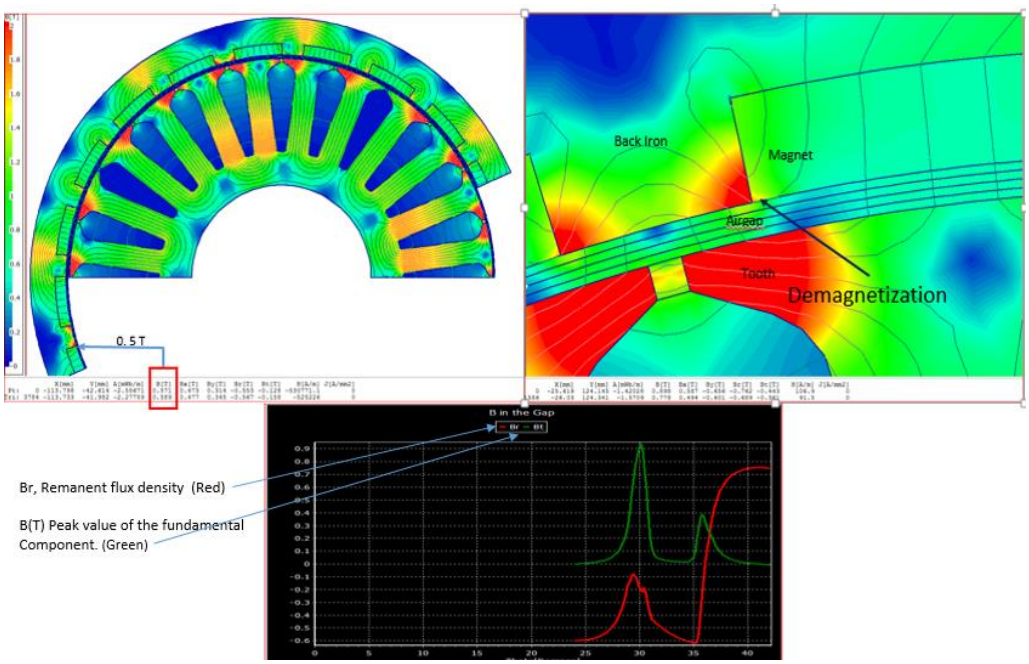

Figure 61. Illustrates, effects of demagnetization (24/20) with current orientation in the negative d-axis

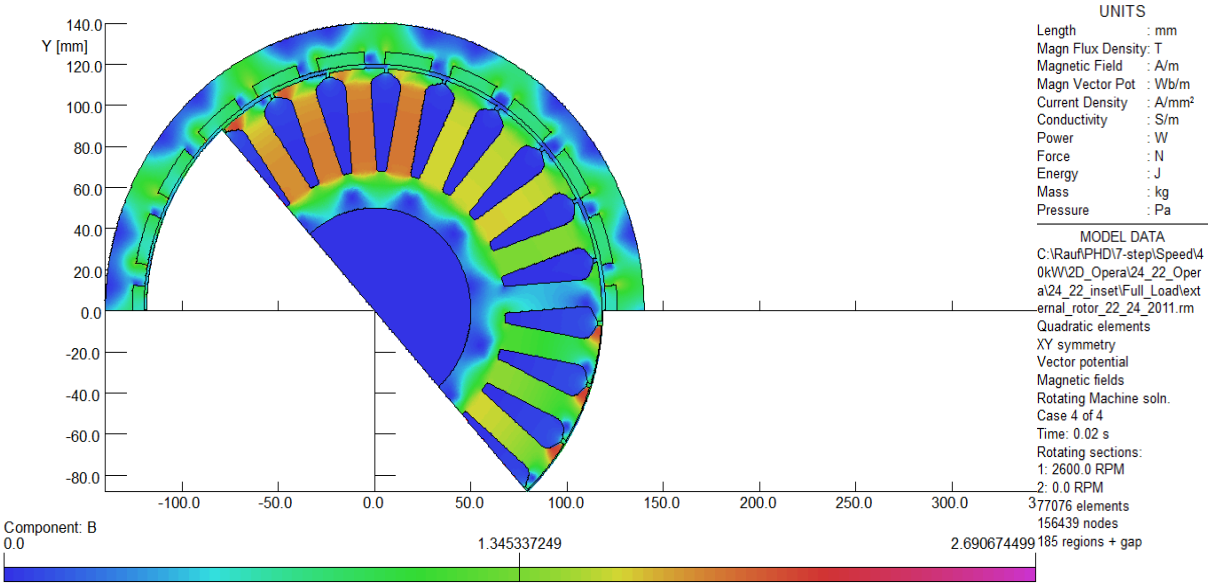

Figure 62. Illustrates, generator on full load flux density plot at 2.0 ms (24/22)

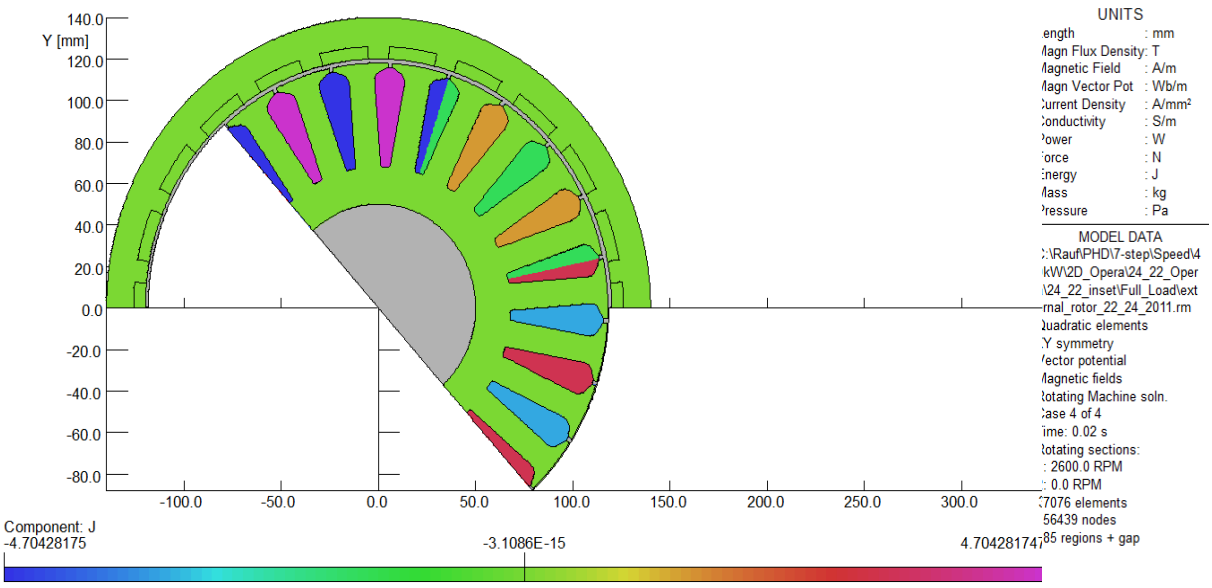

Figure 63. Illustrates, generator on full load current density plot at 2.0 ms (24/22)

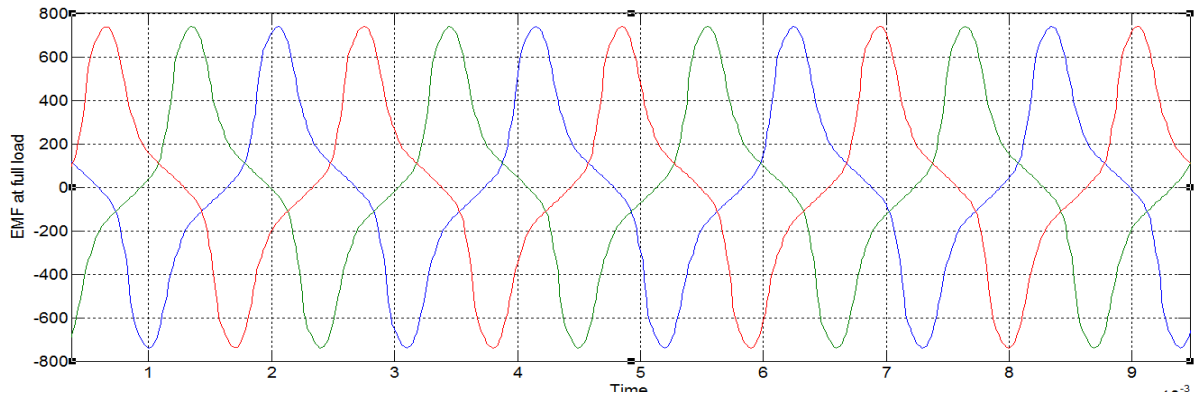

Figure 64. Illustrates 24/22, EMF at full load vs time at 2600 rpm (Opera)

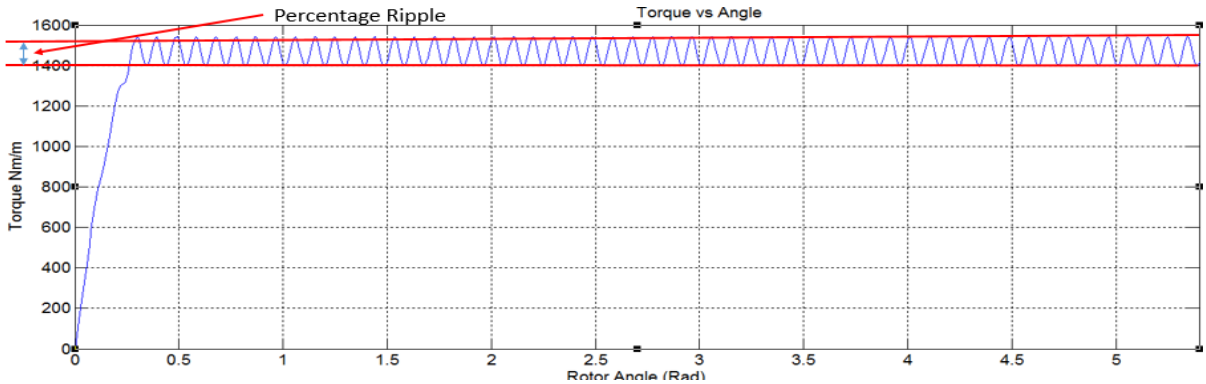

Figure 65. Illustrates 24/22, full load Torque vs Rotor Position at 2600 rpm (Opera)

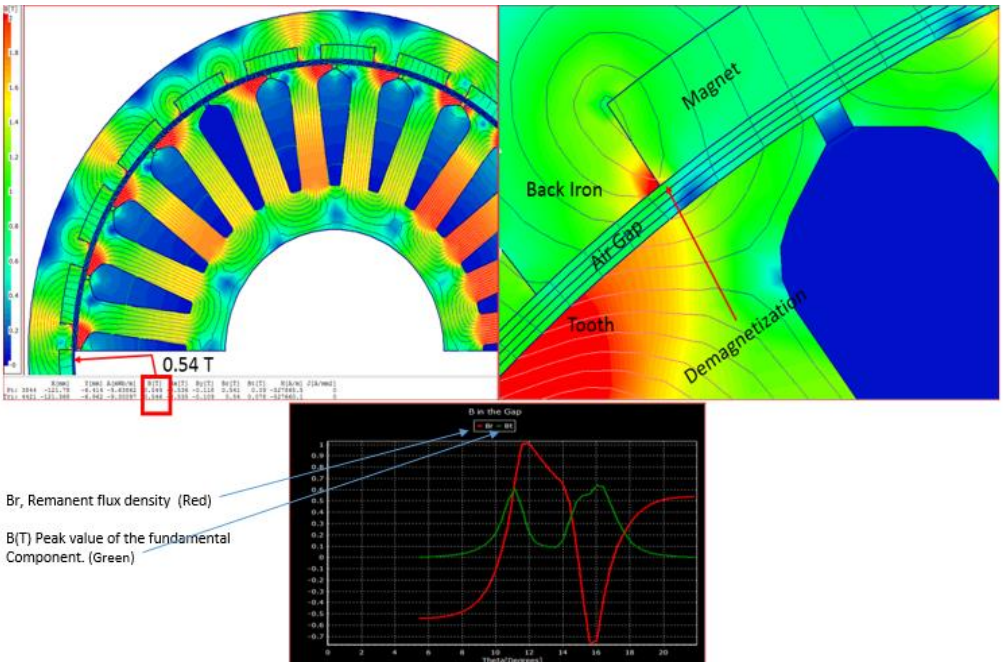

Figure 66. Illustrates, effects of demagnetization (24/22) with current orientation in the negative d-axis

9. Losses and Thermal Analysis

There are two major losses in a PM machine namely electrical and mechanical losses. The electrical losses consist of copper loss and magnetic loss whereas the mechanical losses consist of bearing and windage losses. The mechanical losses are often small in relation to the electrical losses but it may be important if the machine operate at high speed.

9.1. Copper losses

The copper loss often contributes the largest portion of the total losses in a PM machine. The copper loss in a 3 phase PM machine is calculated as follows:

$$P_{cu=}\ 3\ I^{3}\ R_{a} \qquad \text{Eq.111}$$

Where is the winding resistance of one phase and I is the rms value of the stator current. The winding resistance per phase is depending on the total length of conductor per phase and conductor area. The conductor area is a product of the slot area, Aslot, and the slot fill factor SFF. A high slot fill factor will consequently reduce the copper loss. This thermal loss will increase the value of the winding resistance and as a result will proportionally increase the amount of the copper loss. The thermal loss will generate heat and increase both the temperature of the motor winding and its resistance. The value of the winding resistance at any temperature other than the standard temperature (usually specified at 20°C Celsius winding conductors) shall be determined through the following equation

$$R =\ Ref\ [1 -\ \alpha\ (T - Tref)] \qquad \text{Eq.112}$$

Where,

*R***:** the winding conductor resistance at temperature in Celsius,
Rref: the winding conductor resistance at reference temperature which is usually 20°C.

The alpha constant, **α**: is the temperature coefficient of winding conductor material expressing the resistance change factor per degree of temperature change. The material used is copper and has a temperature coefficient value of 0.00393°C.

T: the winding conductor temperature in degree Celsius and
Tref: the reference temperature of winding conductor

9.2. **Iron losses**

A variation of the flux density produces losses in electromagnetic material known as iron losses. This iron loss is divided into hysteresis loss and eddy current loss. In the symmetric cycle, the specific hysteresis loss depends on the peak value and the frequency of the flux density variation and the area of the hysteresis loop. The hysteresis loss is expressed empirically using a relationship from Charles P. Steinmetz as:

$$P_h = K_h \ B^{\beta} \ f \qquad \text{Eq.113}$$

Where K_h is the hysteresis constant, β is the Steinmetz constant depends on the magnetic material used.

The eddy currents loss depends on the time rate of change of the flux density [40]. The eddy currents are circulating currents that are induced in the iron core by the magnetic field around the turns of the coil. For any given core, this loss is proportional to the frequency, the maximum flux density, and the conductivity of the core. The dependence of eddy current loss on flux density and frequency is expressed as below:

$$\mathrm{P_e} = \mathrm{K_e} \ \mathrm{B}^2 \ \mathrm{f}^2 \qquad \text{Eq.114}$$

Measurements of iron losses in magnetic material are traditionally made under sinusoidal flux density, varying frequency and magnitude. The total volumetric iron losses are commonly expressed in the following form for sinusoidally varying magnetic flux density.

$$\mathrm{P_{iron}} = \mathrm{P_h} + \mathrm{P_e} = \mathrm{K_h} \ \mathrm{B}^{\beta} \ \mathrm{f} + \mathrm{K_e} \ \mathrm{B}^2 \ \mathrm{f}^2 \qquad \text{Eq.115}$$

9.3. **Windage**

Windage loss is a loss due to friction between the air and the rotor surface. If the rotor surface area is small, this loss is negligible at moderate rotational speeds Gieras and Wang provide an analytical equation for the windage loss in a small machine that doesn‘t have an internal fan [25].

$$P_{windage} = 2 \ D_{ro}^3 \ L \ N^3 \ 10^{-18} \qquad \text{Eq.116}$$

Where, D_{ro} is the outside rotor diameter (mm), L is the length of rotor core (mm) and N is the motor rotational speed (revs/min).

9.4. **Bearings**

The bearing loss is depending on many factors, such as bearing type, lubrication, shaft load and rotor speed. The friction torque of a bearing is quite complex to calculate if high accuracy is required, but for an estimation it can be done rather easily. In literature, different formulas can be found of varying complexity, for example, Gieras and Wing provide an analytical equation for the expected bearing losses [25]:

$$P_{bearing} = \frac{K * M_{rot} * N}{1000} \quad \text{Eq.117}$$

9.5. **Thermal Model and Analysis**

The main objective of performing detailed thermal analysis of a motor is to predict and determine the individual motor component temperatures, both under steady state and transient conditions. An accurate determination of temperatures, in particular, for the magnets and winding is very important since the efficiency and life time of the motor are directly related to such temperatures. Over the years, numerous authors have published papers concerning the thermal modelling of electric machines [35-36]. The thermal analysis of an electric motor can be carried out using two methods; analytical lumped parameters analysis or FEM and CFD analysis. In this research, a thermal design package Motor-CAD is used in the investigation.

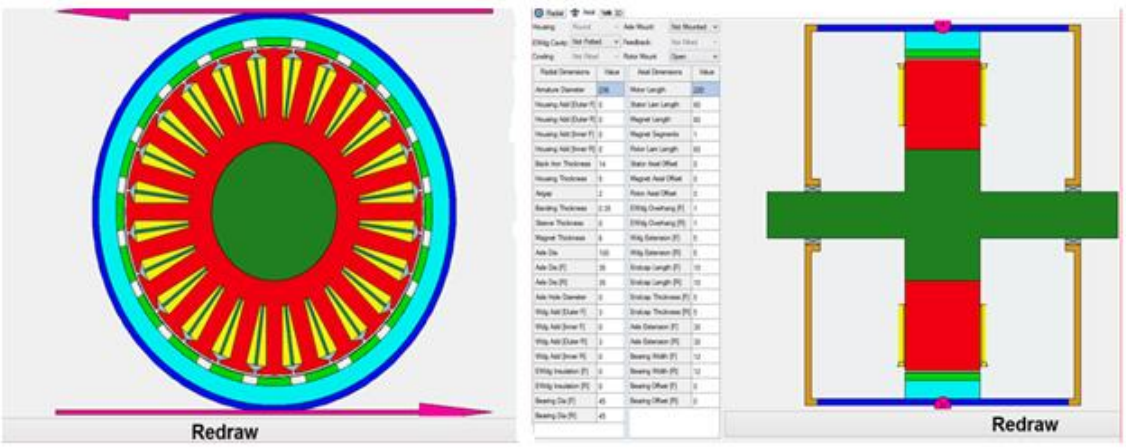

Figure 67. Shows Radial and Axial geometry and actual parameters of the Inset 24_20

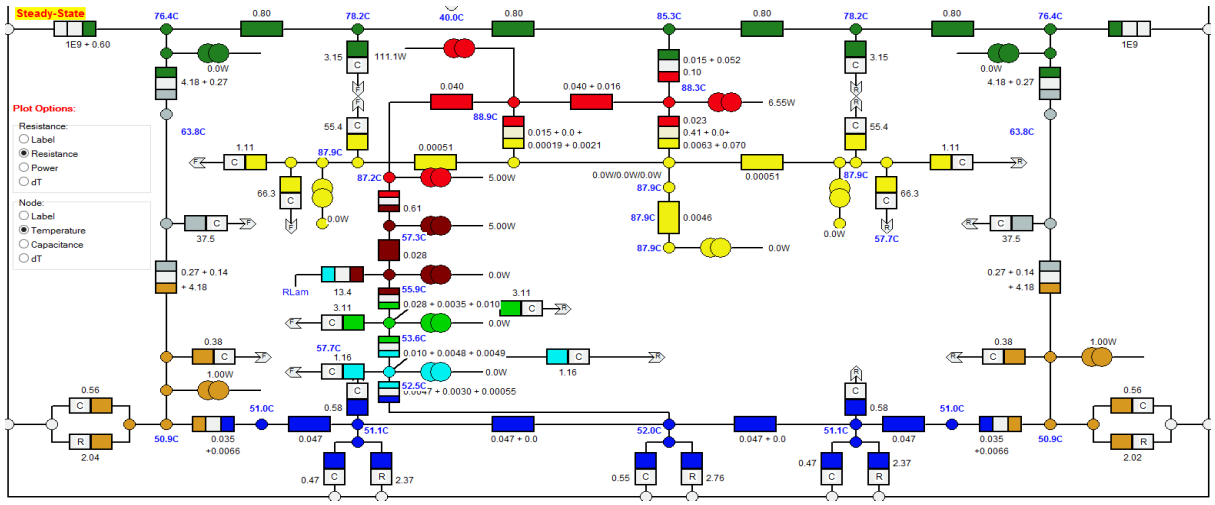

Figure 68. Schematic of thermal resistances placed in the circuit to model heat transfer paths in the machine (steady state transient) (Inset 24_20).

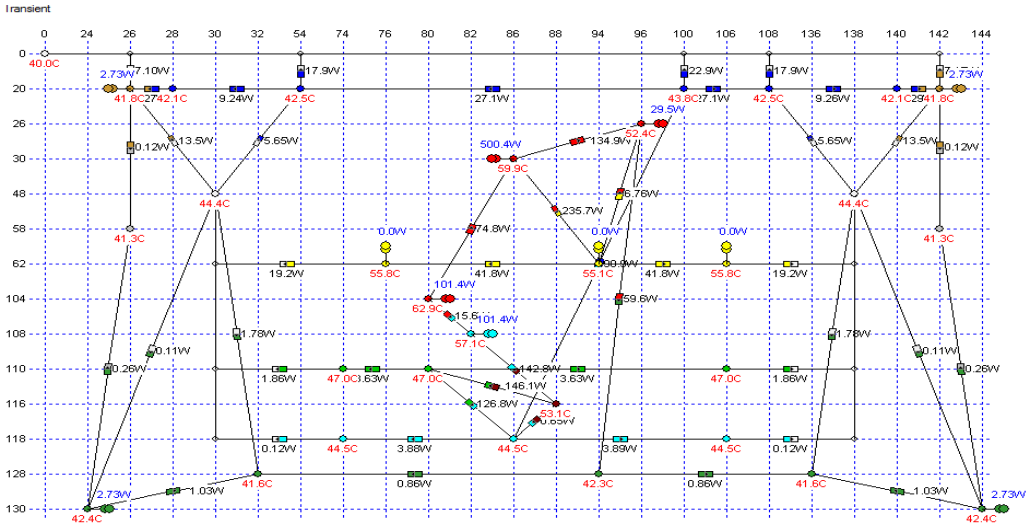

Figure 69. Circuit editor can be used to view predicted temperatures by selecting the radio buttons (inset 24_20)

The Motor-CAD thermal model is based upon lumped parameters analysis. It represents the thermal problems by using equivalent thermal resistance networks which shows a detailed thermal circuit showing all the heat flow paths in the motor as shown in Figures 67 and 68.

Briefly in this technique the electrical machine is divided geometrically into a number of lumped components and each component represents a node which will have a bulk thermal storage and heat generation.

The lumped parameters are derived from entirely dimensional information, the thermal properties of the materials used in the design and constant heat transfer coefficients. The thermal circuit in the steady state consists of thermal resistances and heat sources such as winding, bearing, windage, etc. are connected between motor component nodes to represent heat pathways. For transient analysis, the heat/thermal capacitances are used in representing thermal inertia. By representing the entire motor as a lumped thermal circuit, it is possible to evaluate the significant temperatures to a reasonable degree of accuracy.

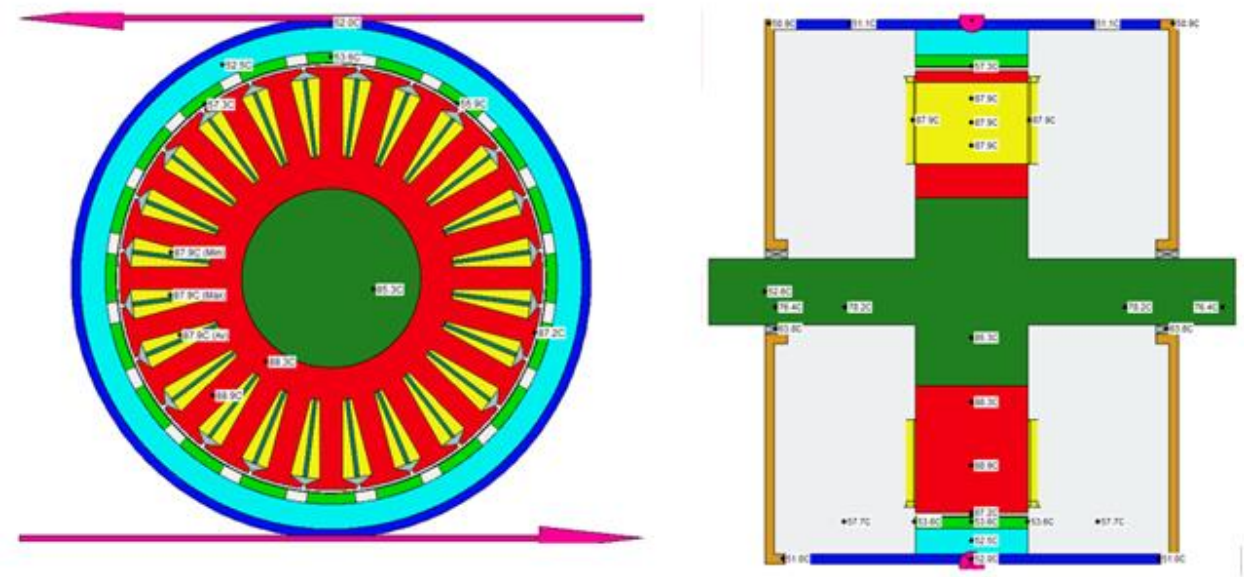

Figure 70.Figure Illustrates predicted temperatures Radial and Axial view (Inset 24_20)

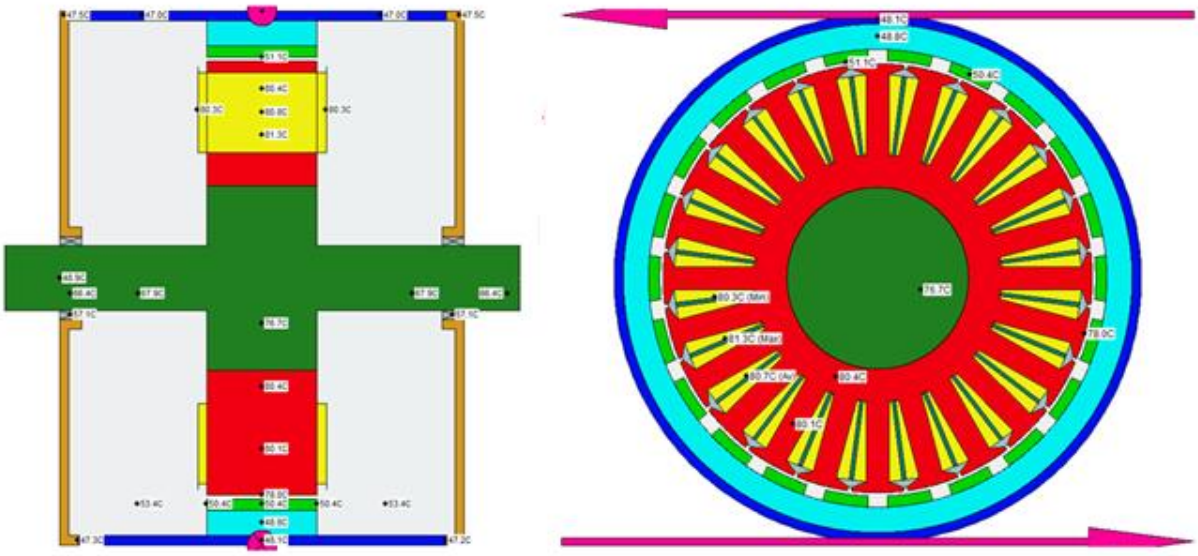

Figure 71. Illustrates predicted temperatures Radial and Axial views (Inset 24_22)

The resistance network is vastly used because this method requires minimal computing power thus giving almost immediate results (for a simple analysis).

The drawback of this method is that motor components are usually modelled by only a single node. To have achieved better simulated accuracy, one must increase the number of nodes. While this is possible, one must be aware of this procedure due to the increasing system complexity, computational time and processing power. The alternative to the resistance network method is the utilization of more sophisticated techniques, namely: Finite Element Analysis (FEA) and Computational Fluid Dynamics (CFD). FEA can only be used to model conduction heat transfer in solid components, while CFD is able to model all heat transfer mechanisms (conduction, convection and radiation). CFD is primarily used in the thermal design of motors since it has the capability to predict complex flow regimes as well as heat transfer, in that regard CFD will not be considered.

10. Comparative analysis Inset & Surface Mount 24/20

Various forms of magnet placement on the rotor lead to certain unique operating characteristics of the machines. The principle of operation of synchronous machines with PM rotors, relationships such as the Magnetomotive force (mmf), induced emf (also known as back emf), and torque are derived for PMSMs.

To obtain these relationships, it is important to understand the stator windings and how the number of turns and their placement in the stator laminations affect them. Factors that affect the windings are pitch, distribution, skew and many other.

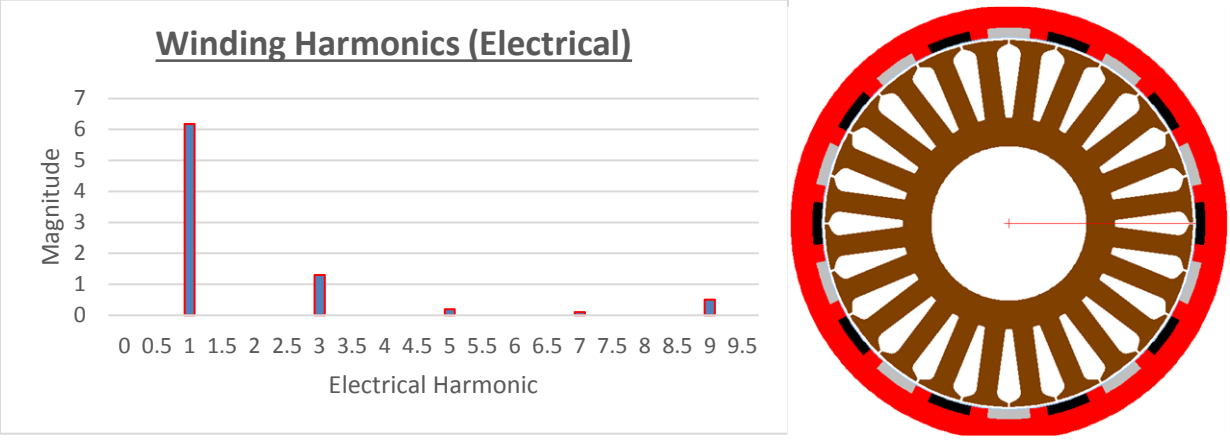

Figure 72. Illustrates winding harmonics 24/20 exterior rotor (Inset)

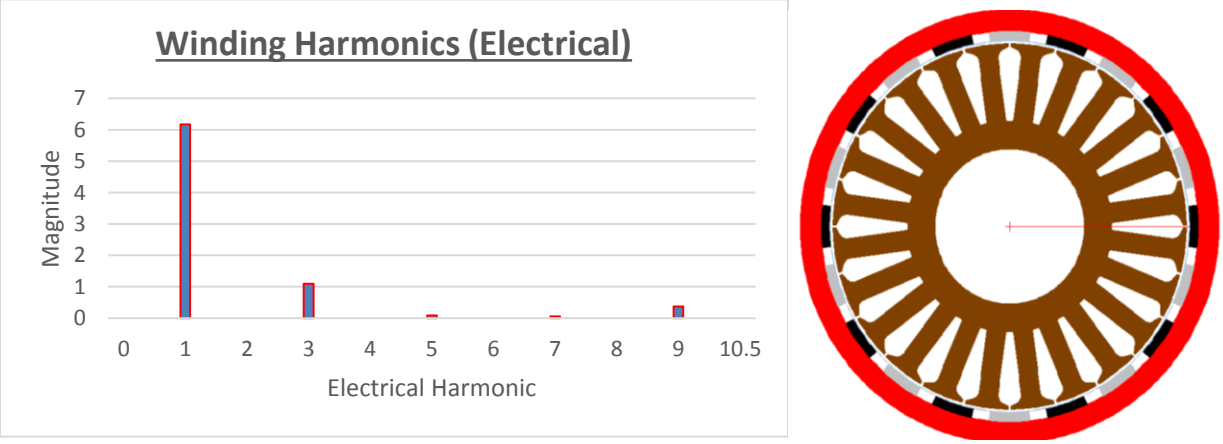

Figure 73. Illustrates winding harmonics 24/20 exterior rotor (Surface Mount)

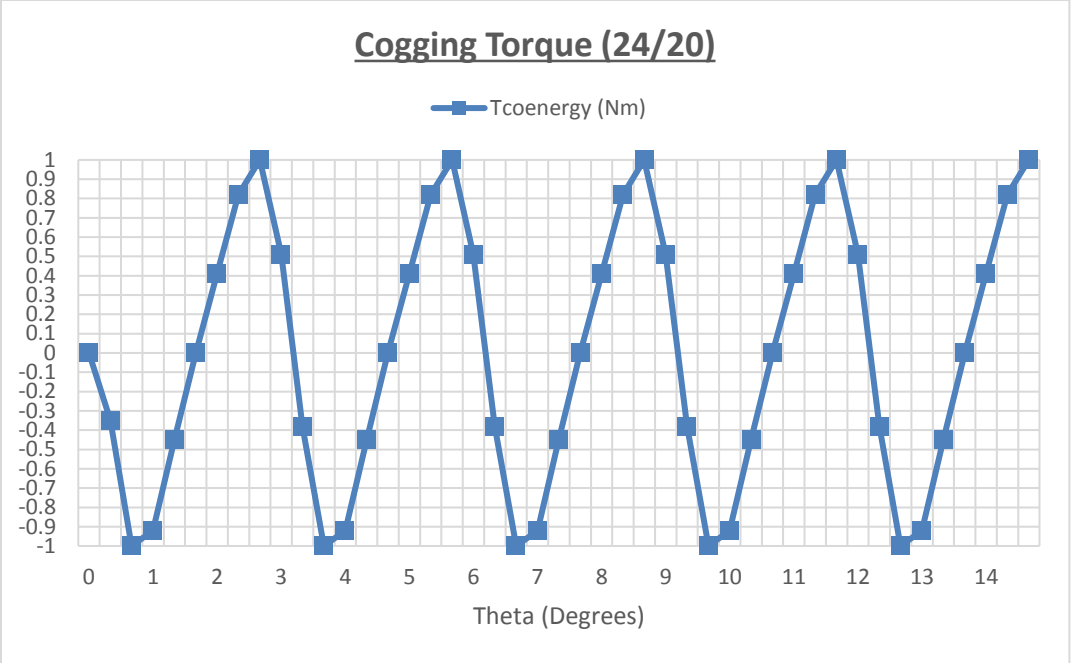

Figure 74. Illustrates Cogging Torque 24/20 Inset

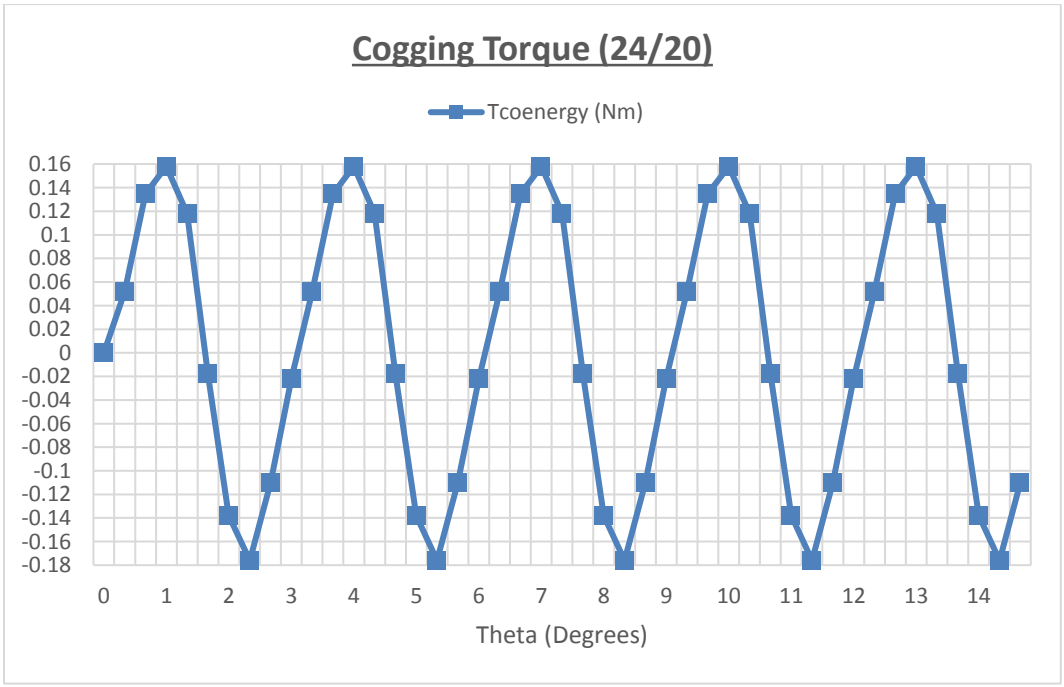

Figure 75. Illustrates Cogging Torque 24/20 Surface Mount

Different ways of arranging magnets on the rotor have created many types of PMSMs and brushless dc machines. Some popular and research-type arrangements and their impact on the air gap flux density, winding inductances, and their influence on reluctance torque, which is capable of enhancing the magnet generated or synchronous torque.

The cogging torque may also be thought of as a reluctance torque due to the reluctance variation presented by the tooth and slot to the magnet current source. Its period is the same as the slot pitch in general during most of the measurements. The cogging torque is alternating and almost symmetric about its angular axis. For radial flux machines, the surface mounted permanent magnet machine is the most widely used topology. However, since the d and q-axis stator winding inductances of such machines are the same, they exhibit zero reluctance torque. The magnets are exposed directly to the armature reaction and, hence, are susceptible to partial irreversible demagnetization. Surface mounted machines also generally have a relatively limited flux-weakening capability. For interior mounted permanent magnets machines (IPMs), since the d-axis inductance is smaller than the q-axis inductance, a reluctance torque exists while the d-axis inductance is high compared to that of an equivalent Surface Mount topology. Therefore, inset permanent mount topologies are eminently appropriate for extended speed and constant power operation in flux-weakening capabilities [38, 39].

The Mean reluctance torque can be calculated as follows:

$$T_{rel} = \frac{mp}{2} * \left(L_d - L_q\right) i_d \, i_q \qquad \text{Eq.118}$$

Where *m* is the number of phases and *p* is the number of pole-pairs and instantaneous currents id and iq.

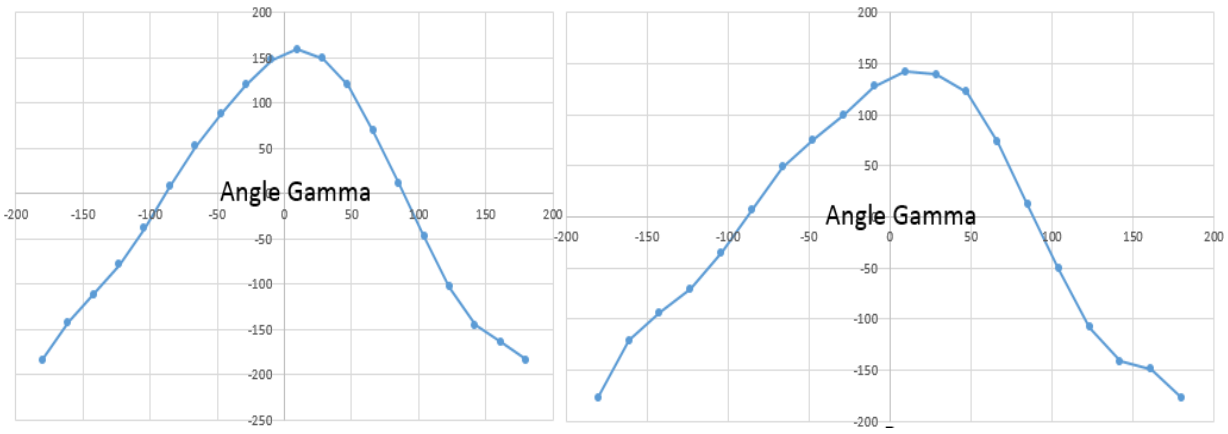

(A) (B)

Figure 76. Illustrates, the effects in torque values with varying angle values between -180 to 180 degrees (A) Surface Mount and (B) Inset Mount (Angle between Iph1 and q axis)

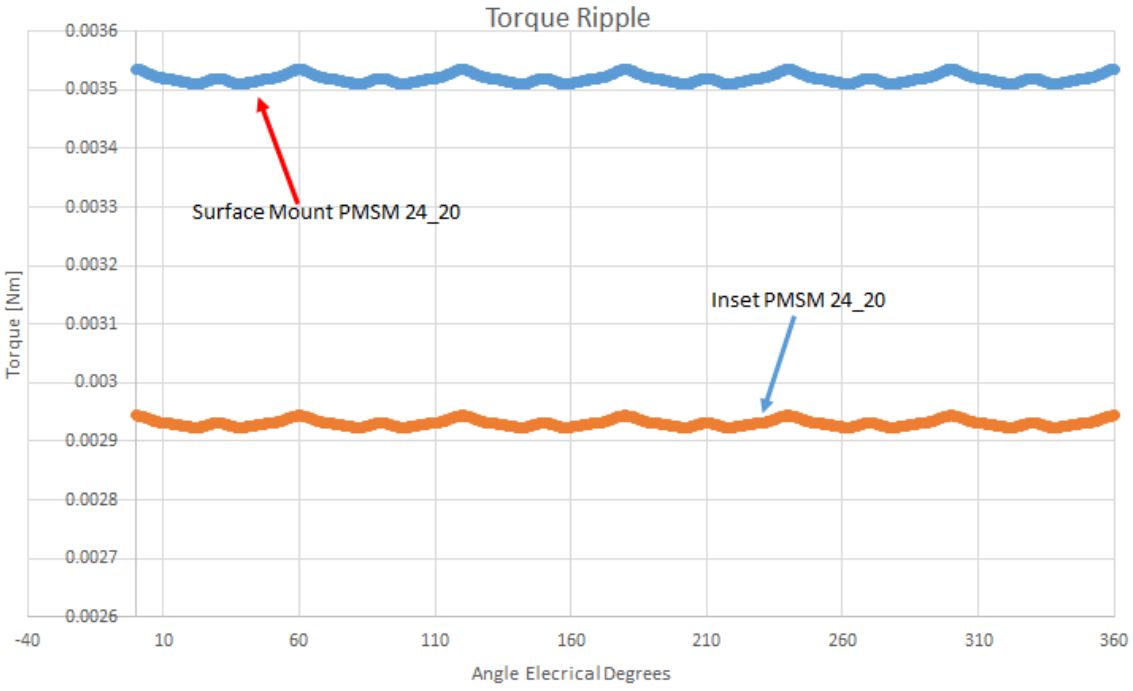

Figure 77. Illustrates Torque Ripple for Surface Mount and inset configuration

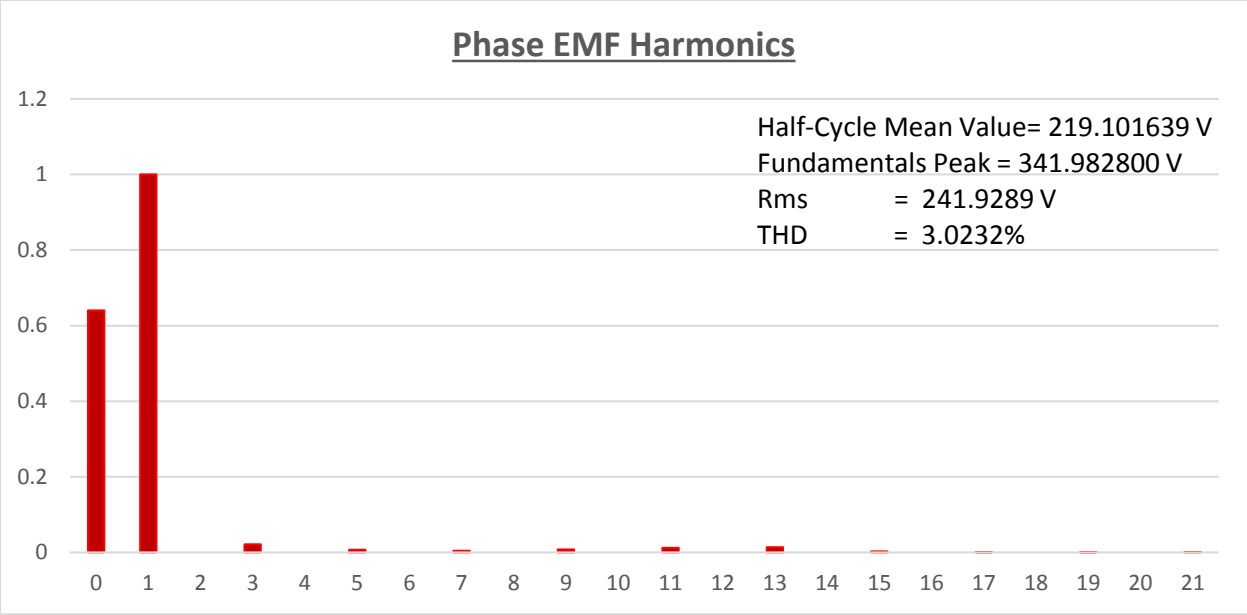

Figure 78. Illustrates Harmonic analysis Inset configuration

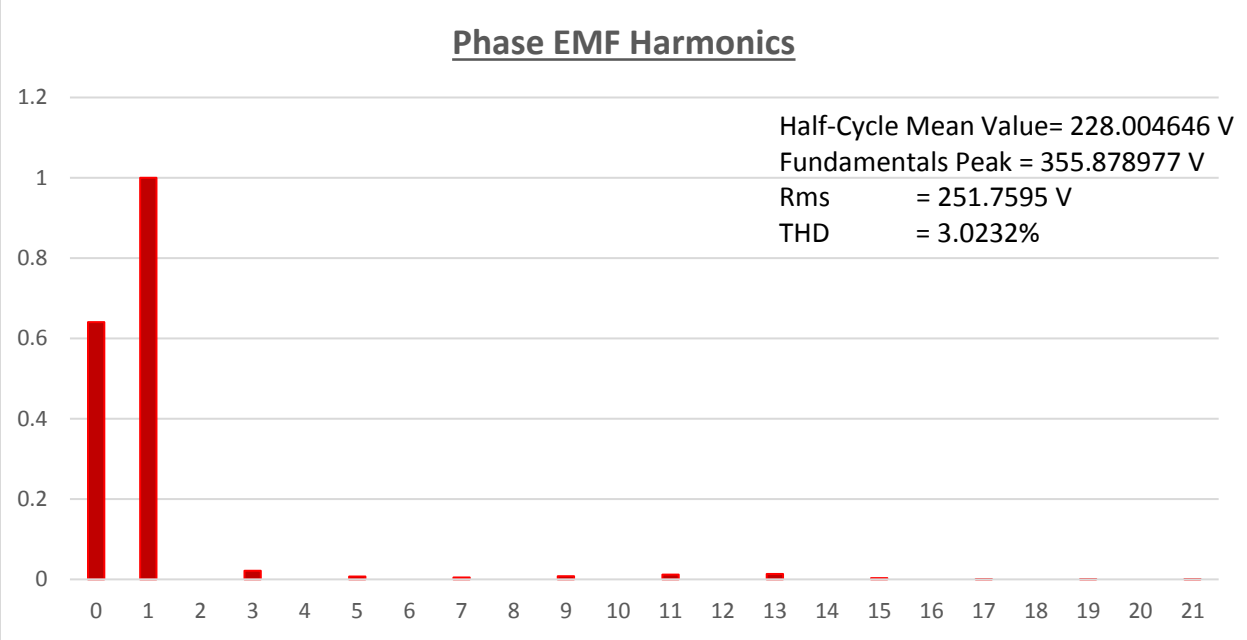

Figure 79. Illustrates Harmonic analysis Surface Mount configuration

11. Conclusion and Further Work

The thesis has described two different radial flux generator topologies for power generation industry, the variable speed integrated generating set capabilities has allowed full engine integration and benefited from a multi pole design.

Some choices have been made in order to restrict the extension of the work. A permanent magnet synchronous machine with a concentrated windings was expected to fulfil the requirements. An extensive comparison between 24 slots and 20 poles and 24 slots and 22 poles. Firstly from the above it can be seen that radial exterior rotor generator with concentrated windings seems to be the selected criteria, this is due to its compactness of the design and of its integration onto a flywheel of a diesel engine. Additionally the concept of concentrated winding for maximizing the fundamental winding factor is presented.

The winding factors of fractional slot machines were closely examined because the winding factor is usually an important parameter for designing of a motor.

It was, however, discovered that in the case of fractional slot machines, the fundamental winding factor does not necessarily indicate the amount of pull-out torque. It was also noticed that some winding arrangements have unwanted properties, which may be, e.g. when the number of slots is especially when $Q_s \approx 2p$, an unbalanced magnetic pull. Besides the winding factor, other reasons are the influence of rotor eddy current loss. This provides quick insight into the influence of the winding layout or rotor eddy current loss and helps to select a feasible winding layout for the application.

The cogging torque values of the analysed fractional slot motor types can be less than 1% of the rated torque. In the case of multi-pole machines a cogging torque as low as 0.05% could be estimated. It was discovered, that when a low cogging torque is required, the least common multiplier LCM appears to be a useful and also easily available parameter. The proper procedure to obtain a low cogging torque and low torque ripple is suggested to be the selection of a high value for the LCM.

When comparing the pull-out torque of the motors belonging to the same frame size category, some differences are to be mentioned. Increasing the pole number and keeping the slot number constant reduces the developed pull-out torque in most of the analysed cases, as the magnet material and the machine size (and airgap diameter) were kept practically constant.

Further increasing of the slot number and keeping the pole number constant increases the developed pull-out torque. According to the results obtained for the slot number, the peak-to-peak value of the torque ripple grows as the number of poles increases.

It was noted that, if the number of poles is increased, the height of the stator yoke as well as the iron area could be decreased. Inset configuration was also selected for two reasons, one to try concentrate flux across the air gap and other to provide a means for implementing field weakening technology for any future work.

Furthermore a short comparison between inset and surface mount 24 slots and 20 poles configuration has been conducted in the final chapters.

The performance of the surface magnet motor was compared to the inset magnet motor. When the slot and pole numbers are low, the surface magnet structure produces higher pull-out torques than the corresponding embedded magnet motor of the same frame size. This is due to the high armature reaction effect occurring in the embedded magnet machine. When the slot and pole numbers are high, the pull-out torque may be similar for both the surface and inset structures.

Compared to the inset magnets, one important advantage of the surface mounted magnets is the smaller amount of magnet material needed in the design (in integer-slot machines). If the same power is wanted from the same machine size, the surface mounted magnet machine needs less magnet material than the corresponding machine with embedded magnets.

This is due to following two facts: in the embedded-magnets-case there is always a considerable amount of leakage flux in the end regions of the permanent magnets and the armature reaction is also worse than in the surface magnet case. Zhu et al. (2002) reported that the embedded magnet structure facilitates extended flux-weakening operation when compared to a surface magnet motor with the same stator design (both machines are equipped with an integer slot winding). He also stated that the iron losses of the embedded magnet machine were higher than that of the machine with surface magnet rotor.

However, there are several other advantages that make the use of inset magnets favourable. Because of the high air-gap flux density, the machine may produce more torque per rotor volume compared to the rotor, which has surface mounted magnets.

This, however requires usually a larger amount of PM-material. The risk of permanent magnet material demagnetization remains smaller.

During the design stage, all the parameters have been analytically determined and the motor models were verified through simulation analytical and in the finite element software*, Speed and opera*, in order to predict the induced back EMF and the produced loading torque. According to the used analytical models, the suggested machine design fulfils the requirements. This was also confirmed with finite element method (FEM) simulations results. Thus, the results showed acceptable correlation between simulations results.

From the comparison between simulation works, it can be concluded that the results are in generally good agreement with the simulation. The generator shows excellent performance and able to satisfy the required specification.

However, there may have been slight errors in simulated results probably due to certain parameters which may have not been set correctly during simulation. In conclusion and analysis of the above results, 24 slot and 20 poles inset configuration is the prime target as it satisfies the requirement, also it would help to keep costs low.

An important element would be build a prototype and evaluate the performance of the two machines. The need to carry out such tests in order to confirm and verify the predicted performance data. For these experimental tests a converter should be constructed and implemented. Furthermore, the implementation of fault tolerance test setup would be interesting test to test the capability of operating under fault condition, field weakening and many other applications highlighted above and off course the full capability of the developed system.

References

[1] Jacek F. Gieras, Rong-Jie Wang and Maarten J. Kamper, Axial Flux Permanent Magnet Brushless Machine: Springer 2008.

[2] Duane C. Hanselman, Brushless permanent magnet motor design: Magna Physics Publishing 2008.

[3] Y.G. Guo and J.G. Zhu, "Study of Permanent Magnet Transverse Flux Motors with Soft Magnetic Composite Core", Faculty of Engineering University of technology Sydney.

[4] Jacek F. Gieras and Mitchell Wing, Permanent Magnet Motor Technology: Design and Application: Marcel Dekker Inc, 2002.

[5] Austin Hughes, Electric Motors and Drives: Fundamentals, types and applications: Elsevier 2006.

[6] Aydin, M, S. Huang and T.A. Lipo, "Axial Flux Permanent Magnet Disc Machines": A Review, Research Report 2004-10, University of Wisconsin Madison USA 2004.

[7] Campbell, P: "Principles of a permanent magnet axial field DC machine," Proceedings of Institute of Electrical Engineers, Volume 121, No. 12, 1974, pp, 1489-1494.

[8] Spooner, E and Chalmers, BJ: "Torus - a slotless, toroidal-stator, permanent magnet generator", IEE Proceedings-B Electric Power Applications, Vol. 139, No. 6, 1992, pp. 497-506.

[9] Christopher Gerada, "Brushless DC machines", PEMC research group University of Nottingham

[10] J. R Hendershot, T.J.E. Miller, Design of Brushless Permanent Magnet machines Motors: Magna Physics Publishing and Clarendon Press, 1994.

[11] T. J. E. Miller, Brushless Permanent-Magnet and Reluctance Motor Drives: Oxford Press Publications, 1989.

[12] Juha Pyrhonen, Tapani Jokinen and Valeria Hrabovcova, Design of rotating electrical machines: John Wiley & Sons, 2008.

[13] Wei Hua, Ming Cheng, Z. Q. Zhu and D. Howe, "Design of Flux-Switching Permanent Magnet Machine, Considering the Limitations of Inverter and Flux-Weakling Capabilities," Industry Application Conference, 2006. 41st IAS Annual Meeting, Conference record of the 2006 IEEE.

[14] Ion Boldea, Synchronous generators: Taylor & Francis Group, LLC, 2006.

[15] E. Spooner and L. Haydock, "Vernier hybrid machines," IEE Proceedings- Electric Power Application, Volume 150, No150, November 2003.

[16] P. Campbell, "The magnetic circuit of an axial flux DC electrical machine," IEEE transaction of magnetics, Volume 11, issue 5, September 1975.

[17] H. Weh and H. May, "Achievable Force Densities for Permanent Magnet Excited Machines in New Configuration," International Conference on Electrical Machines: Munich, Germany, September 1986, pp 1107-1111.

[18] A.J. Mitcham and C. Dullage, "A Novel Permanent Magnet Propulsion Motor for Future Warships", International Naval Engineering Conference on Cost Effective Maritime Defense: Plymouth, UK, 1994, paper 16.

[19] F. Şahin, “Design and Development of a High Speed Axial Flux Permanent Magnet Machine,” PhD Thesis: Technische Universiteit, Eindhoven, 2001.

[20] Vu Xuan Hung, “Modelling of External Rotor Permanent Magnet with concentrated windings,” PhD Thesis: Delft University of Technology, Netherlands, 2012.

[21] A.K. Shawney, Electrical Machine Design: Dhanpat Rai & Co. (P) LTD, 2011.

[22] T.J.E.Miller, Speed Electrical Machines: CD-Adapco 2002 – 2011.

[23] C. Gerada and Keith J Bradley, ”Integrated PM machine design for an aircraft EMA,” IEEE transaction on industrial electronics, Volume 55, Issue 9, September 2008.

[24]R. Krishnan, Permanent magnet synchronous and brushless DC motor drives: CRC Press, Taylor & Francis Group, 2010.

[25] Y. S. Chen, Z. Q. Zhu, and D. Howe, “Calculation of d- and q-axis inductances of PM brushless ac machines accounting for skew,” IEEE Transactions on Magnetics- IEEE Trans Magn: Volume 41, No 10, pp. 3940-3942, 2005.

[26] Juha Saari, “Thermal Modelling of High-Speed Induction Machines”: electrical Engineering Series No 82, Helsinki University of Technology.

[27] G.R Slemon and X. Liu, “core losses in permanent magnet motor,” IEEE Transactions on magnetics: Volume 26, issue 5, September 1990.

[28] K. Ng, Z. Q. Zhu, N. Schofield, “Analytical prediction of rotor eddy current loss in brushless machines equipped with surface mounted permanent magnets,” Electrical machines and systems 2001, ICEMS 2001, Proceedings of the fifth International conference.

[29] T. M. Jahns, and W. L. Soong, “Pulsating torque minimisation techniques for permanent magnet ac motor drives: a review,” IEEE Transaction on Industrial Electronics: vol.43, no.2, pp.321-330, 1996.

[30] M. Aydin, Z. Q. Zhu, T. A. Lipo, and D. Howe, “Minimization of cogging torque in axial flux permanent magnet machines – design concepts”, IEEE Transactions on Magnetics: Volume 43, No.9, pp.3614-3622, 2007.

[31] R.P. Deodhar, D.A. Staton, T.J.E. Miller and T.M. Jahns, “Prediction of cogging torque using the flux-mmf diagram technique,” IEEE Transactions on Industry Applications: Volume 32, Issue. 3, pp. 569-576, 1996.

[32] Pia Salminen, “Fractional slot permanent magnet synchronous motors for low speed applications”, PHD Thesis: Lappeenranta University Technology, 2004.

[33] T.H. Koch, A. Binder, “Permanent Magnet Machines with Fractional Slot winding for Electric Traction,” Proceedings of the International Conference on Electrical Machines: ICEM. Brugge, Belgium, 2006.

[34] J. Wang, Z. P. Xia, and D. Howe, “Three-Phase Modular Permanent Magnet Brushless Machine for Torque Boosting on a Downsized ICE Vehicle”, IEEE transactions on vehicular technology: Volume 54, no. 3, pp. 809-816, 2005.

[35] H.P. Liu, V. Lelos, and C.S. Hearn, “Transient 3-D Thermal Analysis for an Air-Cooled Induction Motor,” IEEE International Electric Machines and drives conference, San Antonio, Texas, 2005.

[36] S.E. Lyshevski, Electromechanical System and Devices, CRC Press, 2008

[37] S. Morimoto, Y. Takeda, T. Hirasa, and K. Taniguchi, “Expansion of operating limits for permanent magnet motor by current vector control considering inverter capacity,” IEEE Transaction on Industrial Application*:* Volume 26 , No 5, pp. 866.871, 1990.

[38] C. Mi and G. Slemon, “Modelling of Iron Losses of Permanent-Magnet Synchronous Motor,” IEEE Transactions on Industry Applications: Volume 39, No 3, and 2003.

[39] P. L. Chapman, The Power Electronics Handbook, CRC Press LLC, 2002.

[40] Cummins Generator Technologies: Internal Projects Team, R. Sattar, R. Seliga and E. Ernest, 2008-2014.

[41] Thomas Reichert, Thomas Nussbaumer and Johann W. Kolar, “Torque Scaling laws for interior and exterior rotor permanent Magnet Machines,” Power Electronic Systems Laboratory, ETH Zurich.

[42] Aritz Egea, “Design of Electric Machines,” Electric Energy Magazine 4: Mondragon Unibertsitatea, 2013.

[43] International Electronic Commission, “IEC 60034:2009”: http://www.inmetro.gov.br/barreirastecnicas/pontofocal/..%5Cpontofocal%5Ctextos%5Cregulamentos%5CSAU_467.pdf

[44] Protean, Electric Protean Ford Truck: http://www.proteanelectric.com/, last accessed the website in 2013.

[45] Cummins Generator Technologies, ”Cummins Europe”, http://www.cumminseurope.com/cummins-power-generation-introduces-the-next-generation-of-high-horsepower-generator-sets.

[46] Richard Martin, “Axial flux permanent magnet machines for direct drive application”, PHD Thesis: School of Engineering University of Durham, 2004.

[47] Lester Chong, “Design of an interior permanent Magnet Machine with Concentrated Winding for Field Weakening Applications,” PHD Thesis: The University of South Wales, 2011.

[48] Microchip, “Brushless DC motor control made easy”, http://ww1.microchip.com/downloads/en/appnotes/00857a.pdf

[49] B. A. Maslow, “Rotary permanent magnet electric motor with varying air gap between interfacing between stator and rotor elements”, USA patent number 6727630, 2004

[50] H.R Cha, “Design of outer rotor IPM type PMSM for 3 wheel electrical Vehicle”, ICEMS 2011, Beijing, China, 2011